

***COMPARATIVE PERFORMANCE
OF DUCTILE AND DAMAGE PROTECTED
BRIDGE PIERS SUBJECTED
TO BI-DIRECTIONAL EARTHQUAKE ATTACK***

*A thesis
submitted in partial fulfillment
of the requirements for the Degree
of
Master in Civil Engineering
at the
University of Canterbury*

*By
Naoto MASHIKO*

*Supervised by
Professor J.B. Mander*

***University of Canterbury
Christchurch, New Zealand
2006***

TABLE OF CONTENTS

Abstract	iv
Acknowledgements	v

1 INTRODUCTION

1.1 Research Objective	1-1
1.2 Literature Review and Previous Study	1-2
1.2.1 Design Code	1-2
1.2.2 Bridge Pier Design in the Previous Study in 1999	1-5
1.2.3 Damage Avoidance Design (DAD)	1-6
1.2.4 Pseudodynamic (PD) Test	1-7
1.2.5 Bi-directional Loading Effect	1-9
1.3 Scope of This Thesis	1-10
1.4 What Then Is Particularly New in This Study	1-11
1.5 References	1-12
1.6 Tables for Chapter 1	1-13
1.7 Figures for Chapter 1	1-14

2 INCREMENTAL DYNAMIC ANALYSIS APPLIED TO SEISMIC

RISK ASSESSMENT OF BRIDGES

Section Summary	2-1
2.1 Introduction	2-2
2.2 Findings from Previous Research	2-3
2.3 Quantitative Risk Assessment	2-4
2.3.1 Step 1: Select ground motion records and modelling the structure --	2-4
2.3.2 Step 2: Perform Incremental Dynamic Analysis	2-5
2.3.3 Step 3: Model the IDA Curve and Statistical Outcomes	2-6
2.3.4 Step 4: Assign Damage Limit State	2-7
2.3.5 Step 5: Hazard-Recurrence Risk Relation	2-8
2.3.6 Step 6: Risk Modelling and Accounting for Uncertainty	2-9
2.4 Identifying Critical Earthquake Ground Motion	2-11
2.5 Case Study of Bridge Piers	2-12
2.5.1 IDA Procedures	2-12

2.5.2 Hazard-Recurrence Risk Assessment -----	2-13
2.5.3 Identifying Critical Earthquake Ground Motions -----	2-14
2.6 Conclusions -----	2-15
2.7 Reference -----	2-16
2.8 Tables for Chapter 2 -----	2-17
2.9 Figures for Chapter 2 -----	2-19

3 THE SEISMIC PERFORMANCE OF THE HIGHWAY BRIDGE PIERS SUBJECTED TO BI-DIRECTIONAL EARTHQUAKE

Section Summary -----	3-1
3.1 Introduction -----	3-2
3.2 Experimental Study: Prototype and Specimen Design -----	3-3
3.3 Experimental Procedure: Pseudodynamic Testing -----	3-4
3.4 Choosing Critical Earthquakes for Pseudodynamic Testing -----	3-7
3.5 Experimental Result -----	3-8
3.5.1 Overview -----	3-8
3.5.2 New Zealand Bridge Pier (SP-1) -----	3-8
3.5.3 Japanese Bridge Pier (SP-2) -----	3-10
3.5.4 Caltrans Bridge Pier (SP-3) -----	3-11
3.6 Comparison of Each Pier's Performance -----	3-12
3.7 Comparative Evaluation of Observed Response with Computational Predictions -----	3-13
3.8 Experimental Results to corroborate the Seismic Risk Analysis -----	3-14
3.9 Conclusion -----	3-14
3.10 References -----	3-16
3.11 Tables for Chapter 3 -----	3-17
3.12 Figures for Chapter 3 -----	3-19

4 PERFORMANCE OF A DAMAGE PROTECTED HIGHWAY BRIDGE PIER SUBJECTED TO BI-DIRECTIONAL EARTHQUAKE ATTACK

Section Summary -----	4-1
4.1 Introduction -----	4-2

4.2 Experimental Program -----	4-3
4.2.1 Prototype Design -----	4-3
4.2.2 Specimen and Construction -----	4-4
4.2.3 Testing Procedures -----	4-5
4.3 Test Results -----	4-8
4.3.1 Cyclic Loading Test -----	4-8
4.3.2 Pseudodynamic Test -----	4-8
4.3.3 Comparison with the New Zealand Code-Design Ductile Bridge Pier -----	4-10
4.4 Conclusion -----	4-11
4.5 References -----	4-12
4.6 Tables and Figures for Chapter 4 -----	4-13

5 CONCLUSIONS AND RECOMMENDATIONS

5.1 Research Summary -----	5-1
5.2 Conclusions -----	5-2
5.3 Recommendations for Future Research -----	5-3

Appendix A – Spread Sheet for Spiral Design

Appendix B – DAD procedures

Appendix C – Photo Albums

Abstract

Incremental Dynamic Analysis (IDA) procedures are advanced and then applied to a quantitative risk assessment for bridge structures. This is achieved by combining IDA with site-dependent hazard-recurrence relations and damage outcomes. The IDA procedure is also developed as a way to select a critical earthquake motion record for a one-off destructive experiment.

Three prototype bridge substructures are designed according to the loading and detailing requirements of New Zealand, Japan and Caltrans codes. From these designs 30 percent reduced scale specimens are constructed as part of an experimental investigation. The Pseudodynamic test is then to control on three specimens using the identified critical earthquake records. The results are presented in a probabilistic risk-based format. The differences in the seismic performance of the three different countries' design codes are examined.

Each of these current seismic design codes strive for ductile behaviour of bridge substructures. Seismic response is expected to be resulting damage on structures, which may threaten post-earthquake serviceability. To overcome this major performance shortcoming, the seismic behaviour under bi-directional lateral loading is investigated for a bridge pier designed and constructed in accordance with Damage Avoidance principles. Due to the presence of steel armoured rocking interface at the base, it is demonstrated that damage can be avoided, but due to the lack of hysteresis it is necessary to add some supplemental damping. Experimental results of the armoured rocking pier under bi-directional loading are compared with a companion ductile design specimen.

Acknowledgements

This research was carried out in the Department of Civil Engineering at the University of Canterbury, under the overall guidance of Professor J.B. Mander. This thesis was supervised by Professor J.B. Mander and Dr. R. Dhakal. I also wish to acknowledge the contribution and motivation in the early stages of the work by the late Emeritus Professor Robert Park. Their constructive and patient advice and guidance are gratefully acknowledged. I would like to express my gratitude to Dr. J. Mackechnie for his kind instruction on concrete design and practice. Financial support for the experimental portion of the work under the FRST funded “Future Building” project is also gratefully acknowledged.

Testing of the column specimens was undertaken with the assistance of technicians J. Maley and R. Newton of the Department of Civil Engineering Structural Laboratory. Their strong support is gratefully acknowledged.

I would like to specially recognize the contributions from fellow ME student Tony Rahardjo who assisted me in constructing the test specimens. Without his help this part of the project would not have been possible. The theoretical development part of Chapter 2 of this thesis was a joint effort with Mr. Rahardjo.

Above all, I wish to thank my wife Aki and my parents for their encouragement and support during the two years of work.

Finally, I gratefully acknowledge the Metropolitan Expressway Public Corporation and the Express Highway Research Foundation in Tokyo Japan, for giving me this precious opportunity and extensive support.

1 INTRODUCTION

1.1 Research Objective

Highway Bridge has very important roles when severe earthquake has happened. The transportation system must be kept their serviceability to recover the damage at a site. After devastating earthquake such as Northridge in 1994 and Kobe in 1995, performance-based earthquake engineering has been proposed, but the practical Seismic Risk Assessment (SRA) methodology to assess the performance of the structures correctly has not been established.

The strong interest to compare each design code such as New Zealand, Japan and Caltrans has also been grown up. Each code has similar design procedures but different values at a certain design step. Therefore, the dimensions and the quantity of the reinforcing bars varied considerably, even if the structures are designed under the common conditions.

Conventional bridge piers are applied to the ductile design which allows the irreparable damage at plastic hinge zone (PHZ) after the severe earthquake. The damage at the PHZ makes it difficult to keep the same service after the earthquake. The Damage Avoidance Design philosophy is established very lately but the seismic performance under the bi-directional earthquake motions.

In this study the proposed new SRA methodology are first developed from a theoretical perspective, and then verified through dynamic analysis and experimentation. Furthermore the DAD bridge pier are explored experimentally and compared to the conventional bridge pier.

1.2 Literature Review and Previous Study

1.2.1 Design Codes

Against the background of the strong interest in comparing seismic design codes for highway bridge piers, design codes from three areas of the world were discussed at an international seminar held in Tokyo in April 1999 entitled “Comparative Performance of Seismic Design Codes for Concrete Structures”. Researchers and the structural engineers representing the three codes by Tanabe et al (1999), and trial design of bridge piers was then carried out by Japanese Society of Civil Engineers (JSCE) members using these codes. The selected three countries are New Zealand, Japan and the USA whose design codes are recognized to be most advanced in the entire world. The design procedures of each design code basically follow the flow chart shown in Figure 1-1. The design force applied to the structure in each code is also determined by the same procedure; however, the factor, which contributes to the design forces, vary considerably due to different seismic experiences based on different earthquake mechanisms and the different properties of the soil. The main factors affecting design forces are the design acceleration spectra curves and the possible effect of a transverse earthquake on all the factors. A summary of the special features in each design code are described in below.

New Zealand

The seismic design of bridge piers in New Zealand is mainly carried out following *Bridge Manual* with reference to *New Zealand Standard (NZS) 3101* for concrete structures and *NZS 4203* for earthquake loadings.

The seismic coefficient can be calculated by the equation below,

$$K_h = Z \cdot R \cdot S_p \cdot K_{h0}$$

where, Z: zone coefficient
 R: risk coefficient
 S_p: Structure coefficient

The specific features in the New Zealand design code are listed below:

1. Adoption of inelastic response spectrum
2. Addition of vertical earthquake influence
3. Addition of transverse earthquake influence

The seismic coefficient, K_h , can be obtained from the inelastic acceleration spectra, shown in Figure 1-2, appropriate to the site subsoil categories. The acceleration spectra curves are drawn for a range of values of the displacement ductility factor μ . The vertical earthquake loading effect is considered when the flexural and shear strengths are assessed. How the effect of vertical EQ force is that two varieties of the cases, the 0.8 and 1.3 times larger axial (vertical) load is applied to the pier, are taken into consideration, then, the severe case (smaller flexural and shear strength) are chosen from two cases. Also, 30% of the longitudinal earthquake force is added into the longitudinal direction with consideration of the transverse earthquake effect.

Japan

The Japanese bridge pier followed the *Standard Specification for Design and Construction of Concrete Structure*, published by JSCE. The acceleration response spectra curve was chosen from *Design specifications for highway bridges*, prescribed by the Japan Road Association (JRA) because there are no curves mentioned in the

JSCE codes book. The seismic coefficient, K_h , can be calculated considering the ductility factor as described below

$$K_h = \frac{K_{h0}}{\sqrt{2\mu_d - 1}}$$

where K_{h0} : Spectral Acceleration

μ_d : Design Ductility Factor

This code has two special features: verification of failure mode and verification of ductility. The devastating shear failures of bridge piers, which are not acceptable, in the Kobe earthquake showed how important it is to keep enough shear strength. The failure modes are assessed so that the shear strength has to exceed the bending strength of the members. The ductility verification can be satisfied if the ratio of bending strength to shear strength is equal to or larger than 2, which corresponds to the ductility factor = 10 approximately. Otherwise, the equation below is applied to check whether the ductility calculated is larger than design ductility or not:

$$\mu = \{ \mu_0 + (1 - \mu_0)(\sigma_0 / \sigma_b) \} / \gamma_b$$

$$\text{where, } \mu_0 = 12 \times (0.5 \times V_{cd} + V_{sd}) / V_{mu} - 3$$

The design spectra are shown in Figure 1-3.

Caltrans

The codes mainly followed are *Bridge Design Specification (BDS)* and *The Improved Seismic Design Criteria for California Bridges (ATC32)*. The seismic coefficient, K_h , can be calculated by the equation below, and the acceleration spectra curve to obtain the value, K_{h0} , is shown in Figure 1-4 (a).

$$K_h = \frac{K_{h0}}{Z}$$

where, Z : reduction coefficient

This code has two special features: consideration of transverse earthquake effect and force-reduction coefficient, Z. When determining the lateral seismic force, it is multiplied by 40% because of the transverse earthquake consideration. On the other hand, the New Zealand code takes into consideration a 4% increase as the transverse earthquake and the Japanese code does not consider this bi-directional earthquake effect. The force reduction factor, Z, is determined assuming the characteristic ground motion period corresponding to the peak of the input energy spectrum. The force reduction coefficient, Z, is obtained from the figure shown in Figure 1-4 (b).

1.2.2 Bridge Pier Design in the previous study in 1999

In this section, the results of the three prototype bridge design results by the international committee organized by the Japanese Society of Civil Engineers, Tanabe (1999), are summarized.

Common design conditions for the three piers were set to keep fair comparisons among the three specimens. The Peak Ground Acceleration (PGA) for the input Earthquake and the soil condition were decided at 0.4g (approximately 4m/sec²), which is equivalent to the 1g (9.8m/sec²) elastic response acceleration, and stiff ground, consisting of rock or firm subsoil, respectively. In addition, the heights of the piers, H (defined to be the distance from the bottom of a pier to the level at which the horizontal seismic force is assumed to act on the superstructure), were chosen as 7.0m. The weight of the superstructure was assumed to be 7,000kN,

based on the existing normal highway bridge which has a 40m span and a 10m width. The summarized common conditions are listed in Table 1-1 and described in Figure 1-5.

The seismic coefficient values in accordance with the natural period of each bridge pier are described in Figure 1-4. The design results of the previous study are listed in Table 1-2 and the section dimensions are shown in Figure 1-6. The New Zealand pier has the smallest cross section (1.5*1.5m) area because the New Zealand designer carried out the design under the basic conception of maximizing the pier natural period and minimizing the design seismic coefficient by determining that the pier should have a small cross sectional area and a low reinforcement ratio. The Japanese and USA cross sections were larger than that of New Zealand. One reason for the Japanese pier being larger was that the Japanese response spectra curve has a long plateau between 0.3 and 0.7sec with 1.0g (maximum value) which keeps the seismic coefficient higher. On the other hand, the main reason for making the USA cross section larger was the transverse earthquake load effect, which made the design moment required larger by 40%.

1.2.3 Damage Avoidance Design (DAD)

Even after a big earthquake, highway bridges must keep providing the serviceability for emergency vehicles. However, the current conventional seismic designs allow damage induction around the plastic hinge region and this leads to permanent lateral deformation which may interrupt the smooth transport of emergency service vehicles in the aftermath of an after earthquake in that area. As long as the ductile design philosophy is remained, irreparable damage to structures is inevitable. After the Kobe earthquake in 1995, the bridge engineers used the index to determine whether the bridge pier would be rebuilt or repaired by measuring the

residual deformation. Then, if the index measured value was less than approximately 15cm or 1/60 drift, then the bridge piers were judged to be repaired. From this experience learnt from Kobe Earthquake, the seismic design code for the highway bridge in Japan described in Japanese design code, “*Specification of Highway Bridge*” (2002) proposed a clear regulation to keep the residual drift within 1/100 (1%) drift. The concept of Damage Avoidance Design (DAD) was developed in the early 60s by Housner (1963). Two state-of-the-practice examples of rocking structures may be found in New Zealand: the South Rangitikei Railway Bridge, and an industrial chimney at the Christchurch Airport.

Further exploration by Mander and Cheng (1997) established the DAD principle. The DAD pier is constructed separately from the foundation, and sits on the foundation through the two solid steel interface plates at both ends of the pier and foundation to avoid any damage around the interface due to the contact during the seismic event. Several experimental studies by Mander and Cheng (1997) were carried out to investigate the seismic capacity of the DAD piers designed on this principle and no damages and no residual drifts were found throughout the tests even though the maximum 8.2% drift had been applied. However, these tests were carried out in one direction of loading. In a real situation, bridge piers could be subjected to multi-directional earthquake forces; therefore, the simultaneous bi-directional loading test is necessary for the DAD pier to make sure the validity of the DAD pier even under bi-directional seismic event.

1.2.4 Pseudodynamic (PD) Test

The Pseudodynamic (PD) test is a strong and efficient tool exposing the seismic performance behaviours of structures during the real earthquake since it is

organized by combining the advantages of both experimental and the dynamic analytical approaches.

Several experimental methods have been developed so far to assess the seismic capacity of the RC structures properly. The characters of the conventional three varieties of the tests are summarized in Table 1-3. The Cyclic Loading (CL) Test is the most common and reasonable method from the facility cost point of view, which can provide the fundamental seismic data of the structures associated with the pre-decided displacement path such as the clover leaf type path. The tests require only hand jacks and a strong floor or wall, which is available at most of the institutions, and no additional equipment is usually required. The results obtained would be the fundamental aspect of structural seismic capacity, such as the ductility or strength degrades, under an ideal symmetric displacement path. The Shaking Table (ST) Test may be most ideal and closest test method to a real earthquake situation. The specimens are set on a table controlled by high speed hydraulic actuators and the exactly same acceleration for the EQ records can be applied. However, the dimension of the specimens is usually limited, due to the hydraulic actuator's capacity to maintain the proper acceleration in the whole test procedure. Also, the top weight for the gravity load and the amplitude and time step of input earthquake must be calculated carefully following the similarity law.

The Pseudodynamic (PD) test method was developed about 30 years ago by Takanashi et al. (1975) and is thought to be the most efficient and powerful alternative to both STT method and dynamic analytical method, especially when the real response behaviours, such as the damage state during and after a certain earthquake are need to be investigated.

On the other hand, considerable number of the dynamic analysis programs running on conventional personal computers has been developed recently and the accuracy and reliability of the results improved as the new theories are applied to them. Also, the cost of running the computer becomes cheaper. Considering these background, the dynamic analysis is strong and reasonable tool for the seismic research except that the dynamic analysis method is needed to assume the simplified model for the properties of structures such as the lateral load and displacement relationship and hysteresis damping factors. On the contrary, the PD test does not need to assume the property of the structures because these properties can be obtained from the experimental specimens directly except for the intrinsic damping factors. Therefore, the more reliable results can be obtained than in the ordinary dynamic analytical method. The comparison between the PD test and Dynamic Time History Analysis are summarized in Table 1-4.

1.2.5 Bi-directional Loading Effect

The earthquake forces are applied to the structure from various directions randomly and simultaneously in the real event. However, in the typical seismic design procedure, only one (longitudinal or transverse) directional force is applied to the structures. According to the different contexts of each design code, there are different ways of considering this effect, as summarized in Table 1-5. This range of consideration indicates that no one uniform theory has yet been established and it is necessary to develop such a theory. Mutsuyoshi (1994) established the bi-directional Pseudo Dynamic (PSD) test to clarify the effect of simultaneous bi-directional earthquake forces. The test results show obviously that the lateral load capacity in one direction decreases considerably in accordance with the interaction by the displacement progress in the orthogonal direction. It was also confirmed by

Hayakawa and Kawashima (2003) that the measured ultimate displacement when the pier was collapsed was smaller than that of the unidirectional test due to the same interaction effect as that of the decrease of the lateral load capacity. These interaction effects cannot be explained by the extra force addition to the principal direction, for example, 40% extra load is applied to one main direction in the USA code. Before the Northridge and Kobe earthquake in 1994 and 1995 respectively, the insoluble phenomena had been simply taken into consideration as the additional multiplied safety factor. Since then, however, the newly established theories have been actively adopted. Judging from these trends, the further research on this bi-directional interaction effect is necessary to achieve the aim of design code revision.

1.3 Scope of this thesis

Following this introductory section, chapter 2 presents a seismic risk analysis methodology. The purpose of this development is to select ground motions that are irrelevant for experimental investigations. This is become in destructive model tests there is only one opportunity to correctly identify performance modes and general behaviour attributes. Therefore it is imperative that such a test be tried back into a risk base context where a level of confidence can be expressed in the outcome.

Chapter 3 presents an experimental investigation where the seismic performance of three bridge piers designed to New Zealand, Japan and Caltrans specifications. Damage states following DBE and MCE are investigated.

Chapter 4 presents an alternative views on how bridge is used to develop and constructed. Damage Avoidance Design is used to develop an experimental specimen. The base of the bridge pier is “Damage Protected” by using armoured details along with energy dissipators. The test results are compared with the companion New Zealand designed specimen described in Chapter 3. Finally, Chapter 5 presents a

summary of this research and the principal conclusions. Recommendations for future research as an outcome of this work are also given.

1.4 What then is particularly new in this thesis

As mentioned previously, this research explores the use of a newly developed Seismic Risk Assessment (SRA) methodology. This proposed methodology can be applied Performance-Based Earthquake Engineering as a tool to estimate the damage outcome corresponding to a certain level of an earthquake. Furthermore, this methodology makes it possible to select a critical input earthquake motion for a one-off experimental test.

The three bridge piers designed following to New Zealand, Japan and Caltrans experimentally explored. The seismic performances of the bridge are examined by a way of bi-directional Pseudodynamic (PD) test method under the same earthquake input. The validity of SRA methodology is examined with the results of these tests.

The Damage Avoidance Design bridge pier is also explored using bi-directional PD test. As the longitudinal reinforcing bars are disconnected and boundary of between the column and the base are armoured by thick steel plates, the bridge pier can avoid the damage.

1.5 References

- Hayakawa R., Kawashima K., and Watanabe G., 2003, Effect of Bilateral Loadings on the Flexural Strength and Ductility of Reinforced Concrete Bridge Piers, *Japan Society of Civil Engineers Journal of Earthquake Engineering*, Vol 27, pp1-4 (in Japanese).
- Housner G.W., 1963, *The Behavior of Inverted Pendulum Structures During Earthquake*, Bulletin of the Seismological Society of America, Vol. 53, No. 3, pp. 403-417
- Japan Road Association, 2002, *Specification of the Highway Bridge*, Vol. V, Seismic Design, Japan
- Mander J.B., Cheng C-T., 1997, *Seismic Resistance of Bridge Piers Based on Damage Avoidance Design*, National centre for Earthquake Engineering research, Technical Report NCEER-97-0014, December 10
- Mutsuyoshi H., and Machida A., Tanzo W., and Mashiko N., 1994, Inelastic Seismic Response Behaviour of RC Bridge Pier Using Pseudo-Dynamic Test Method, *Transactions of the Japan Concrete Institute*, Vol. 16., pp265-272
- Takanashi K., Udagawa M., Seki M., Okada T., and Tanaka H., 1975, Nonlinear earthquake response analysis of structures by a computer-actuator on-line system, *Bulletin of Earthquake Resistant Structure Research Centre 8 Institute of Industrial Science*, University of Tokyo, Tokyo, Japan.
- Tanabe T, 1999, *Comparative Performance of Seismic Design codes for Concrete Structures*, Vol. 1, Elsevier, New York

1.6 Tables for Chapter 1

Table 1-1: Common conditions for the bridge pier designs studied in 1999

Height	Weight of Superstructure	PGA	Soil Condition
m	kN	gal	
7.0	7,000	400	Very stiff

Table 1-2 Prototype bridge pier design properties studied in 1999

Contents	Code	Unit	New Zealand	Japan	Caltrans
Natural Period	T	sec	0.852	0.57	0.546
Diameter	D	mm	1500	1800	1800
PHZ	PHZ	mm	1500	3600	2700
$P/A_g f'_c$ ($f'_c=24\text{MPa}$)			0.15	0.11	0.11
Main Bar			40-D32	40-D51	64-D35
($f_y=345\text{MPa}$)	ρ_t	%	1.43	2.52	1.90
Spiral at PHZ			8-D13@180	4D19@150	2D19@150
($f_y=345\text{MPa}$)	ρ_s	%	0.47	0.47	0.74

Table 1-3 The Conventional Experimental Test Methods

Type of Tests	Pros	Cons
CLT	Simple facility is required Can get comparable data to other tests	Not representative of real earthquake situation
STT	Similar to reality	Hard to follow the sequences Need consideration of scale effect
PD	Simple facility is required Can get real behaviour	Need to establish the online control system Need proper damping assumptions

Table 1-4 The Dynamic Time History Analysis Methods vs PSD Test

Types	Pros	Cons
Computer Analysis	Low cost recently Can analyse lots of cases	Need simplified structural properties and model Need verification with experimental results
PD	Can observe the sequential damage events	In accuracy of viscous damping factor

Table 1-5 The way of considerations for the bi-directional earthquake interaction

Country	New Zealand	Japan	U.S	Europe
Code	Bridge Manual 3.4 and 5.2.2	JSCE	Caltrans 3.21.9.2	EC8/2-4.2.1.4
Design consideration	100% of effects in one direction and 30% of effects in the orthogonal direction are taken into account based on a square root of sum of square method	Design the longitudinal and transverse direction separately	Longitudinal loading is combined with 40% of the corresponding actions from the transverse direction	Design ground acceleration is increased 1.3 times the original one
Equations	$V_d = \sqrt{V^2 + (0.3V)^2}$	N/A	$V_d = V + 0.4V$	$a_g = 1.3a_g$

1.7 Figures for Chapter 1

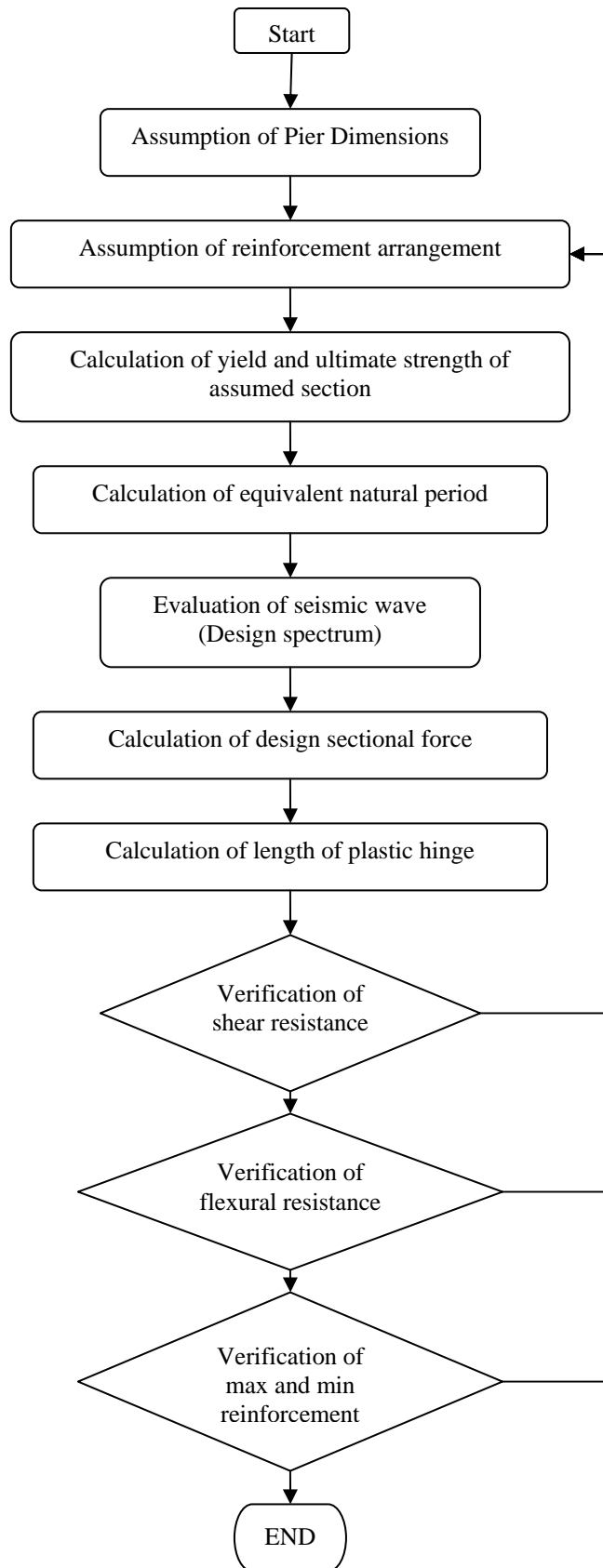


Figure 1-1 The flow chart of seismic design procedures

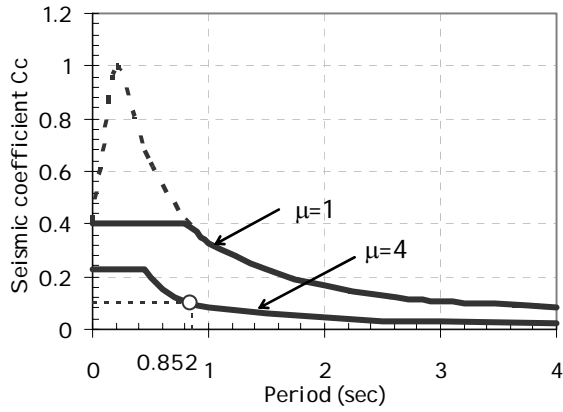


Figure 1-2: Design Spectra for New Zealand Code ($\mu = 4$)

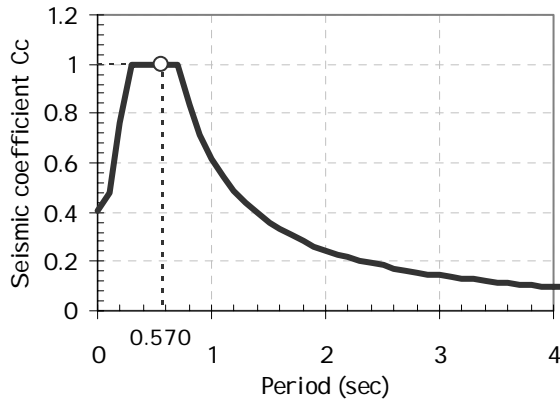
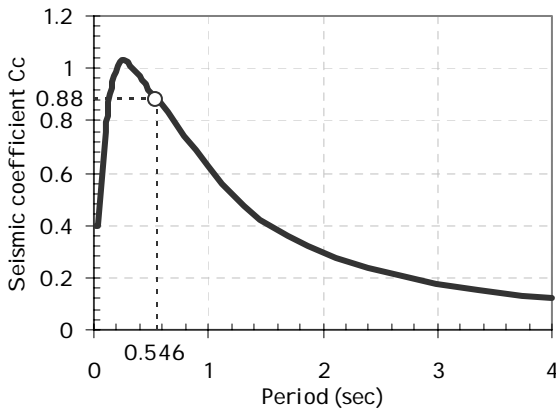
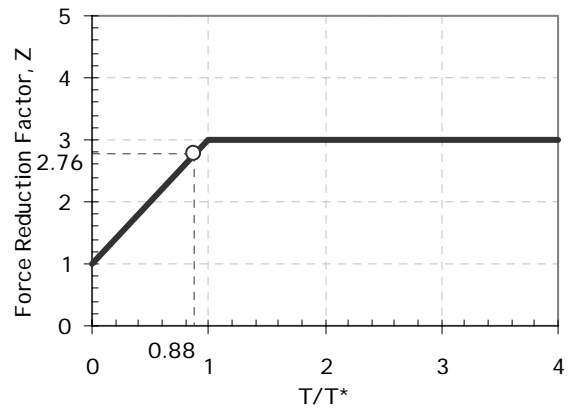


Figure 1-3 The response acceleration spectra of Japanese code



(a) Design Acceleration Spectra



(b) Force Reduction Factor

Figure 1-4 Design acceleration spectra and Force Reduction Factor for Caltrans

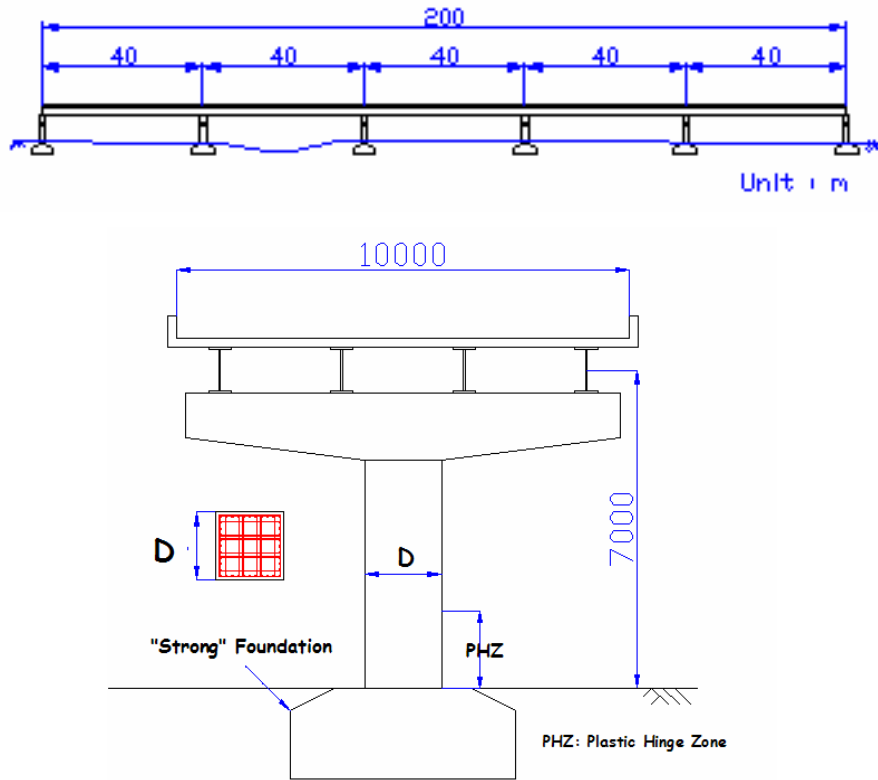


Figure 1-5: The prototype bridge view and bridge pier

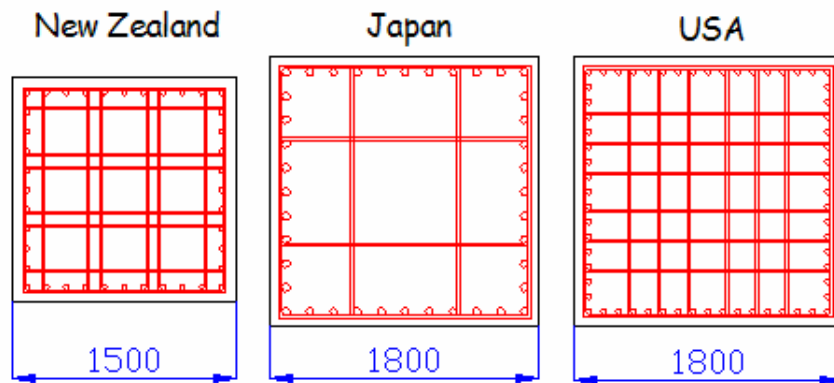


Figure 1-6 Cross Section Dimensions of the Bridge Piers

2 INCREMENTAL DYNAMIC ANALYSIS APPLIED TO SEISMIC RISK ASSESSMENT OF BRIDGES

Summary

Incremental Dynamic Analysis (IDA) is applied in a Performance-Based Earthquake Engineering context to identify critical earthquake ground motions that are subsequently to be used in physical testing or analytical studies to investigate structural response and damage outcomes. This quantitative risk analysis procedure consists of: choosing a suitable suite of ground motions and appropriate intensity measures; performing IDA on a nonlinear model of the prototype structure; summarizing the IDA results and parameterizing them into 10th, 50th, and 90th percentile performance bounds; integrating these results with respect to hazard intensity recurrence relations; and identifying the strength of two or three critical earthquakes that will potentially encompass all damage states through to collapse. An illustrative example of the procedure is given for reinforced concrete highway bridge piers, designed to New Zealand, Japan and Caltrans specifications.

2.1 Introduction

Performance Based Earthquake Engineering (PBEE) procedures require the prediction of the seismic capacity of structures which is then compared to the local seismic demand. The interrelationship between the two gives an inference of the expected level of damage for a given level of ground shaking. Incremental Dynamic Analysis (IDA) is a new methodology which can give a clear indication of the relationship between the seismic capacity and the demand. Engineers can estimate principal response quantities, such as the maximum drift of the structure for a given intensity measure (IM) such as peak ground or spectral acceleration.

The need to identify a critical earthquake for the purpose of an experimental investigation or further advanced analysis and design can be accommodated by the application of IDA. A synthesis of IDA curves into 10th, 50th, and 90th percentile bounds helps the designer to single out critical ground motions which can then be used in physical testing or advanced analysis to investigate structural damage with a certain level of confidence.

This chapter first considers reviews the evolution of the principal ideas that have lead to IDA, and then goes on to develop the IDA process specifically for bridge structures. What is new here is the way in which IDA results are quantitatively modelled and then integrated into a probabilistic risk analysis procedure whereby the seismic intensity-recurrence relationship (the seismic demand) is viewed with respect to the damage propensity of a specific bridge structure (structural capacity). Confidence intervals and damage outcomes for given hazard intensity levels, such as the Design Basis Earthquake (DBE) or a Maximum Considered Earthquake (MCE) earthquake, can be evaluated.

2.2 Findings from Previous Research

Cornell et al (2002) proposed that given a spectral acceleration (S_a), it was possible to predict a drift demand, (D') by:

$$D' = a(S_a)^b \quad (2-1)$$

where a = a coefficient determined by non-linear time history analyses and b is an exponent.

Luco and Cornell (2000) showed that for moment frames a value of $b=1$ should suffice. This is in keeping with Newmark's well-known equal displacement principle. It suggests that for moderate period structures (without major strength degradation) the inelastic displacement demands are similar to the demands imposed on a linear structure with no bounds on when collapse may be imminent.

Lee and Foutch (2002) compared the difference between the median responses and both the 84th and 95th percentile values. With respect to the median response, their results showed a multiplier between 1.5 and 2 for the 84th percentile and a multiplier greater than 2.0 for the 95th percentile values. This result is consistent with the findings of Martinez (2002) who found that similar variability of results from some 20 earthquake ground motions scaled so that they each had a one-second spectral acceleration of $S_a(T=1 \text{ sec}) = 1g$. This variability explains the distribution curves that show the spread of results away from the median values.

In order to investigate the likely seismic performance of multi-storey precast concrete buildings, Matthews (2004) adopted the method given by Equation (2-1). Then based on analysis he derived a protocol for super-assembly specimen testing that was a physical representation of a family of typical prototype precast concrete buildings. Matthews (2004) carried out his study on 3, 6, 9, and 12 storey precast concrete structures, and from these studies fragility curves were developed and DBE

and MCE drift demands were assessed for New Zealand seismicity. Matthews (2004) found that for New Zealand designed precast concrete buildings the ratio of drift demand for the 2% in 50 years MCE to the 10% in 50 years DBE is about 1.8. He showed that between a suite of some 50 earthquakes response outcomes were lognormally distributed with a log normal coefficient of seismic demand of $\beta_D=0.55$.

In order to estimate structural performance under seismic loads, Vamvatsikos and Cornell (2004) presented a procedure called “Incremental Dynamic Analysis (IDA)”. This approach involves performing nonlinear dynamic analyses of a prototype structural system under a suite of ground motion records, each scaled to several intensity levels designed to force the structure all the way from elastic response to final global dynamic instability (collapse). From IDA curves, limit states can be defined. The probability of exceeding a specified limit state for a given intensity level can also be found. Furthermore, the final results of IDA are in a suitable format to be conveniently integrated with a conventional seismic hazard curve in order to calculate mean annual frequency of exceeding a certain limit-state capacity.

2.3 Quantitative Risk Assessment

2.3.1 Step 1: Select ground motion records and modelling the structure

In order to perform IDA, a suite of ground motion records are needed. In their previous study, Vamvatsikos and Cornell (2004) used 20 ground motion records to analyse mid-rise buildings in order to provide sufficient accuracy of seismic demands. The same ground motions were adopted for this study and are presented in Table 2-1. These earthquakes have Richter magnitudes in the range of 6.5-6.9 with moderate epicentral distances mostly in the range of 16 to 32 km; all these ground motions were recorded on firm soil. Figure 2-1 (a) shows response spectra for each of the 20

earthquake ground motions scaled to the same IM that is a PGA of 0.4g. A significant degree of variability is evident with respect to the median spectral curve. Figure 2-1 (b) presents a plot of the lognormal coefficient of variation (β_D), sometimes referred to as the dispersion, across the spectrum. For this suite of earthquakes it is evident that the PGA serves as an appropriate IM, provided that the period is less than about 1.6 seconds.

A nonlinear computational model of the prototype structural system should then be developed. A check should be made that the dispersion of response demand (β_D) in the neighbourhood of the natural period is reasonable. If the dispersion is excessive, then an alternative IM should be considered and this step should be repeated until the dispersion is reasonable.

2.3.2 Step 2: Perform Incremental Dynamic Analysis

Once the model and the ground motion records have been chosen, IDA is performed. To start the analysis, the earthquake record chosen has to be scaled from a low IM to several higher IM levels until structural collapse occurs.

For each increment of IM, a nonlinear dynamic time history analysis is performed. Analyses are repeated for higher IM's until structural collapse occurs. Locating the maximum drift observed in an analysis gives one point in the PGA versus maximum drift plot domain. As shown in Figure 2-2 (a), connecting such points obtained from all the analyses using an earthquake record with different IM's gives the IDA curve for that individual earthquake. This process is then repeated for all earthquakes in the suite, as is illustrated in the left side of Figure 2-2 (b). It may also be of interest to analyse the variability of the response outcomes for a given level of IM. Results typically show a lognormal distribution of drift (displacement) outcomes. The

lognormal Coefficient of Variation (β) is then plotted as shown in the right side of Figure 2-2 (b).

2.3.3 Step 3: Model the IDA curve and statistical outcomes

In their previous study, Vamvatsikos and Cornell (2004) modelled their IDA curves by using multiple interpolation spline functions. It is considered that such an approximation is cumbersome and not particularly useful for subsequent analysis. Therefore, in this study several single functional relations were explored, and the Ramberg-Osgood equation (R-O), Park and Paulay (1975) was adopted as the most suitable. The R-O relation is given by:

$$\theta = \frac{S_a}{K} \left(1 + \left| \frac{S_a}{S_c} \right|^{r-1} \right) \quad (2-2a)$$

in which θ = drift; K = the initial slope of the IDA curve in initial proportional range; S_c = “critical” earthquake acceleration that occurs at the onset of large drifts that subsequently lead to collapse; S_a = earthquake acceleration; and r = constant.

The R-O equation can also be written in the form

$$\frac{\theta}{\theta_c} = \frac{S_a}{S_c} + \left(\frac{S_a}{S_c} \right)^r \quad (2-2b)$$

where $\theta_c = S_c / K$ is a “critical” drift.

The significance of the three required control parameters (S_c , r , and either θ_c or K) may be examined in Figure 2-3 (a). As the value of the constant r increases the curve tends toward a bilinear case (when $r \rightarrow \infty$). If the input IM is greater than the “critical” value (i.e. $S_a > S_c$) then the response is such that $\theta > 2\theta_c$ and structural instability (collapse) is imminent.

In Equation (2-2) the three control parameters (S_c , r , and either θ_c or K) are estimated using nonlinear least squares analysis for each individual earthquake ground

motion IDA data set. Figure 2-3 (b) illustrates the fit between the IDA data points and the fitted R-O curve for one specific case.

Although the results for each of the control parameters are different, they can then be examined collectively and a statistical analysis on the parameters can be performed. Studies show that the parameters are lognormally distributed. Therefore by ascertaining median values of each parameter the 50th percentile IDA response can be represented by an individual R-O median curve. Likewise by examining variability of individual IDA distributions, parameters that represent curves of other bounds of interest, such as the 10th and 90th percentiles may be found. Figure 2-3 (c) illustrates the fitted IDA curves for the suite of 20 earthquakes along with the 10th, 50th and 90th percentile response demand.

2.3.4 Step 4: Assign damage limit states

Once the three (10th, 50th and 90th percentile) lines have been generated, it is possible to determine the expected drift for an earthquake with a certain level of the intensity. Emerging international best practice for seismic design is tending to adopt a dual level intensity approach that is (i) a DBE represented by a 10% in 50 years ground motion; and (ii) a MCE represented by a 2% in 50 years earthquake.

Several damage limit-states can be defined on the IDA curves developed. In their previous research, Vamvatsikos and Cornell (2004) applied building use criteria of Immediate Occupancy (IO) and Collapse Prevention (CP) limit-states to their IDA curves based on building use criteria. In this study, the definitions of damage limit states were extended by adopting Mander and Basoz (1999) definitions of damage states for bridges, as listed in Table 2-3. Two damage states can be easily defined as follows.

DS=1 is for elastic behaviour, it therefore concludes at the onset of damage which is best defined at the yield drift (displacement) of the structure. Also, DS=5 commences at the onset of collapse, and as described above this is best defined when $\theta > 2\theta_c$.

The other damage stages (DS=2, 3, and 4) are more subjective in their definition. It is suggested that the boundary separating DS=3 and DS=4 be defined at that level of drift where the structure would be deemed to have suffered irreparable damage such that the structure would likely be abandoned; as evidenced by: (i) excessive permanent drift at the end of the earthquake; (ii) severe damage to critical elements such as buckling of longitudinal reinforcing bars or the fracture of transverse hoops and/or longitudinal reinforcing bars.

Finally, the boundary separating DS=2 and DS=3 should be defined as that level of damage that would necessitate temporary loss of function due to repairs that need to be undertaken for reinforced concrete structures, this usually occurs when spalling of cover concrete is evident. This displacement can also be found by analysis when the cover concrete compression strain exceeds the spalling strain at say $\varepsilon_{spall}=0.008$ at drifts below this boundary (i.e., DS=2) damage is considered to be slight and tolerable. The result of assigning damage states to the IDA fractile curves is illustrated in Figure 2-4.

2.3.5 Step 5: Hazard–Recurrence Risk Relation

A return period dependant scale factor λ_T such that $S_a^{(T=Tr)} = \lambda S_a^{(T=475yrs)}$ is required to scale spectra to required return periods (or annual probabilities), as required for the serviceability limit state and for various combinations of structural importance level and reference return period of 475 years. Values for the return period factor have been derived by drawing a representative line through the hazard curves

(PGA as a function of a return period) for various structural periods as illustrated in Figure 2-5. This curve is given by:

$$S_a^{(T=Tr)} = \lambda_T S_a^{(T=475)} = S_a^{(T=475)} \left(\frac{Tr}{475} \right)^q = \frac{S_a^{(T=475)}}{(475 p_a)^q} \quad (2-3)$$

in which $S_a^{(T=Tr)}$ = PGA relevant to its return period ; $S_a^{(T=475)}$ PGA at a return period of 475 years (10 percent probability in 50 years); Tr = return period; p_a = annual probability ($p_a=1/Tr$); and q = an exponent based on local seismic hazard-recurrence relations. The values of q for the design codes of New Zealand, Japan and Caltrans are determined to be 0.333, 0.418 and 0.29 respectively according to the data in each design code.

2.3.6 Step 6: Risk modelling and accounting for uncertainty

From the IDA curves developed, the curves can be modified more elegantly by substituting hazard curves based on Equation (2-3) into Equation (2-2) as given by:

$$\theta = \frac{S_a^{(T=475)}}{K(475 p_a)^q} \left(1 + \left| \frac{S_a^{(T=475)}}{S_c (475 p_a)^q} \right|^{r-1} \right) \quad (2-4a)$$

Or

$$\frac{\theta}{\theta_c} = \frac{S_a^{(T=475)}}{S_c (475 p_a)^q} + \left(\frac{S_a^{(T=475)}}{S_c (475 p_a)^q} \right)^r \quad (2-4b)$$

Note that the parameters S_c , θ_c , and r are dependent on confidence interval. According to Martinez (2002), who found an appropriate closed form of the cumulative lognormal probability density function, the confidence can be estimated from:

$$CI_{\%} = \frac{100}{1 + \left(\frac{x_{CI}}{\tilde{x}} \right)^{1.8/\beta_{CI,D}}} \quad (2-5)$$

where $\beta_{C/D}$ = composite lognormal coefficient of variation; and \tilde{x} = median of the distribution of variable x . Using this expression the value of the parameter $x(CI)$ for a given confidence interval CI can be estimated from

$$x(CI) = x(CI = 50\%) \left[\frac{100}{CI} - 1 \right]^{0.55\beta_{C/D}} \quad (2-6)$$

The integrated curves presented graphically in Figure 2-6 can be used to estimate the annual probability of exceeding the limit-state.

An example of the resulting integrated risk curves is presented graphically in Figure 2-6 (a). It can be used to estimate the annual probability of exceeding a given damage state with a certain degree of confidence.

In the foregoing analysis it must be emphasised that the resulting variability in response results entirely from the randomness of the input motion that is the seismic demand. This is because the computational modelling is conducted using crisp input data. However, the structural resistance both in terms of strength and displacement capacity is also inherently variable. Moreover, the computational modelling, although it may be sophisticated, is not exact; there is a measure of uncertainty that exists between the predicted and the observed response.

To encompass the randomness of seismic demand along with the inherent randomness of the structural capacity and the uncertainty due to inexactness of the computational modelling it is necessary to use an integrated approach as suggested by Kennedy et al (1980). The composite value of the lognormal distribution can be expressed as

$$\beta_{C/D} = \sqrt{\beta_C^2 + \beta_D^2 + \beta_U^2} \quad (2-5)$$

in which β_C = coefficient of variation for the capacity; β_D = coefficient of variation for the demand = 0.25 (assumed in this study); and β_U = lognormal dispersion parameter for modelling uncertainty = 0.2 (assumed in this study).

The hazard recurrence curves including the uncertainty from the computational modelling can be seen as the dotted line with $\beta_{C/D} = \sqrt{0.38^2 + 0.2^2 + 0.25^2} = 0.5$ in Figure 2-6 (a). For detailed assessment, additional confidence intervals can also be plotted with the 95th, 80th, 70th and 60th percentile curves as shown in Figure 2-6 (b).

2.4 Identifying Critical Earthquake Ground Motion

When carrying out physical tests using actual earthquake records to experimentally explore damage outcomes, one is faced with the dilemma of choosing what earthquake should be adopted from a suite of eligible candidate records. Results from the foregoing IDA analysis along with the desired experimental outcomes can be used as a basis for choosing appropriate earthquakes. To be roughly 90% confident about the experimental outcomes, one should closely examine the earthquake records that fall within the 85 to 95 percentile range as potential candidates that will lead to critical performance. These candidate records can be identified from IDA results at the IM level necessary to obtain a desired damage outcome. First, it is suggested that the IM level that coincides with the DBE be chosen. Secondly, the IM level at the MCE (2% in 50 years) is used as a basis for final destructive testing. The critical earthquakes at the DBE and MCE levels may not necessarily be the same.

Once several earthquakes in the 85 to 95 percentile range have been identified, then dynamic analyses should be conducted to examine and compare the resulting time history responses. Factors other than displacement or drift that might influence failure should also be evaluated and compared. Amongst other things these might include:

- Cyclic loading effects that could potentially lead to low cycle fatigue.
- Amplifications of overturning (rocking) effects by large axial load and secondary P- Δ moments.
- Amplification of pier moments arising from higher mode effects.
- Bidirectional and torsional motion response.

2.5 Case Study of Bridge Piers

In this section, an IDA example applied to PBEE is presented. The risk assessment based on the IDA procedure for three piers is performed. Also, the three critical earthquakes for one-off series of Pseudo Dynamic (PD) tests were selected.

The three bridge piers selected for the comparative study were initially designed by Tanabe (1999) using three different seismic design codes from NZ, Japan and USA. All three piers were 7m high and were taken from a “long” multi-span highway bridge on firm soil with a 40m longitudinal span and a 10m transverse width. The weight of the super-structure reaction at each pier is assumed to be 7,000kN. The elevation view of both the whole bridge and the pier and the design parameters for the three piers is illustrated in Figure 2-7.

2.5.1 IDA Procedures

Before performing the Increment Dynamic Analysis (IDA), the three reinforced concrete circular bridge piers were modelled as the single-degree of freedom system and were analysed using Takeda hysteresis model as presented in Figure 2-7. The dynamic time history inelastic analyses were carried out for the 20 selected earthquake records using a nonlinear structural analysis program RUAUMOKO [Carr (2003)]. The data obtained from the IDA are plotted and the dispersions for the three piers are graphically presented in Figure 2-8 (a). The 20 fitted IDA curves with the 10th, 50th and

90th percentile curves for each bridge pier are shown in Figure 2-8 (b). The five damage states based on the HAZUS damage scale were then assigned into these three curves, as shown in Figure 2-8 (c). The Hazard-Recurrence Curve in Figure 2-8 (e) are generated by combining the site-dependant hazard curves as shown in Figure 2-8 (d) and the IDA curves shown in Figure 2-8 (c).

2.5.2 Hazard-recurrence risk assessment

The more detailed hazard recurrence curves with 95th, 90th, 80th, 70th, 60th and 50th percentile curves are graphically presented in Figure 2-9 (a). From this quantitative risk analysis it is evident that for each of the three bridge designs one can be 95 percent confident of survival without collapse for a DBE with a 10 percent probability in 50 years. For a rarer event, such as an MCE that has a 2 percent probability of recurrence in 50 years, it is evident the ones confidence in the performance is substantially reduced. For the New Zealand and Caltrans designs, one can only be some 80 percent confident that the bridge will survive without collapse this implies there is a 20% chance of collapse. Moreover, for each design there is roughly a 25 percent chance that irreparable damage will occur.

Figure 2-9 (b) and (c) present respectively the IDA curves and Hazard recurrence curves plotted with two bullets obtained from the analytically predictions. The prediction analyses were conducted using EQ13 with 400 gal PGA as the DBE and EQ4 with 800gal PGA as the MCE respectively. Figure 2-9 (b) shows that DBE and MCE are close to the 90th and 50th percentile curves respectively. Therefore, the maximum drifts obtained have 90 and 50 percent confident. The analytical results show that New Zealand and Japanese bridge piers will be slightly damaged by the DBE with 90 percent confident and by the MCE 50 percent confident. Caltrans bridge pier will be damaged moderately in the DBE and MCE with 90 percent and 50 percent

confident respectively. Figure 2-9 (c) shows that the two analytical predictions are within the area between the 50th percentile and 90th percentile lines with consideration of uncertainty of computational modelling. Taking consideration of the uncertainty, the hazard recurrence curves can predict the maximum drift of the structures precisely.

2.5.3 Identifying critical earthquake ground motions

Before selection of the critical earthquakes, the dual stages of PGA corresponding to the DBE and MCE were determined. The PGA for the DBE, which has 10% probability of exceedance in 50 years (475-year mean return period), was determined to be 0.4g. The PGA for the MCE, which has 2% probability of exceedance in 50 years (2450-year mean return period), was determined to be 0.8g for typical Japanese seismicity. As shown in Figure2-10, the earthquake selection can be conducted by looking over the IDA curves of the 20 earthquakes and the three (90th, 50th and 10th percentile) fractile curves. The DBE can be any of the 20 earthquake curves, which passes through or very close to the point where the 90th percentile IDA curve and the horizontal line at 0.4g (PGA of the DBE). One such earthquake has been identified a EQ13 in Figure 2-10, that is EQ13 tended to be stronger than the 90% of all earthquakes when scaled at 0.4g PGA. The second earthquake (EQ4) serves as the MCE and it was chosen such that it passed through or was very close to the point of intersection of the 50th percentile IDA curve and the horizontal line at 0.8g (PGA of MCE). This earthquake (EQ4) represents the average strength of the all earthquakes scaled at 0.8g PGA. The third earthquake (EQ17) serves as another devastating MCE and it was chosen such that it runs very close to the 90th percentile IDA curve. This earthquake (EQ17) represents the upper-bound limit of the all earthquakes scaled at 0.8g PGA. The examples of the three critical earthquakes selected by this process are

presented in Figure 2-11 (a). The response of the New Zealand designed bridge pier for these three critical earthquakes are shown in Figure 2-11 (b).

2.6 Conclusions

This chapter has presented a study based on using IDA in the context of a quantitative seismic risk assessment. The following conclusions are drawn:

1. It is important to analyse bridge structures under high level of shaking as large displacements can occur that can lead to structural collapse. The IDA approach is a systematic method for achieving this end. It is possible to parameterise the outcomes using the Ramberg-Osgood (R-O) function. Statistical analysis of the control parameters in the R-O equation give a good indication of the level of shaking needed to cause collapse.
2. A seismic risk analysis can be developed when IDA is combined with site-dependent hazard-recurrence relations and compiled with damage indices. In this way, risk can be posed as the probability of the hazard times the consequential outcome for a given level shaking in terms of structural damage for a level of confidence in that outcome.
3. The IDA methodology can be adapted to identify critical earthquakes along with their required intensity for advanced analysis or physical testing.

2.7 REFERENCES

- Carr A.J., 2004, *RUAUMOKO: Inelastic Dynamic Computer Program*, Computer Program Library, Department of Civil Engineering, University of Canterbury, Christchurch, New Zealand.
- Cornell C.A., Jalayer F., Hamburger R.O., and Foutch D.A., 2002, *Probabilistic Basis for 2000 SAC Federal Emergency Management Agency Steel Moment Frame Guidelines*, ASCE Journal of Structural Engineering, April, pp 526-533
- Kennedy R.P., Cornell C.A., Campbell R.D., Kaplan S., and Perla H.F., 1980, *Probabilistic Seismic Safety Study of an Existing Nuclear Power Plant*, Nuclear Engineering and Design No.59, pp315-338
- Luco N., and Cornell C.A., 2000, *Effects of Connection Fractures on SMRF Seismic Drift Demands*, ASCE Journal of Structural Engineering, January, pp 127-136
- Mander J.B., and Basoz N., 1999, *Enhancement of The Highway Transportation Lifeline Module in Hazus*, Federal Emergency Management Agency
- Martinez M.E., 2002, *Performance-Based Seismic Design and Probabilistic Assessment of Reinforced Concrete Moment Resisting Frame Structures*, Master of Engineering Thesis, Department of Civil Engineering, University of Canterbury, Christchurch, New Zealand.
- Matthews J., 2004, *Investigating The Load Path of Floor Diaphragm Forces Following Severe Damaging Earthquakes*, Ph. D thesis, Department of Civil Engineering, University of Canterbury, Christchurch, New Zealand
- Montgomery D.C., and Runger G.C., 1999, *Applied Statistics and Probability for Engineers*, John Wiley, New York
- Park R., and Pauley T., 1975, *Reinforced Concrete Structures*, John Wiley, New York.
- Tanabe, T., 1999, *Comparative Performance of Seismic Design codes for Concrete Structures*, Vol. 1, Elsevier, New York.
- Vamvatsikos D., and Cornell C.A., 2004, *Applied Incremental Dynamic Analysis*, Earthquake Spectra Vol.20 No.2.

2.8 Tables for Chapter 2

Table 2-1 Selection of 20 Strong EQ Motions

No	Event	Year	Station	ϕ^{*1}	M^{*2}	R^{*3} (km)	PGA (g)
1	Loma Prieta	1989	Agnews State Hospital	90	6.9	28.2	0.159
2	Imperial Valley	1979	Plaster City	135	6.5	31.7	0.057
3	Loma Prieta	1989	Hollister Diff. Array	255	6.9	25.8	0.279
4	Loma Prieta	1989	Anderson Dam	270	6.9	21.4	0.244
5	Loma Prieta	1989	Coyote Lake Dam	285	6.5	22.3	0.179
6	Imperial Valley	1979	Cucapah	85	6.9	23.6	0.309
7	Loma Prieta	1989	Sunnyvale Colton Ave	270	6.9	28.8	0.207
8	Imperial Valley	1979	El Centro Array #13	140	6.5	21.9	0.117
9	Imperial Valley	1979	Westmoreland Fire Sta.	90	6.5	15.1	0.074
10	Loma Prieta	1989	Hollister South & Pine	0	6.9	28.8	0.371
11	Loma Prieta	1989	Sunnyvale Colton Ave	360	6.9	28.8	0.209
12	Superstition Hills	1987	Wildlife Liquefaction Array	90	6.7	24.4	0.180
13	Imperial Valley	1979	Chihuahua	282	6.5	28.7	0.254
14	Imperial Valley	1979	El Centro Array #13	230	6.5	21.9	0.139
15	Imperial Valley	1979	Westmoreland Fire Sta.	180	6.5	15.1	0.110
16	Loma Prieta	1989	WAHO	0	6.9	16.9	0.370
17	Superstition Hills	1987	Wildlife Liquefaction Array	360	6.7	24.4	0.200
18	Imperial Valley	1979	Plaster City	45	6.5	31.7	0.042
19	Loma Prieta	1989	Hollister Diff. Array	165	6.9	25.8	0.269
20	Loma Prieta	1989	WAHO	90	6.9	16.9	0.638

¹ Component, ² Moment Magnitudes, ³ Closest Distances to Fault Rupture, and Source: PEER Strong Motion Database, <http://peer.berkeley.edu/smcat/>

Table 2-2 R-O modelling and the Parameter Identification

No	New Zealand			Japan			Caltrans		
	S _c g	θ _c %	r	S _c g	θ _c %	r	S _c g	θ _c %	r
1	0.80	2.1%	25	1.05	2.1%	24	0.86	1.7%	28
2	1.80	4.3%	15	1.50	2.1%	26	1.20	1.7%	25
3	1.05	4.2%	28	0.70	2.0%	32	0.66	2.0%	27
4	1.80	4.0%	18	1.30	2.0%	29	1.22	2.1%	32
5	1.60	6.7%	15	1.10	2.2%	19	0.95	1.9%	43
6	1.20	4.4%	34	1.05	2.1%	30	0.90	2.1%	42
7	0.75	2.3%	5	0.95	2.3%	24	0.82	2.1%	45
8	0.78	2.0%	36	1.30	2.2%	27	1.05	1.9%	43
9	0.60	2.0%	9	0.80	1.6%	32	0.65	1.2%	32
10	0.70	4.7%	20	0.53	2.0%	28	0.38	1.3%	15
11	0.78	3.7%	25	1.02	1.7%	34	0.80	1.2%	36
12	0.60	2.9%	15	0.80	1.5%	14	0.65	1.3%	25
13	1.20	4.8%	24	0.80	2.3%	28	0.66	1.7%	21
14	1.40	2.5%	18	1.70	1.9%	31	1.60	1.9%	25
15	1.00	2.6%	19	1.10	1.9%	35	1.05	1.9%	36
16	3.50	5.6%	18	1.40	2.5%	31	1.24	2.4%	21
17	0.60	4.0%	25	0.65	1.6%	41	0.52	1.4%	34
18	2.10	3.8%	11	2.10	2.4%	21	1.80	2.3%	8
19	1.05	4.6%	19	0.84	2.6%	24	0.70	2.4%	30
20	3.10	5.0%	35	1.95	2.2%	17	1.60	1.9%	12
10 th	2.90	5.9%	34.8	1.83	2.5%	37.1	1.60	2.4%	46.0
50 th	1.32	3.8%	20.7	1.13	2.1%	27.4	0.97	1.8%	29.0
90 th	0.60	2.5%	12.3	0.70	1.7%	20.2	0.58	1.4%	18.3
β	0.61	0.34	0.41	0.38	0.15	0.24	0.40	0.21	0.36

Table 2-3 Damage States Index in HAZUS (1999)

Damage State	Failure Mechanism	Repair required	Outage
DS1 None	Pre-Yielding	None	No
DS2 Minor/Slight	Post-Yielding Minor spalling	Inspect, Adjust, Patch	< 3 days
DS3 Moderate	Post Spalling, Bar buckling	Repair components	< 3 weeks
DS4 Major/Extensive	Degrading of strength, Bar fracture	Rebuild components	< 3 months
DS5 Complete/Collapse	Collapse	Rebuild structure	> 3 month

Table 2-4 The Three Selected Critical Earthquakes

	PGA ^{*5} (g)	Component	Event	year	Station	φ ^{*1}	M ^{*2}	R ^{*3} (km)	PGA ^{*4} (g)
EQ13 DBE	0.376	EW	Imperial Valley	1979	Chihuahua	282	6.5	28.7	0.254
	0.400	NS				012			0.270
EQ4 MCE	0.800	EW	Loma Prieta	1989	Anderson Dam	270	6.9	21.4	0.244
	0.787	NS				360			0.240
EQ17 MCE	0.800	EW	Superstition Hills	1987	Wildlife Liquefaction Array	360	6.7	24.4	0.207
	0.700	NS				90			0.181

¹ Component, ² Moment Magnitudes, ³ Closest Distances to Fault Rupture, ⁴ Original Peak Ground Acceleration and ⁵ Peak ground Acceleration for the PSD test

Source: PEER Strong Motion Database, <http://peer.berkeley.edu/smcat/>

2.9 Figures for Chapter 2

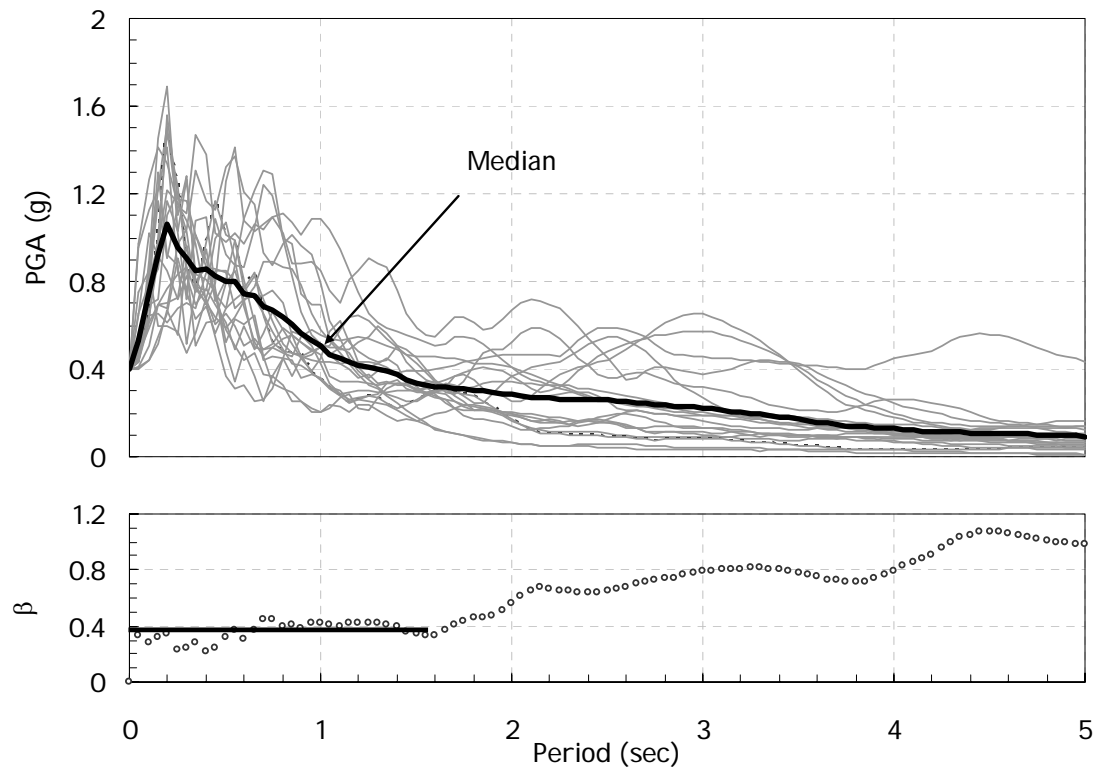
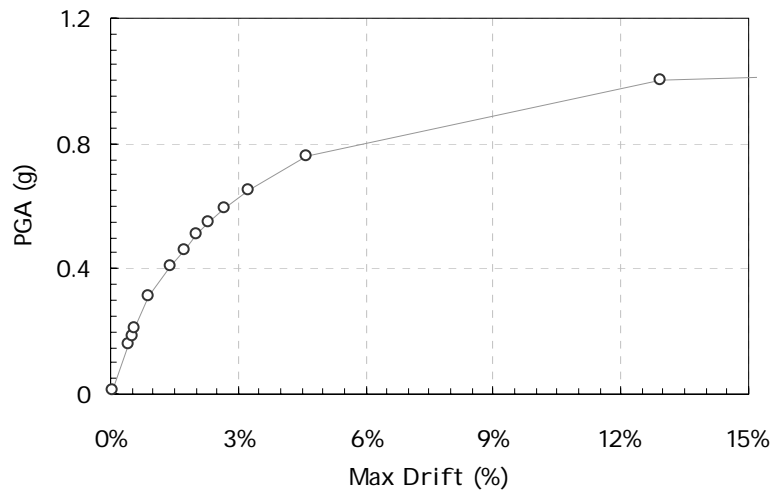
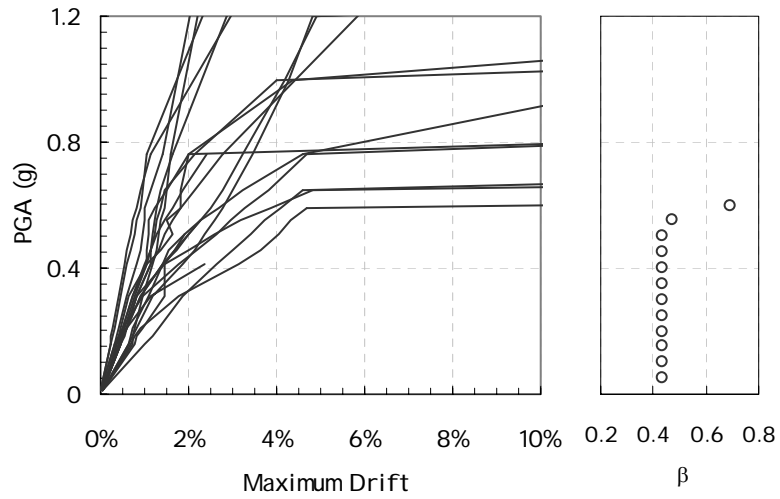


Figure 2-1 STEP 1: Selection of ground motion records normalised to Intensity measure of PGA=0.4g

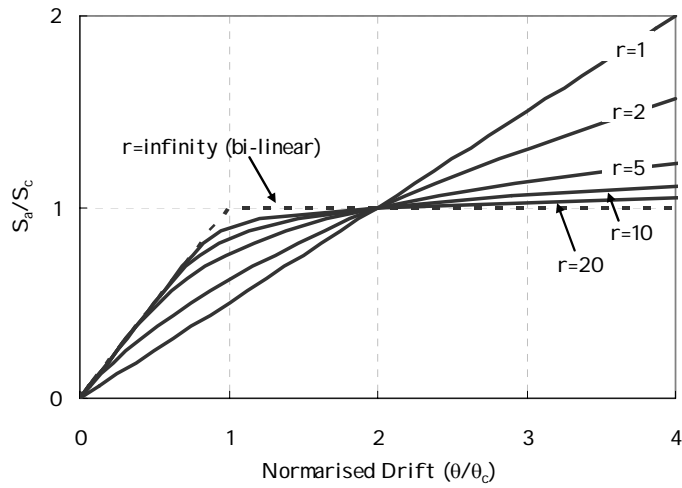


(a) IDA data points for one earthquake

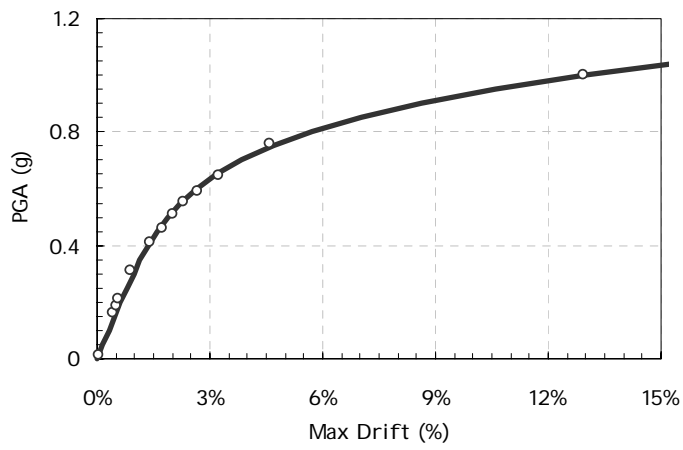


(b) Lined IDA data points of 20 EQs and Coefficient of Variation (β)

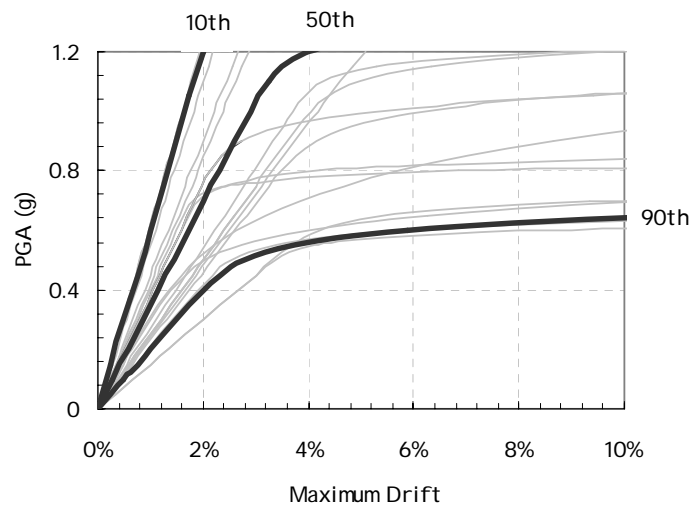
Figure 2-2 STEP 2: IDA data plots and Coefficient of Variation (β)



(a): Ramberg-Osgood equation for the IDA modelling



(b): An example fit of R-O model with IDA data points for one earthquake



(c): Fitted IDA curves and the 10%, 50% and 90% fractiles

Figure 2-3 STEP 3 Modelling IDA Curves and Generating Response Demand Curves

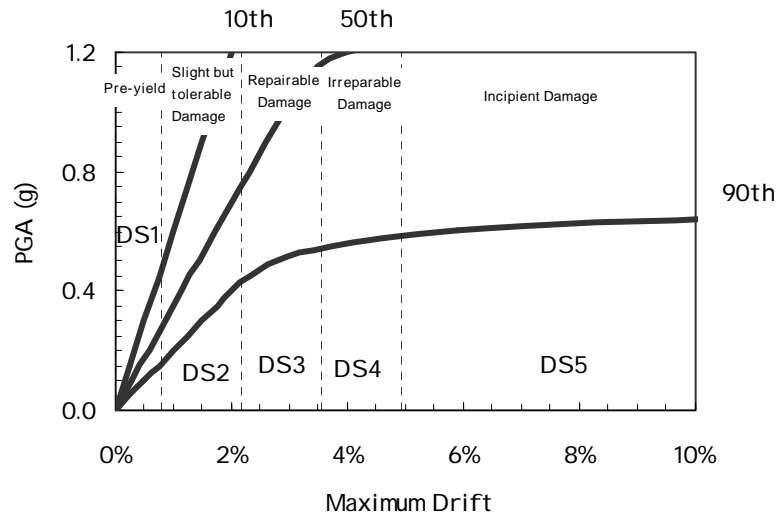


Figure 2-4 STEP 4: Assigning damage states to the IDA fractile curves

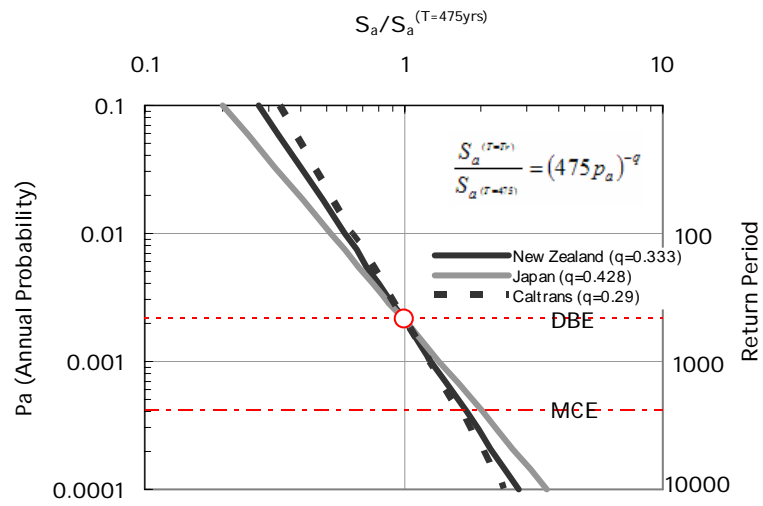
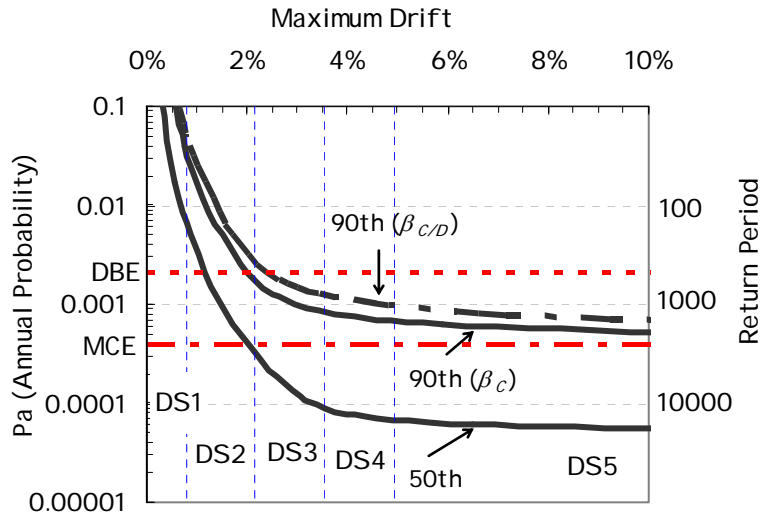
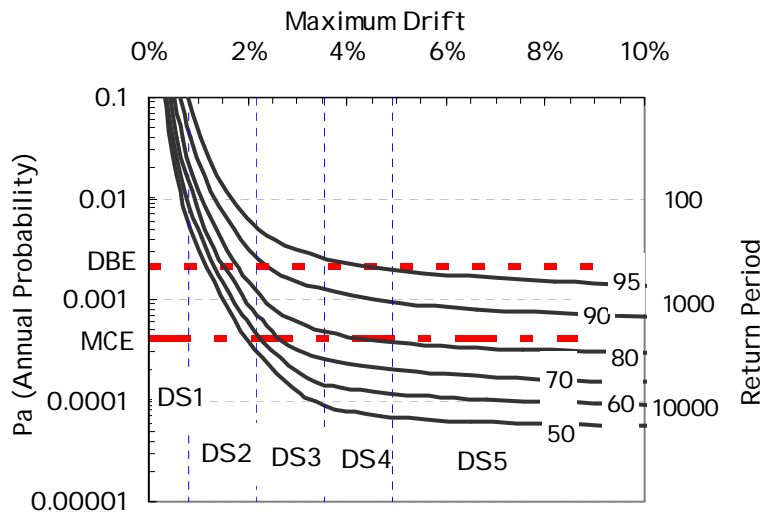


Figure 2-5 STEP 5 Hazard Intensity recurrence relation

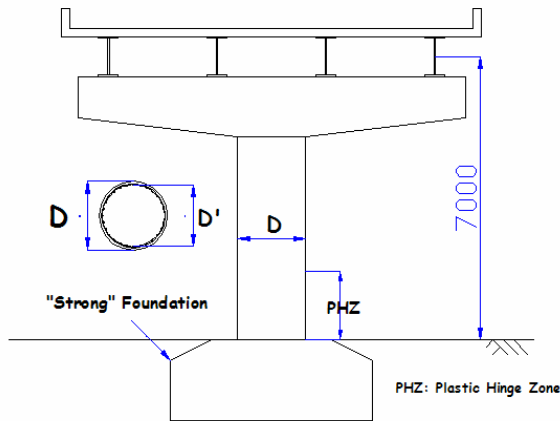
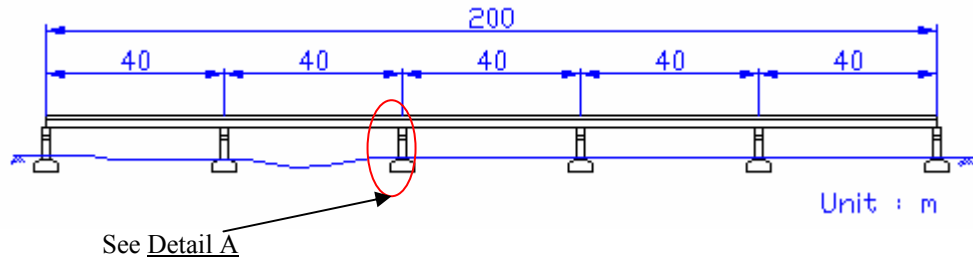


(a) Candidate intervals of response expectations based on demand randomness only and also the composite 90 percentile curve based on randomness of demand and capacity modelling uncertainty

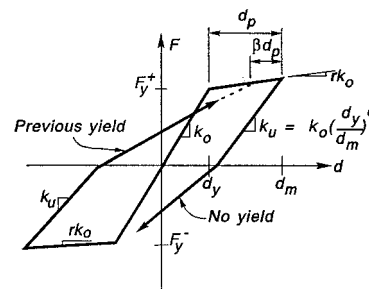


(b) Composite confidence interval curves with demand and capacity modelling uncertainty

Figure 2-6 STEP 6 Quantitative Risk Assessment



Detail A



Takeda Model

	New Zealand	Japan	Caltrans
D	1700	2000	2000
D'	1540	1834	1838
PHZ	1700	4000	3000
$P/A_g f'_c$	0.15	0.11	0.11
Bar	28-D32	28-D51	32-D41
ρ_t	0.99%	1.82%	1.34%
Spiral	R20@170	R20@115	R20@85
ρ_s	0.49%	0.61%	0.78%

ρ_t : the ratio of the longitudinal bars area to the pier's cross sectional area, ρ_s : the volume ratio of the volume of the spiral to the volume of the confined concrete

Figure 2-7 The Prototype Bridge Pier and Modelling Outline

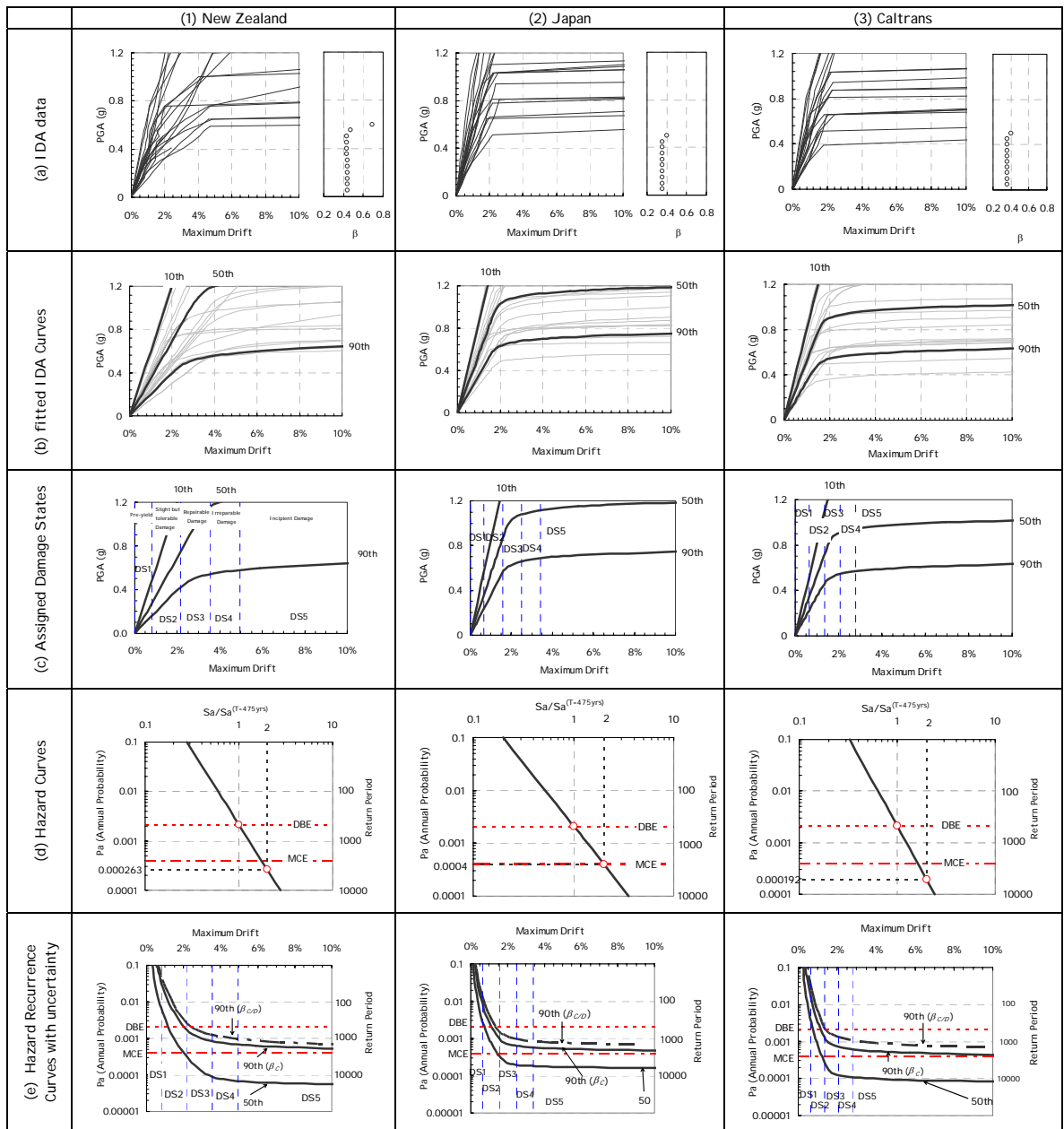


Figure 2-8 IDA procedures for the New Zealand, Japan and Caltrans Bridge piers

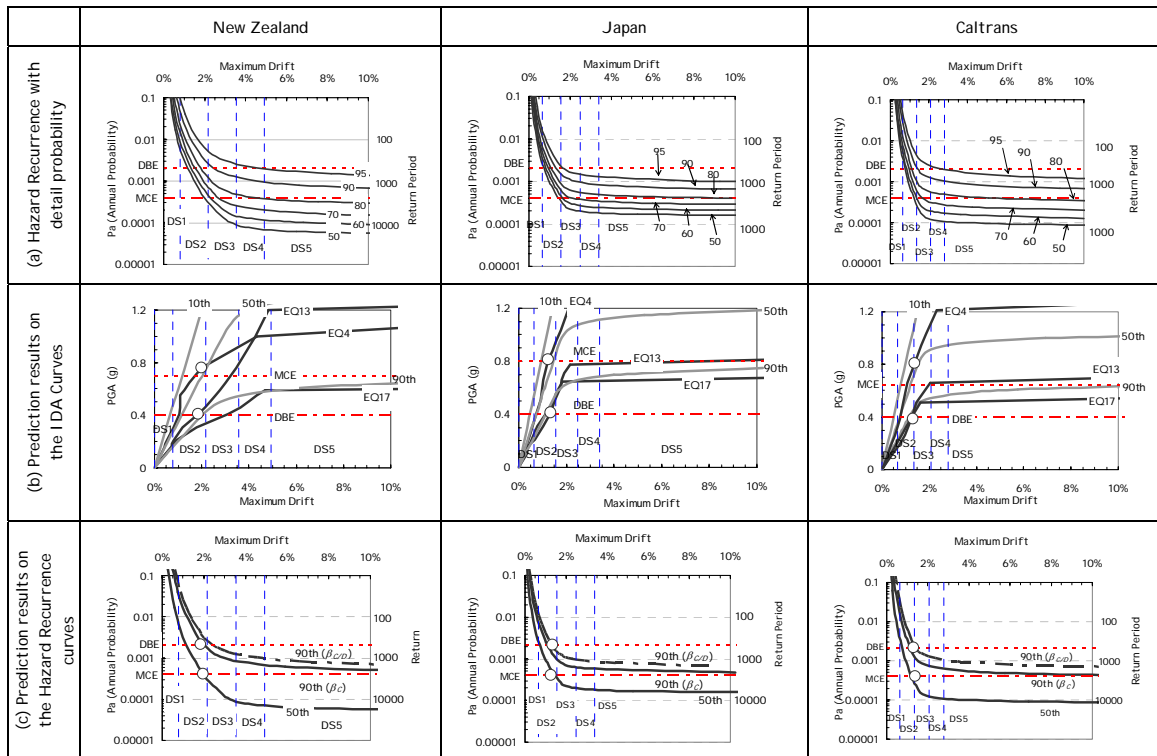


Figure 2-9 Risk Hazard Assessment for the New Zealand, Japan and Caltrans Bridge piers

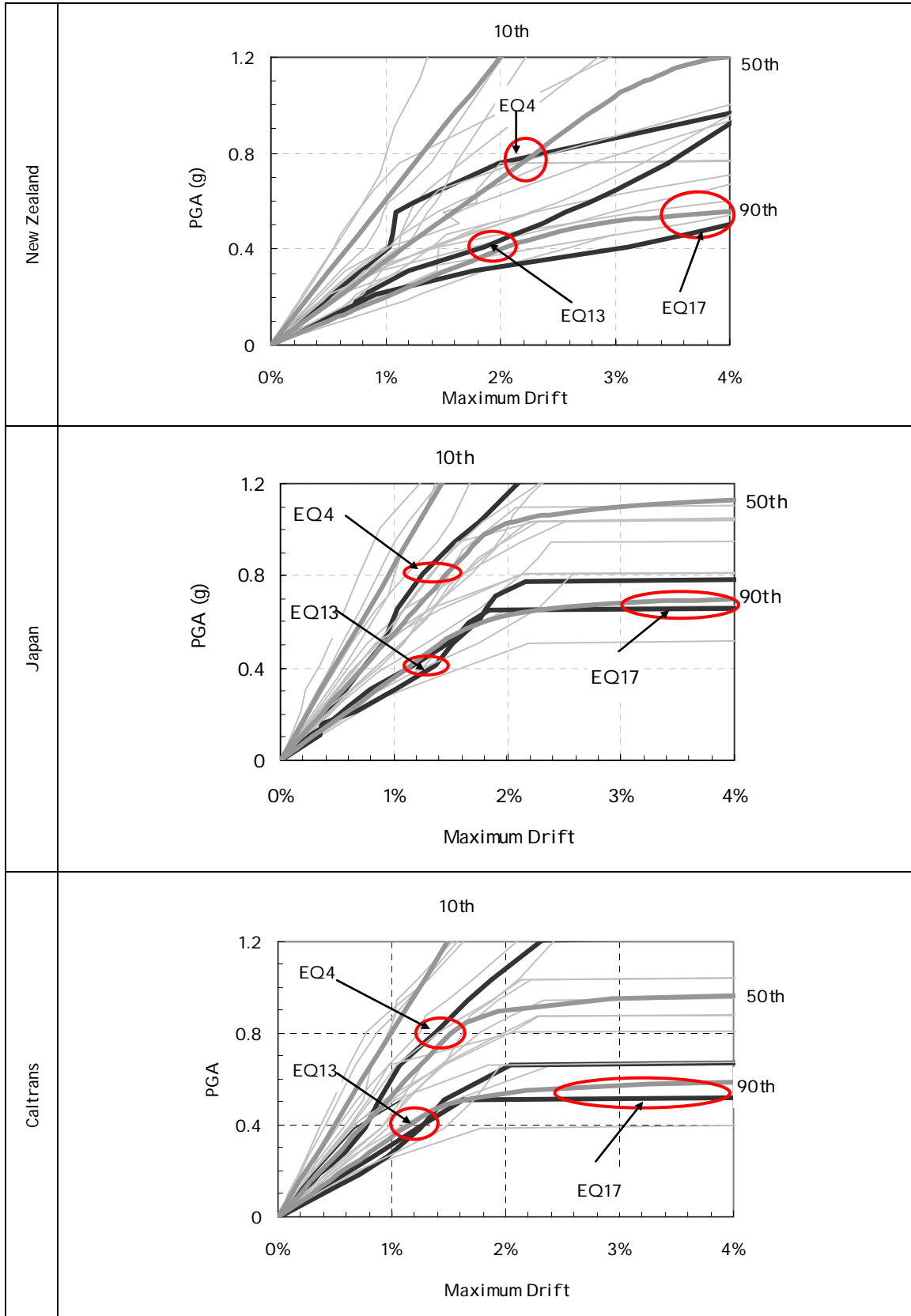
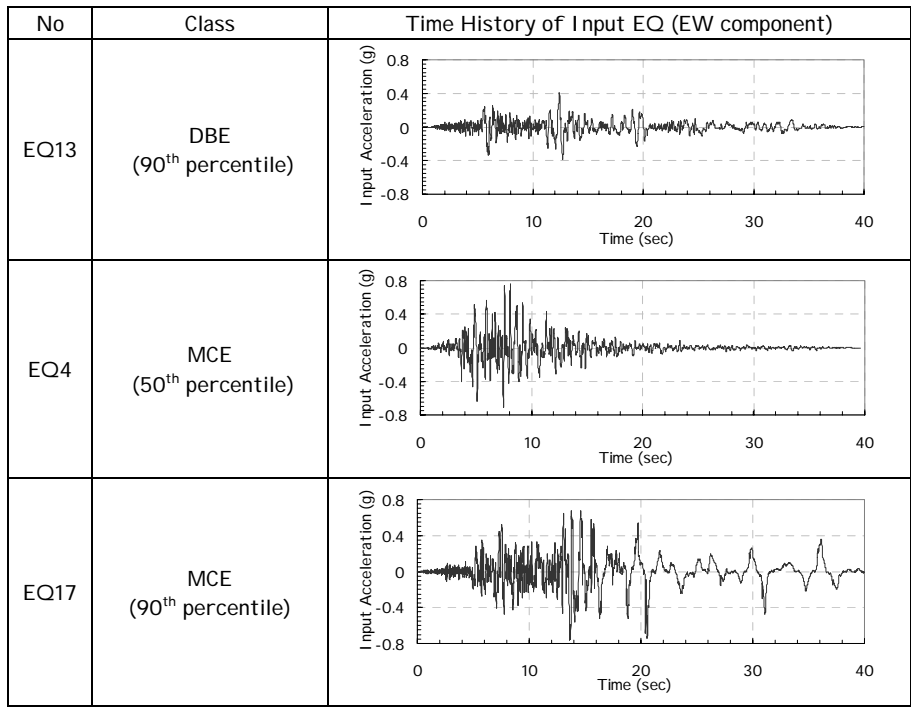
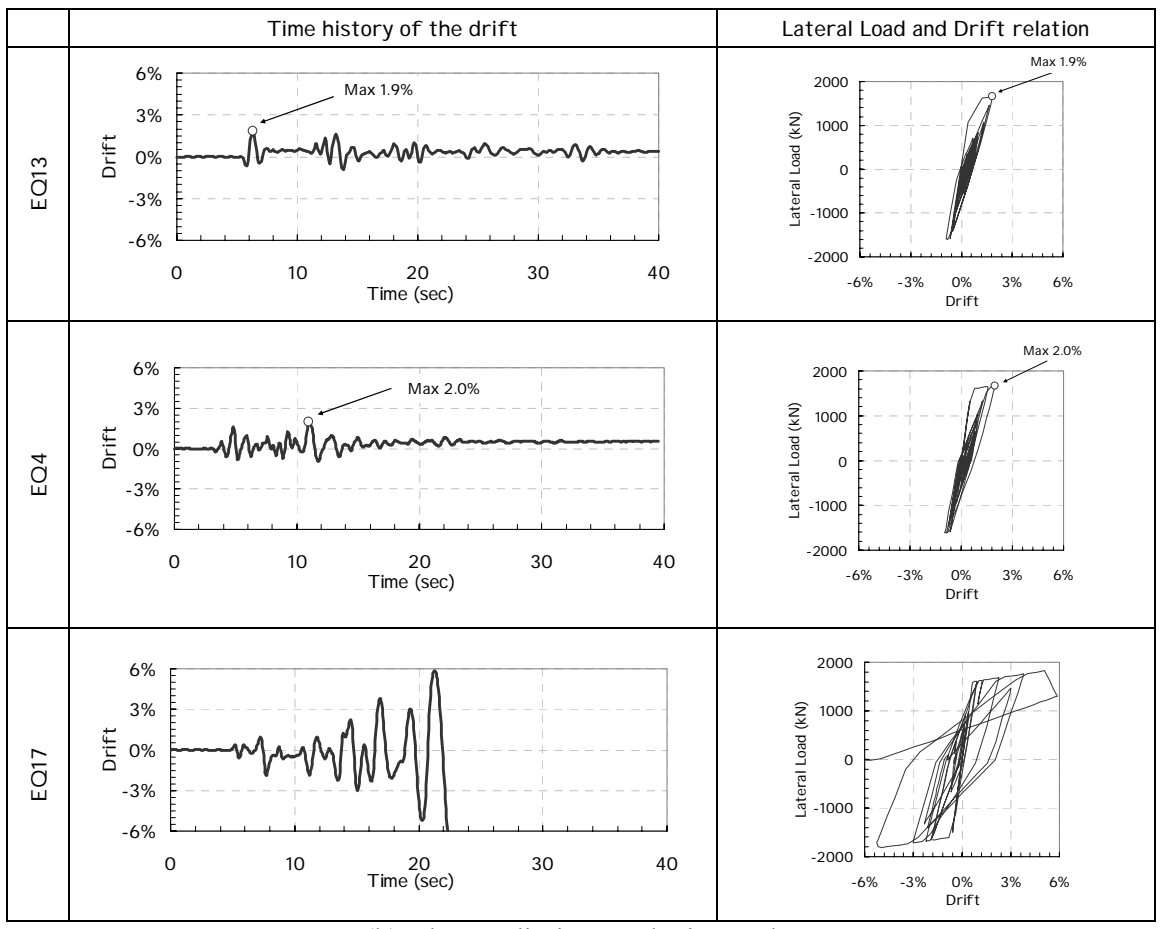


Figure 2-10 The Three Selected Critical Earthquakes with three fractile curves



(a) Three Input Earthquakes



(b) The prediction analysis results

Figure 2-11 An example of the Dynamic Analysis for the New Zealand Bridge Pier

3 PERFORMANCE OF DUCTILE HIGHWAY BRIDGE PIERS SUBJECTED TO BI-DIRECTIONAL EARTHQUAKE ATTACK

Summary

Circular reinforced concrete highway bridge piers, designed in accordance with the requirements of New Zealand, Japan and Caltrans specification, are experimentally investigated to assess their seismic performance. Pseudodynamic test procedures are developed to perform experiments on the three pier specimens. The experiments are performed on each pier using three earthquake ground motions: (i) a Design Basis Earthquake (DBE) (10% in 50years) with a 90 percent probability of non-exceedance; (ii) a maximum considered event (MCE) (2% in 50years) representing a median response (i.e. with a 50% probability of non-exceedance); and (iii) a MCE representing 90 percent probability of non-exceedance. Damage states after the earthquakes are assessed and mapped to a quantitative risk assessment. Although differences between pre-test computational predictions and Pseudodynamic test observations are shown to exist, the experimental results validate the expected seismic risk assessment damage outcomes for the three countries. It is concluded that each bridge pier designed to the three countries specifications can provide satisfactory seismic performance for the design basis earthquake events [500 year return period]. However, for maximum considered earthquakes [2500 year return period] the performance of the New Zealand pier was less than satisfactory, resulting in collapse due to insufficient strength. For the other two countries, in spite of certain detailing deficiencies, the piers survived the MCE without collapse.

3.1 Introduction

Following recent devastating earthquake events such as the 1994 Northridge (USA) Earthquake and the 1995 Hyogoken-Nanbu (Kobe-Japan) earthquake, there is a growing interest to compare seismic performance of bridge piers designed according to the codes of different countries. This is because both the loading requirements and structural detailing procedures vary considerably, even though the magnitude of hazard exposure is similar. As part of a cooperative four-country international project Tanabe (1999) designed four bridge piers, in accordance with New Zealand, Japan, Caltrans and Euro design codes. The main purpose of this international project was to identify differences in the cross section dimensions and reinforcing details; to clarify the reasons for these differences; and to assess the seismic performance using computational dynamics. This comparative research was restricted to uni-directional earthquake motions. Given that simultaneous bi-directional earthquake motions occur in reality, and computational prediction may differ from real response due to modelling simplifications, it is considered desirable to conduct a dual computational-experimental approach to investigate the seismic risk exposure of bridge piers.

Takanashi et al. (1975) developed the “Pseudodynamic” (referred to as PD hereafter) test method for experimentally determining the seismic performance of critical components using real earthquake ground motions as input. The PD test method is well known as an effective approach in assessing the seismic performance of critical elements under real earthquakes. The PD test method consists of two parts. First, the structure is represented “virtually” as a computational model, for which the equations of motion are formulated and analysed in a normal fashion. Next, the tangential stiffness of the structure is measured physically at each time-step increment and an updated value is used in subsequent computational modelling. As the PD test is conducted at a much slower rate than real time,

the inertial effect on the physical test specimen does not exist, but needs to be accounted computationally.

Mutsuyoshi et al. (1994) and Kawashima et al. (2003) investigated bridge pier behaviour under the bi-directional earthquake motions by PD tests. It was confirmed by their experimental studies that both strength and deformability in a given direction deteriorated as a result of displacements induced by motion orthogonal to that direction. In their papers, this effect is referred to as the “simultaneous bi-directional interaction effect”. Different values for this effect are taken into account in each design code since insufficient research has been conducted on this subject.

In this study, three highway bridges are designed. Each bridge design consists of a common 40 m span superstructure (deck) supported on a 7 m tall single column pier. The three designs differ in that they are separately designed and detailed according to the prevailing seismic design standards of New Zealand, Japan and California. For experimental investigation, specimens representing 30% scaled models of these three bridge piers were constructed and tested using the PD method at the University of Canterbury. Bi-directional PD tests were carried out on these specimens using three earthquakes chosen based on the results of a rigorous Incremental Dynamic Analysis (IDA) as explained in the previous chapter. Observed damage to the piers was assessed in terms of post-earthquake serviceability. The observed performance of each bridge design was then analysed to obtain a quantitative measure of the seismic risk.

3.2 Experimental Study: Prototype and Specimen Design

The properties of the three prototype bridge piers designed using New Zealand, Japan and Caltrans specifications are shown in Figure 3-1 (a) and Table 3-1 respectively. Elasto-plastic design basis push-over curves for the three prototypes are also shown in Figure 3-1 (a).

Push-over curves based on moment-curvature analyses using both the design strength and the measured strength of the materials are also presented in Figure 3-1 (a).

Although the For Design Basis Earthquakes (DBE) with 10% probability of occurrence in 50 years (return period = 475 years) in different countries will undoubtedly vary, a common earthquake having peak ground acceleration of $PGA = 0.4g$ was adopted to represent the DBE in all countries. The transverse (spiral) reinforcement was arranged and detailed following the design recommendations of each design code. The calculation for the design of transverse reinforcement carried out in this study is presented in Appendix A.

Figure 3-1 (b) and Table 3-1 present details of the 30% scaled specimens. The provided longitudinal and transverse reinforcement ratios, ρ_t and ρ_s , were aimed at keeping the same proportional force capacities as in the prototypes.

Each specimen was constructed in three phases: (i) the rectangular base block; (ii) the circular column; and (iii) the rectangular head block. The concrete was poured separately for each part. Following the pouring of the bases and prior to pouring of the piers, strain gauges were attached to the spirals over the lower 0.1 to 0.3D (where D is the diameter) of the column. Threaded rods (6mm diameter) were placed over the lower portion of the column for the measurement of curvature. Cardboard tube formwork was placed and held securely over the tied reinforcing cages, then the concrete was cast.

Table 3-1 presents the measured material properties of concrete and reinforcing steel. The compression strength of the concrete was measured at 28 days and at the time of testing using 100×200 mm cylinders.

3.3 Experimental Procedure: Pseudodynamic Testing

Details of the experimental setup and PD testing procedures are given in Figure 3-2 and 3-3. Figure 3-2 (a) presents an East-West elevation view from the north direction of a typical specimen set up in the test rig. Once, the specimens were set in the DARTEC

universal testing machine, a constant axial force of 630kN was applied via ball joints attached to the top and bottom plattens and the specimens. A plan view of the specimen setup is shown in Figure 3-2 (b). L-shaped loading frames and counterweight baskets were attached to the base block of the specimen in each direction. These were connected by 30mm diameter high strength threaded bars. Lateral loads were applied in both the E-W and N-S direction via 800kN hydraulic actuators that were connected to the specimen head block and L-shaped load frames via universal joints. In each lateral loading direction 1000kN capacity load cells were installed in series with the actuators.

Figure 3-3 (a) presents the instruments installed as part of the overall experimental system. To monitor the global response, the rotary potentiometers (pots) were installed (located 2.1m from the bottom of the columns) to measure the total displacements. To infer rotations, curvatures and longitudinal strains, 5 layers of EW and NS pairs of spring loaded pots were installed over the lower-portion of the columns along with 3 additional rotary pots to measure the deformation profile. As mentioned previously, strain gauges were affixed to the spiral reinforcement to enable the calculation of confining stress.

Figure 3-3 (b) presents the concept of the PD testing at the $(n+1)^{th}$ time step. To conduct the PD test, two main physical systems linked together are required. One is an “analysis and control system”, which analyses the response of the piers based on the equation of motion, $ma_{n+1} + cv_{n+1} + kx_{n+1} = -ma_{g(n+1)}$ and also controls the “experimental system”. The other system is the “experimental system” which plays a role in moving the specimen to the position calculated by the “analysis and control system”

In the “analysis and control system”, the position for the next step (x_{n+1}) is calculated and sent to the “experimental system”. This is based on the measured restoring forces ($F_n = k_n x_n$) from the “experimental system” at the current (n^{th}) step and also based on the earthquake ground motion at the next step, a_{gn+1} , whose whole data set is stored in the form of

an acceleration time history. Then, the “experimental system” moves the specimen to the position (x_{n+1}) and the measured restoring forces ($F_{n+1}=k_{n+1}*x_{n+1}$) are returned to the “analysis and control system”. This cyclic procedure is repeated until the input earthquake data sets are terminated.

There are several complexities inherent to the PD tests arising from the combination of scale factors in the “Analysis and Control System” such as (1) the time step increment, (2) the amplitude of input earthquake, (3) the mass of the superstructure, and (4) the damping factor. The values in the “analysis and control system” always corresponded to the full-scale prototype dimensions, whereas the displacements were scaled 30% only when sent to the “experimental system”. On the other hand, the lateral loads measured during the course of the experiment were scaled up by a factor of 11.11 ($1/0.3^2$) when being sent back to the “analysis and control system”. These scale factors are in accordance with constant acceleration, constant stress and constant strain similitude.

The determined input values for the PD tests are the superstructure weight (7000 kN) as described in Chapter 1 and the damping factor (5%) in this analysis and the input earthquakes in time series format.

The time step (Δt) for the numerical integration in the PD algorithm as well as the input earthquakes was chosen as 0.03 sec. This was based on the numerical stability using the central difference method (Chopra 2000). The percentage of displacement increments below the ram’s resolution was confirmed to be small enough to conduct PD test.

(i) The Stability of Numerical Integration

$$\omega\Delta t = \frac{2\pi}{T} * \Delta t = \frac{2 * 3.1415}{0.57} * 0.03 = 0.331 < 2.0 \quad \text{--- OK!!}$$

in which T is the natural period of Japanese Pier described in the reference book (Tanabe 1999) as described in Chapter 1.

(ii) The displacement increment vs The ram’s minimum resolution

Ram's resolution = $200 \text{ mm} / 2048 = 0.1 \text{ mm}$

The Percentage of Disp Increments below the Rams resolution is

3.0% in EW direction and 2.4% in NS direction < 5 % --- OK!!

3.4 Choosing Critical Earthquakes for Pseudodynamic Testing

In this study, three input earthquakes (EQ1, EQ2 and EQ3) with two intensity levels of earthquakes were chosen according to the Incremental Dynamic Analysis (IDA) discussed in Chapter 2 (Figure 3-4).

As observed in Northridge (1994) and Kobe (1995) earthquakes, when earthquakes stronger than the DBE used in the design occur, structures are damaged severely. Therefore, the development of a seismic performance assessment method with two or three intensity levels of earthquakes is becoming the current trend. Single level of assessment with 0.4g PGA earthquake (representing DBE) have been carried out for all three piers (Tanabe 1999). Hence, investigation of their seismic performance with a higher (stronger) level of earthquake, the so called Maximum Considered Earthquake (MCE), is considered to be important for earthquake engineers to establish the dual assessment methodology.

First, EQ1 with a peak ground acceleration of $\text{PGA}=0.4\text{g}$ was selected as the DBE, which has a 10% probability of exceedance in 50 years (475 year mean return period). Then, EQ2 was used with $\text{PGA}=0.8\text{g}$ to represent a median (50 percentile) MCE, which has a 2% probability of exceedance in 50 years (2450 year mean return period). The first 20 sec of each complete record was used for the input earthquakes, since the main shock occurs in this range. These two earthquakes were connected together with 5sec zero acceleration data between them to measure values such as residual drift and natural period under free vibration. Finally EQ3 was used with $\text{PGA}=0.8\text{g}$ to represent more intensive MCE with a 90 percent confidence of non-exceedance.

3.5 EXPERIMENTAL RESULTS

3.5.1 Overview

Figure 3-5, Figure 3-6 and Figure 3-7 respectively present the seismic performance of the three bridge piers (SP-1, 2 and 3), designed to the New Zealand, Japan and Caltrans codes. Each of these figures of results presents: (a) a plan view of the bidirectional orbit of drift response, (b) load-displacement hysteresis curves, (c) the time-history of response drift in accordance with the three earthquakes, and (d) and (e) show photographs of particular damage states during each earthquake (as defined by the HAZUS (1999)). Table 3-2 presents the five damage states, defined to assess the damage of the bridge pier, during and after each earthquake. These are DS1 (none), DS2 (slight/minor), DS3 (Moderate), DS4 (extensive) and DS5 (complete). The damage state descriptions are based on strain measurements and visual observations. Throughout this section, only the EW response of the bridge piers is discussed in detail since the critical earthquake component was aligned to the EW direction. The damage states inspected were yielding of bars, cracking, spalling of cover concrete, buckling of bars, and fracturing of bars. Yielding was judged after the tests from the data measured by the vertical potentiometers. All other damage states were surveyed by visual observation during the test. In addition, the maximum drift, the maximum lateral load during each earthquake and the residual drift after each earthquake are also described in this section.

3.5.2 New Zealand Bridge Pier (SP-1)

Figure 3-5 presents the experimental results of the seismic performance of the New Zealand bridge pier. Note that part (d) and (e) of Figure 3-5 show photographs of bar buckling at a drift of 3.6% and at the end of the test showing low cycle fatigue fractures of longitudinal bar. The seismic performance of the New Zealand bridge pier is described in detail based on damage observed after each earthquake as follows:

EQ1 (0-25sec)

When judged from the longitudinal bar strain inferred by external instrumentation, yield occurred at 5.61sec when the drift exceeded 0.30% eastwards. The lateral load when the pier yielded was 63.3kN. Several horizontal cracks were observed 150mm apart during the test, but these cracks closed after the earthquake ceased. The maximum drift and lateral load measured were -1.65% at 13.83 sec and 159 kN at 6.2 sec, respectively. The residual drift was -0.167%. The damage state after EQ1 (PGA=0.4g for the 90 percentile DBE) was assessed as slight, that is DS2, since the pier exceeded the yield drift value and cracks appeared.

EQ2 (25-50sec)

The maximum drift (-2.48%) occurred at time=36.9sec with horizontal flexure cracks spaced about 50 mm apart over the lower 2D range (approximately 1m) of the pier. The cracks were found to be more intensive than for EQ1 but the residual crack width was still relatively small (not more than 0.2 mm). The cover concrete remained in satisfactory condition and no spalling was observed. The residual drift was -0.25%. The damage state following EQ2 (PGA=0.8g for the 50 percentile MCE) remained at DS2.

EQ3 (50-100sec)

The important damage events observed under EQ3 were spalling, buckling, initial bar fractures and severe bar fractures, which resulted in the strength degrading rapidly forcing the termination of the test. The first spalling and bar buckling occurred on the East face of the pier at 63.7 sec with 2.5% drift and 68.4 sec with 3.6% drift, respectively. Subsequently, the first bar fracture occurred at 71.7sec at a drift of 6.0%. This was easily identified by a banging noise together with a sudden drop in lateral load resistance. The major degradation of strength started at 74.5 sec when the top of the pier was at a drift of 6.52%. Thereafter, the lateral load strength of the pier decreased to 80% (from 78.7kN to 62.6kN), while the drift of the pier increased 1.75% (from 6.53% to 8.27%). This degradation phenomenon was assessed as a

serious damage signalling a potential collapse of the pier and the test was terminated. Due to an effective collapse; it was clearly evident that the damage state was DS=5.

3.5.3 Japanese Bridge Pier (SP-2)

Figure 3-6 presents the experimental results of the seismic performance of the Japanese bridge pier. The two photographs show (d) cover spalling at a drift of 2.7%; and (e) the specimen at the end of testing. Details of the seismic performance of the Japanese bridge pier showing each of the three earthquake follow:

EQ1 (0-25sec)

The Japanese bridge pier (SP-2) yielded when the drift reached -0.20% at 5.61 sec. During the earthquake, two principal horizontal cracks formed, one at the bottom of the pier and the other 300 mm from the bottom; however these cracks closed after the earthquake. The maximum drift and the corresponding lateral load measured were -1.48% and -327 kN at 13.02 sec respectively. The residual drift was -0.05% indicating slight damage, thus DS=2 for the DBE.

EQ2 (25-50sec)

The maximum drift (-1.76%) was measured when the lateral load was -355kN at 30.18sec with horizontal cracks approximately 100 mm apart appearing throughout the bottommost 60 cm (equal to the diameter of the pier). The cracks were found to be more intensive than those under EQ1. Nevertheless, no residual cracks were visible. The residual drift was -0.11% and the damage state after EQ2 remained at DS=2.

EQ3 (50-100sec)

The extent of damage resulting form EQ3 was restricted to cover concrete spalling, which occurred at 66.1 sec at a drift of 2.7%. At the end of the earthquake, the residual drift

was 0.11%. As some repairs were necessary to restore full working order the damage state are measured as DS=3.

3.5.4 Caltrans Bridge pier (SP-3)

Figure 3-7 shows the experimental results of the seismic performance of the Caltrans bridge pier. A visual view of the extent of damage in the later part of the experiment is shown in the two photographs (d) and (e). The seismic performance of the Caltrans bridge pier for each earthquake is described as follows:

EQ1 (0-25sec)

The Caltran's pier (SP-3) yielded at 5.58sec with -0.24% drift when the lateral load was -93.9kN. Several horizontal cracks spaced every 200 mm from the bottom of the pier were found during EQ1, but these cracks closed after the earthquake terminated. The maximum drift and the corresponding lateral load were 1.53% and 232kN respectively measured at 13.11sec. The residual drift was -0.12% indicating slight damage, thus the damage state was DS=2.

EQ2 (25-50sec)

The maximum drift (1.95%) was measured at 36.0 sec with horizontal cracks (approximately 50 mm apart) around the bottommost one-diameter range (0.6 m) of the pier. The lateral load corresponding to the maximum drift was 259 kN. The cracks were found to be more intensive than those under EQ1 but still they were less than 0.1mm in width. The cover concrete remained intact and no spalling was observed. The residual drift was -0.13% with the damage state remaining at DS=2.

EQ3 (50-100sec)

The damage events found under EQ3 were cover concrete spalling and bar buckling on the East side. The spalling and buckling occurred at 65.1 sec and 70.2 sec when the pier drifts were 3.7% and -5.29%, respectively. The residual drift was -0.20%. As the damage to

the longitudinal buckled bars lead to an irreparable condition, the damage state at the end of testing was considered to be DS=4.

3.6 Comparison of Each Pier's Performance

Seismic performance of each of the three specimens under each of the three successive earthquakes are arranged separately to give nine force-displacement hysteresis graphs along with three drift time-history responses, as shown in Figure 3-8. Under the DBE (EQ1) the load-displacement relationships ((a)-1, (b)-1 and (c)-1) show that all the bridge piers exhibited limited hysteresis response and only a minimal residual drift remained at the end of EQ1. Although the stiffness of the New Zealand pier (SP-1) is less than the others due to its smaller diameter and lower lateral strength, the maximum displacement response of each pier did not differ considerably. The rounded nature of the hysteresis loops near their peaks is due to the phenomenon of “simultaneous bi-directional interaction effect” (Mutsuyoshi, 1994), where the lateral load in a particular direction tends to be reduced by its orthogonal movement. Comparison of the drift time-histories, shown in Figure (d)-1, before the maximum peak response at approximately 13.7 sec, indicates that the responses of all piers were similar, but due to different yield points after the peak was attained the responses varied, particularly the New Zealand pier (SP-1).

Under EQ2, it is interesting to note that in spite of the previous response, the responses of the three piers are similar from 25 to 37 sec until the first large inelastic excursion took place. The response at that time was largest in the weakest and most flexible of the three piers; i.e. SP-1. However, as the ductility demand on each of the three piers was still modest at this stage ($\mu < 2.5$), it is not surprising that the residual drifts were small and hence the damage state in all cases remained at DS=2.

Only under the largest of the three ground motions the responses became significantly different. The large shaking portion of EQ3 (90th percentile MCE) led to a maximum drift of

8% and effective collapse of the New Zealand pier. Being stronger and stiffer, the Japanese and Caltrans piers performed better, but nevertheless still sustained 4.4% and 6.0% drifts resulting in final damage states of DS=3 and DS=4, respectively.

3.7 Comparative Evaluation of Observed Response with Computational Predictions

The seismic performance of the New Zealand bridge pier was compared with a computational prediction using the nonlinear dynamic time history analysis program RUAUMOKO, (Carr, 2003). The modelling approach along with key parameters is presented in Figure 3-9 (a). The pier was modelled as a single mass on a column. Using the material strength measured in the laboratory, a nonlinear moment-curvature based pushover analysis was conducted and used as the basis for assigning macro model properties for the time history analysis.

The PD tests were carried out with three earthquakes continuously, whereas the time-history analyses were conducted for each earthquake separately. Therefore, the damage accumulated by the previous earthquake was not taken over to next analysis. The comparison between experimental observations and the computation prediction is graphically presented in Figure 3-9 (b) in the forms of (1) hysteresis curves and (2) time-history of the drift for each of the three earthquakes. From the time history of the drift, during EQ1, the response of the PD experiment and the analytical/computational prediction are in phase, although the predicted response tends to have a consistent offset of +0.4% as a result of the first large inelastic excursion following 6 sec. This residual drift is largely due to inaccuracies in the Takeda model which neglects some of the pinching characteristics exhibited in the experiment. Similar agreement with the harmonics of the response, but with some offset, is evident for EQ2. EQ3 inflicted serious damage as observed both in the experiment and analysis. The analysis is in agreement with the experimental observation that collapse is expected after 72

sec. This outcome is in spite of the modelling differences observed in the hysteresis curves when the response exceeds 3% drift.

3.8 Experimental Results Applied to the Seismic Risk Analysis

Figure 3-10 presents a comparison between the theoretical prediction carried out in Chapter 2 and the outcomes for the PD test. Figure 3-10 (a) shows that the PD results (shown by solid bullets) and the computational prediction (shown by circles) are close for both EQ1 and EQ2. That is, it is possible for earthquake engineers to expect the maximum drift in accordance with a certain level of confidence.

The Hazard Curve (the ratio of the PGA for the MCE to that of the DBE as a function of the annual probability) shown in Figure 3-10 (b) is integrated into the IDA curves in Figure 3-10 (c). From the prediction, the damage state of the New Zealand bridge pier can be estimated to be less than DS2 for the 90th percentile DBE; and to be more than DS3 for the 50th percentile MCE. The test results were plotted in the same range as the computational result. It is confirmed that the prediction methods established in Chapter 2 can provide a satisfactory estimate of the overall behaviour that includes the final damage state.

3.9 Conclusion

The bi-directional PD test system was developed and used for three highway bridge piers designed according to the seismic design codes of New Zealand, Japan and Caltrans. The input ground motions were selected from a suite of 20 earthquakes based on the results of Incremental Dynamic Analysis (IDA). The IDA procedure was coupled with the hazard exposure and be applied as a tool for seismic risk assessment.

Based on the experimental investigation reported herein, the following specific conclusions can be drawn.

1. All three bridge piers, designed to New Zealand, Japan and Caltrans Standards were only slightly damaged (DS=2) under the DBE. It could hence be concluded that one can be highly confident that for bridges designed and detailed in accordance with existing specifications can be quickly restored after a design basis earthquake.
2. For motions stronger than the DBE, irreparable damage can be expected. For a maximum considered event (MCE) with 2 percent probability in 50 years there is approximately 30 percent chance that structural collapse will occur.
3. The second devastating (90th percentile) MCE motion inflicted serious damage to the New Zealand bridge pier and the experiment was terminated after seven longitudinal reinforcing bars fractured and the specimen became unstable. The damage found in the Caltrans pier during the test resulted in longitudinal bar buckling and core concrete crushing. Such damage cannot be easily repaired and a rebuild would be normally necessary. Nevertheless the residual drift was small enough for the emergency vehicles pass over the highway. The damage of the Japanese pier was small and repairable; this improved performance was largely due to the higher strength inherent in that pier design.

3.10 References

- Carr A.J., 2004, *RUAUMOKO: Inelastic Dynamic Computer Program*, Computer Program Library, Department of Civil Engineering, University of Canterbury, Christchurch, New Zealand
- Chopra A.K., 2000, *Dynamics of structures (second edition)*, Prentice Hall, New Jersey
- Hayakawa R., Kawashima K., and Watanabe G., 2003, Effect of Bilateral Loadings on the Flexural Strength and Ductility of Reinforced Concrete Bridge Piers, *Japan Society of Civil Engineers Journal of Earthquake Engineering*, Vol 27, pp1-4 (in Japanese)
- Mander J.B., and Basoz N., 1999, *Enhancement of The Highway Transportation Lifeline Module in Hazus*, Federal Emergency Management Agency
- Mutsuyoshi H., and Machida A., Tanzo W., and Mashiko N., 1994, Inelastic Seismic Response Behaviour of RC Bridge Pier Using Pseudo-Dynamic Test Method, *Transactions of the Japan Concrete Institute* Vol. 16, pp265-pp272
- Takanashi K., Udagawa M., Seki M., Okada T., and Tanaka H., 1975, Nonlinear earthquake response analysis of structures by a computer-actuator on-line system, *Bulletin of Earthquake Resistant Structure Research Centre 8 Institute of Industrial Science*, University of Tokyo, Tokyo, Japan
- Tanabe, T., 1999, *Comparative Performance of Seismic Design codes for Concrete Structures*, Vol. 1, Elsevier, New York

3.11 Tables for Chapter 3

Table 3-1 Dimensions of Prototype and Specimens and measured material properties

		Code	Unit	New Zealand	Japan	Caltrans
Prototype Details	Diameter	D	mm	1700	2000	2000
	Pitch circle diameter of long. bar	D'	mm	1540	1834	1838
	Plastic Hinge Zone Length	PHZ	mm	1700	4000	3000
	Weight of superstructure	P	kN	7000	7000	7000
	$P/A_g f'_c$			0.15	0.11	0.11
	Longitudinal reinforcing bars			28-D32	28-D51	32-D41
	Longitudinal steel volume	ρ_t	%	0.99	1.82	1.34
	Diameter and pitch of Spiral in PHZ			R20@170	R20@115	R20@85
	Spiral steel volume	ρ_s	%	0.49	0.61	0.78
	Concrete	f'_c		25	25	25
	Longitudinal reinforced bars	f_y		500	500	500
Details of Test Specimens	Diameter	D	mm	500	600	600
	Gravity Load	P	kN	630	630	630
	Longitudinal reinforcing bars			24-D10	24-D16	32-D12
	Longitudinal steel volume	ρ_t	%	0.96	1.71	1.28
	Spirals in PHZ			R6@50	R6@35	R6@25
	Spiral steel volume	ρ_s	%	0.51	0.60	0.83
	Concrete measured strength	f'_c	MPa	41.2	38.5	40.7
	Longitudinal steel: yield strength	f_y	MPa	539	517	528
	ultimate tensile strength	f_{su}	MPa	677	697	689
	strain hardening	ϵ_{sh}	%	1.8	1.4	1.8
	strain at ultimate tensile strength	ϵ_{su}	%	14.6	16.4	14.1
	Spiral steel: yield strength	f_y	MPa	461	461	461
	ultimate tensile strength	f_{su}	MPa	633	633	633
	strain hardening	ϵ_{sh}	%	1.4	1.4	1.4
	strain at ultimate tensile strength	ϵ_{su}	%	19.6	19.6	19.6

ρ_t : the ratio of the longitudinal bars area to the pier's cross sectional area; ρ_s : the volume ratio of the volume of the spiral to the volume of the confined concrete; and ϵ_{sh} and ϵ_u are the measured strains at the onset of the strain hardening and ultimate strength respectively.

Table 3-2 Damage States Index HAZUS (1999)

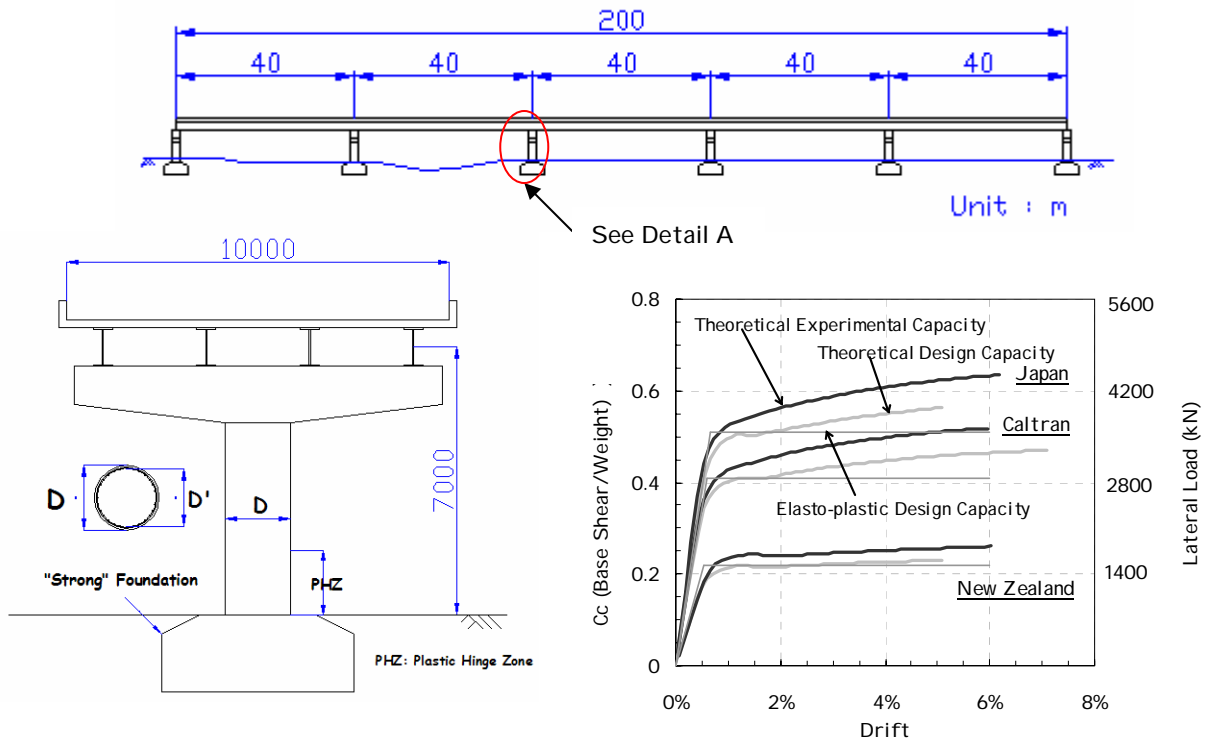
Damage State	Failure Mechanism	Repair required	Outage expected
1 None	First Yield	None	No
2 Minor/Slight	Cracking, Minor spalling	Inspect, Adjust, Patch	< 3 days
3 Moderate	Spalling, Bar buckling	Repair components	< 3 weeks
4 Major/Extensive	Degrading of strength, Bar fracture	Rebuild components	< 3 months
5 Complete/Collapse	Collapse	Rebuild structure	> 3 month

Table 3-3 Parameters for the IDA

IDA	New Zealand			Japan			Caltrans		
	S_c	θ_c	r	S_c	θ_c	r	S_c	θ_c	r
	g	%		g	%		g	%	
10 th	2.90	5.9	34.8	1.83	2.5	37.1	1.60	2.4	46.0
50 th	1.32	3.8	20.7	1.13	2.1	27.4	0.96	1.8	29.0
90 th	0.60	2.5	12.3	0.70	1.7	20.2	0.581	1.4	18.3
β_D	0.61	0.34	0.41	0.38	0.15	0.24	0.40	0.21	0.36
$\beta_{C/D}$	0.69	0.46	0.52	0.50	0.35	0.40	0.51	0.38	0.48

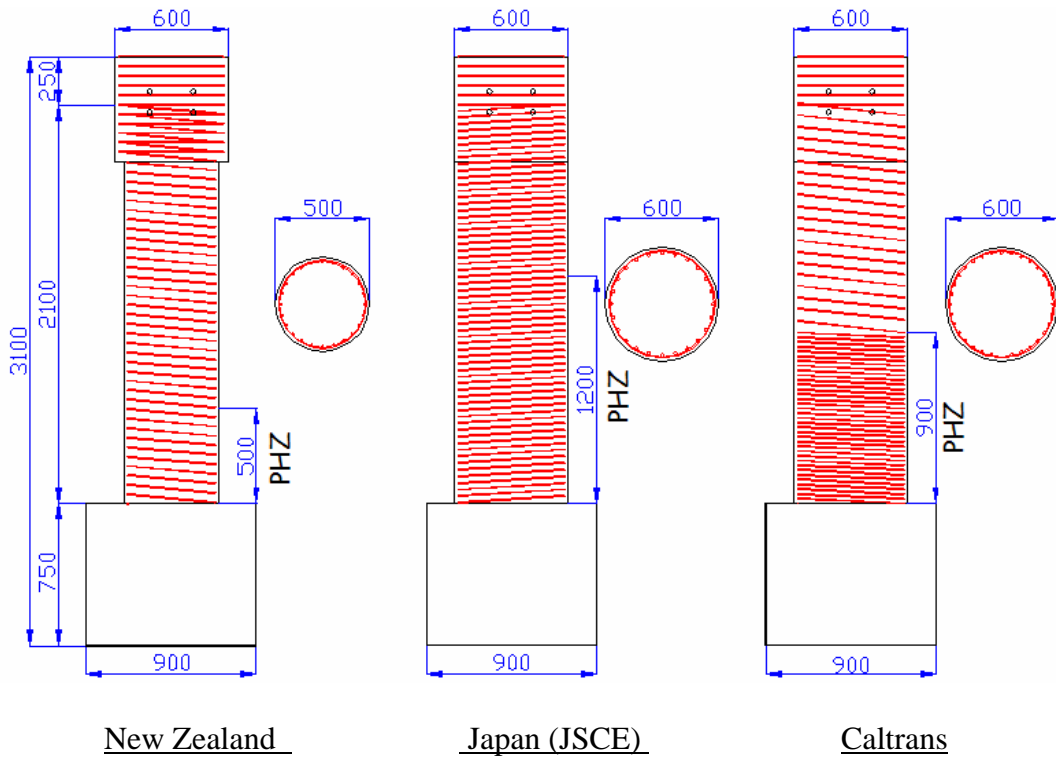
S_c is the critical value of the PGA, r is the multiplier for the R-O equation and θ_c is the critical drift, where $2\theta_c =$ drift of collapse..

3.12 Figures for Chapter 3



Detail A

(a) Prototype Bridge



New Zealand

Japan (JSCE)

Caltrans

(b) 30% scaled Specimens

Figure 3-1 Prototype Bridge and 30% scale reduced Specimens for Pseudodynamic Experimentation

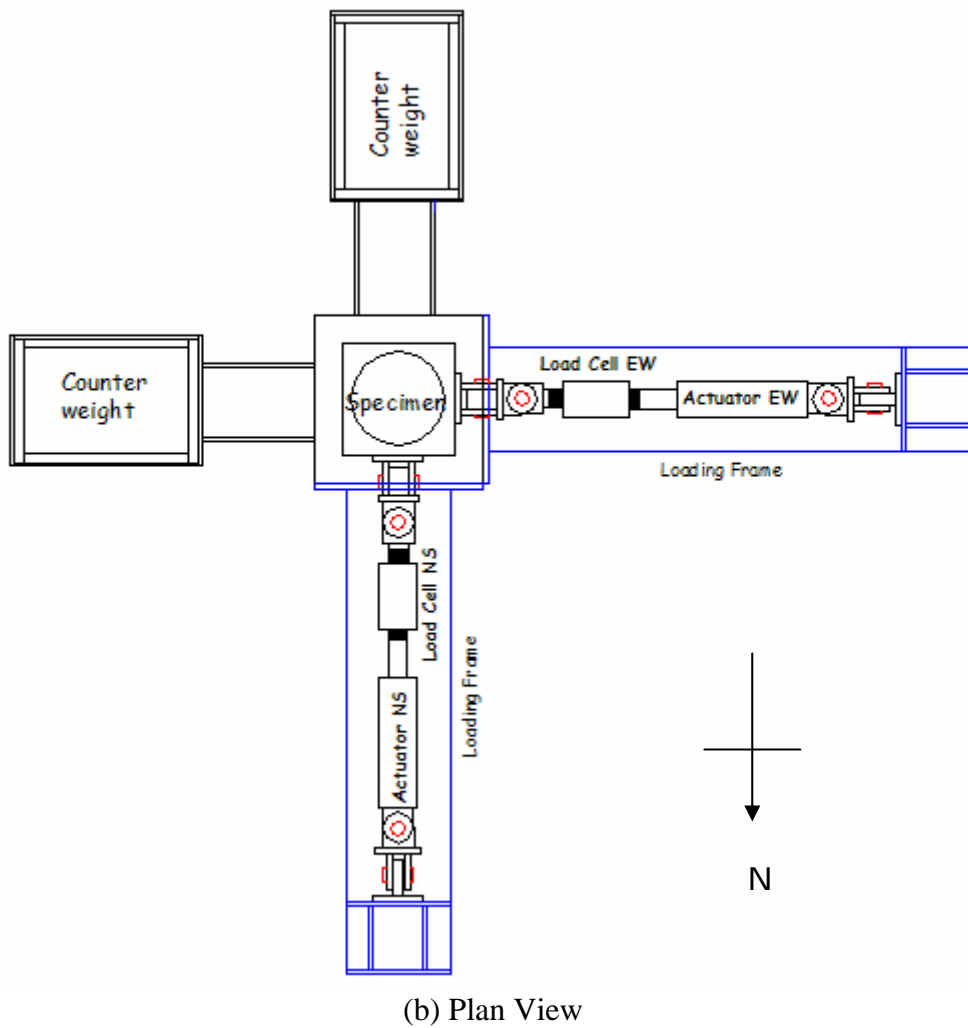
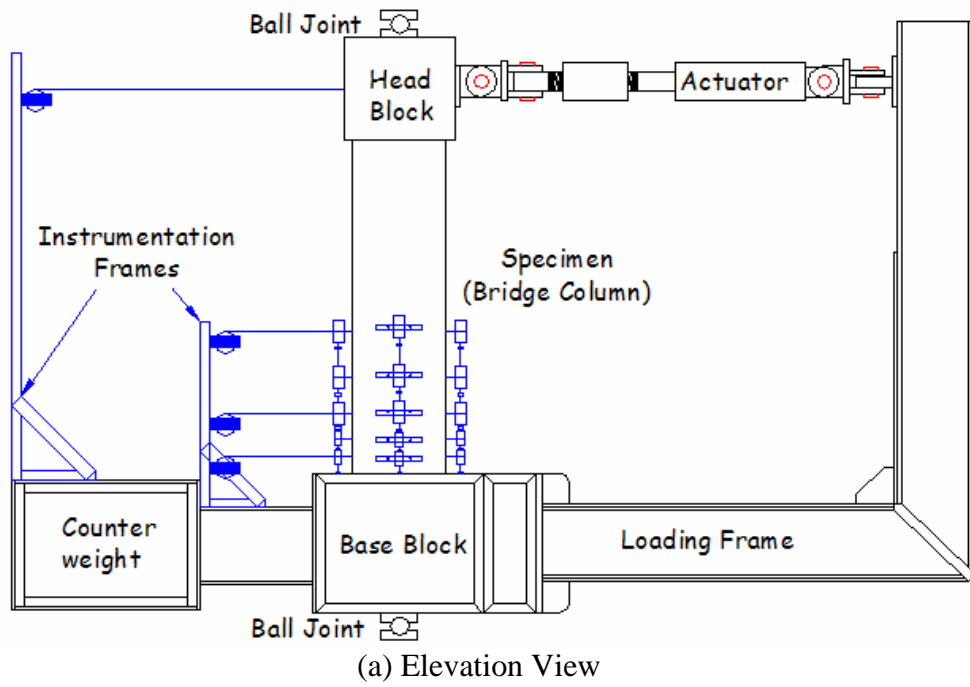
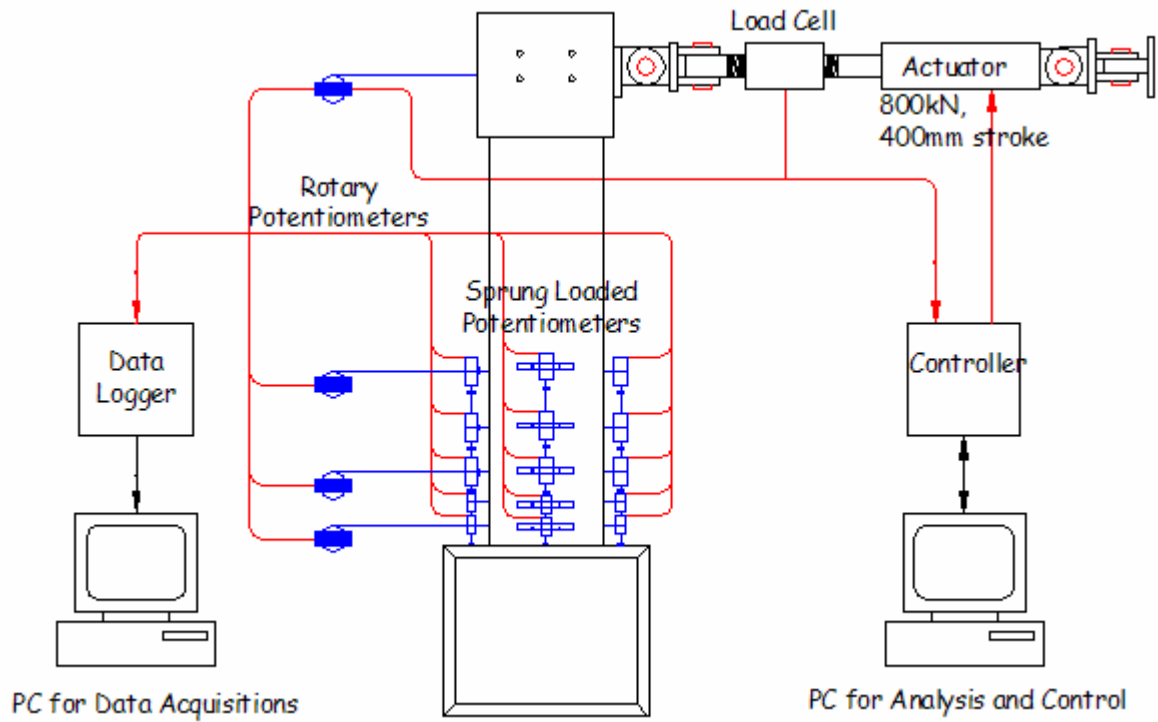
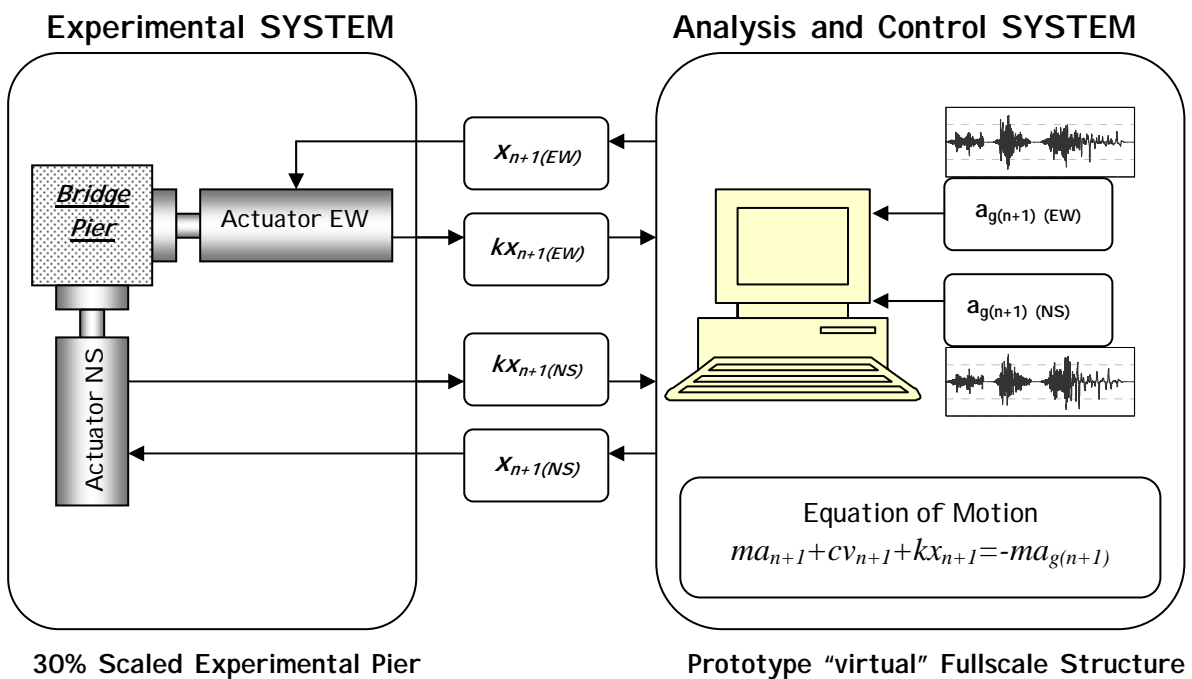


Figure 3-2 Experimental Setup

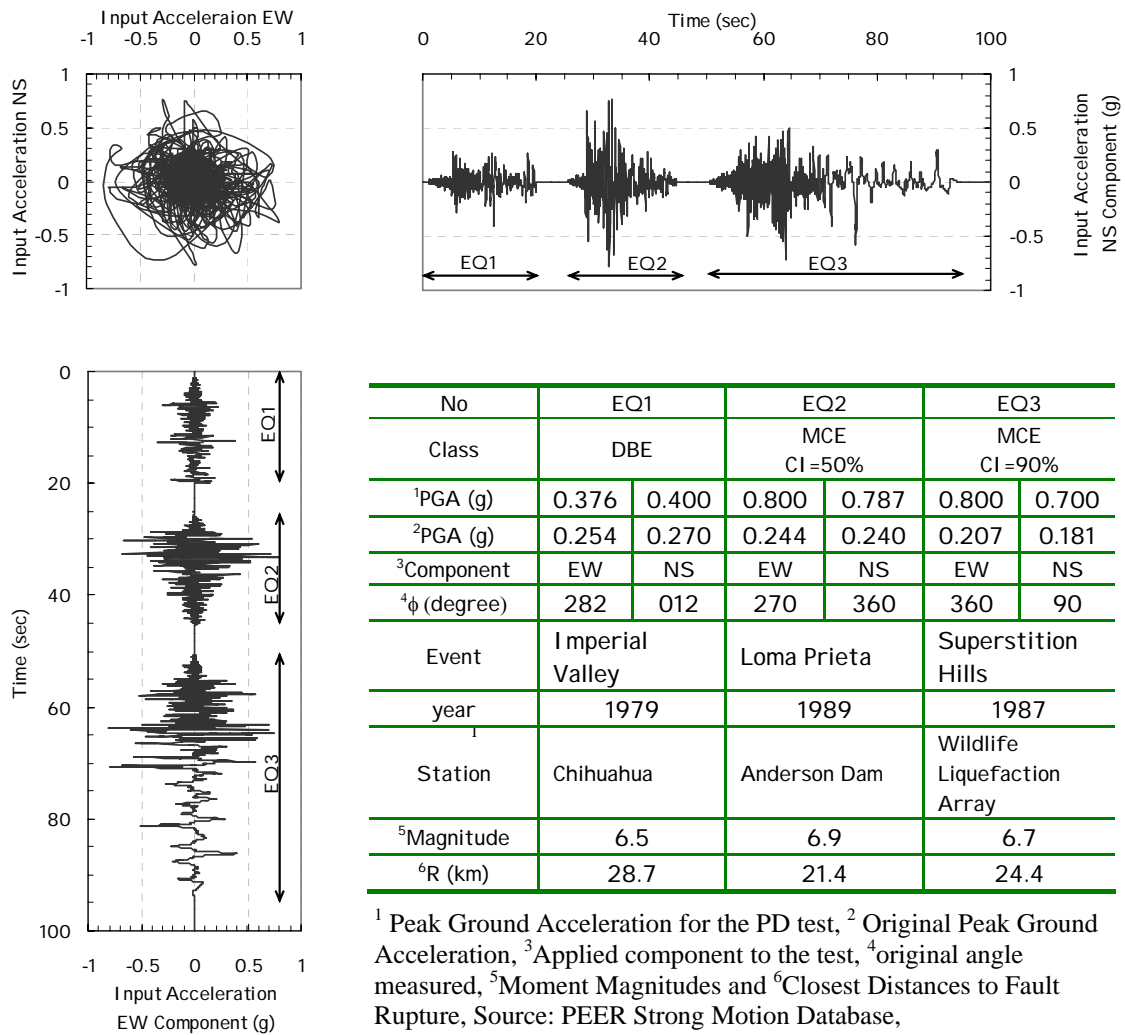


(a) Instrumentation and Data Acquisition System



(b) Bi-directional Pseudodynamic Test Concept at the $(n+1)^{\text{th}}$ step

Figure 3-3 Data Acquisition and Experimental Control for the Bi-directional Pseudodynamic Experiments



¹ Peak Ground Acceleration for the PD test, ² Original Peak Ground Acceleration, ³ Applied component to the test, ⁴ original angle measured, ⁵ Moment Magnitudes and ⁶ Closest Distances to Fault Rupture, Source: PEER Strong Motion Database, <http://peer.berkeley.edu/smcat/>

Figure 3-4 Detail of Earthquakes used in Pseudodynamic testing sequence

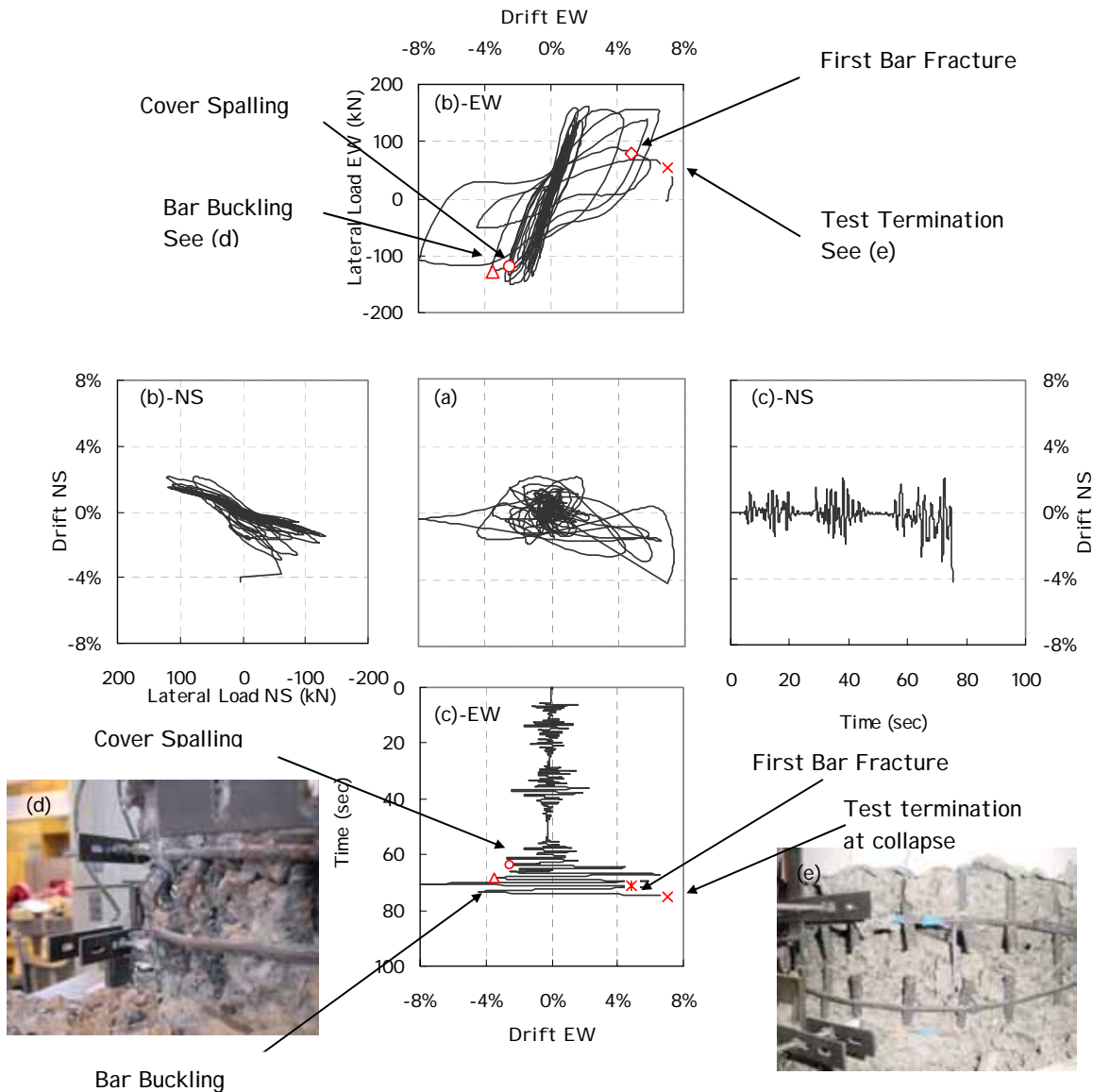


Figure 3-5 Experimental Results of the Seismic Performance of the New Zealand Pier (SP-1) showing (a) Plan view of bi-directional drift orbit; (b) Load Displacement Curve; (c) Time History of the Drift; (d) Photograph showing bar buckling at drift of 3.6%; and (e) photograph at end of test showing longitudinal low cycle fatigue bar fracture.

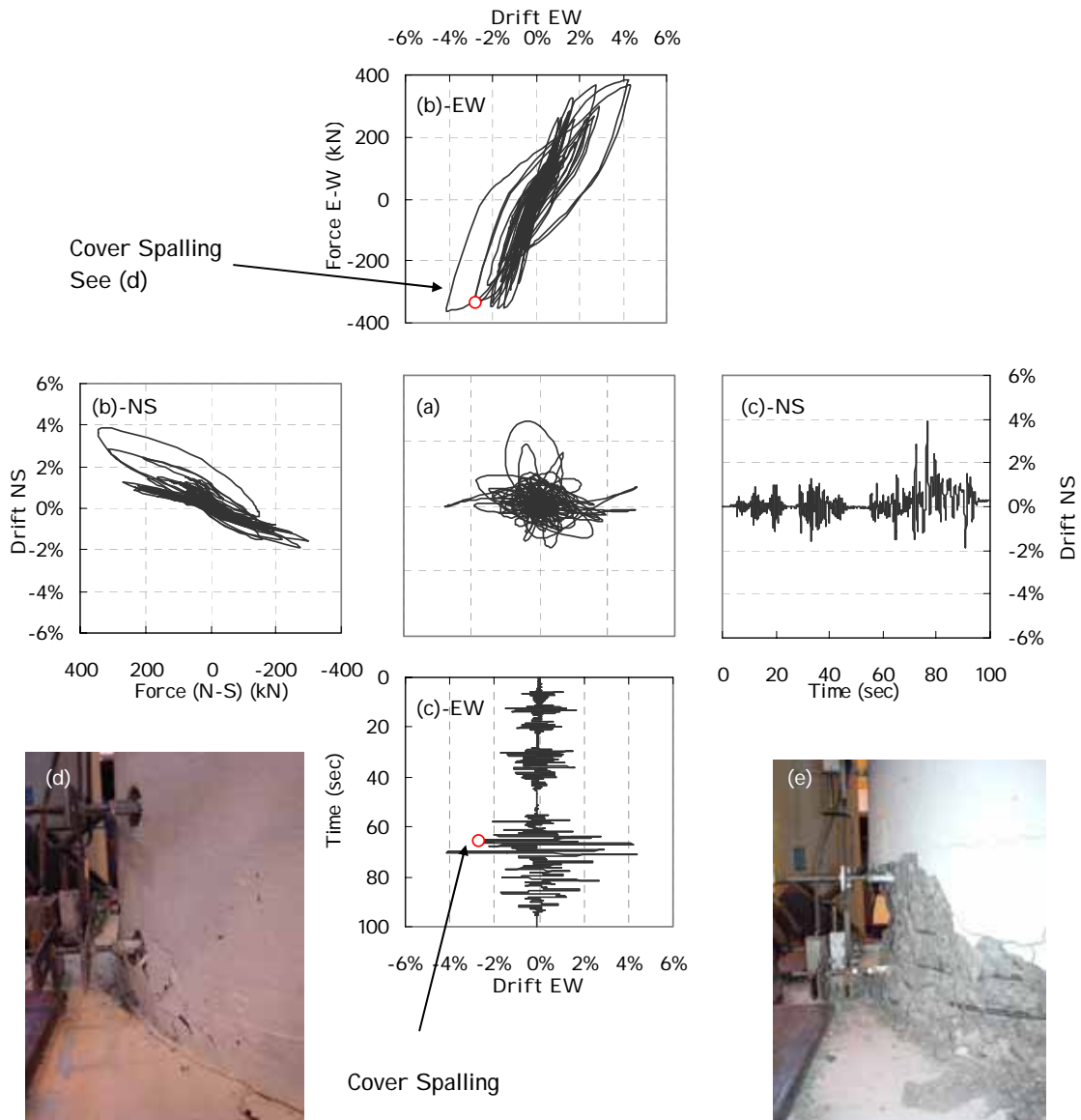


Figure 3-6 Experimental Results of the Seismic Performance of the Japanese Pier (SP-2) showing (a) Plan view of bi-directional drift orbit; (b) Load Displacement Curve; (c) Time History of the Drift; (d) Photograph showing cover spalling at drift of 2.7%; and (e) photograph at end of test.

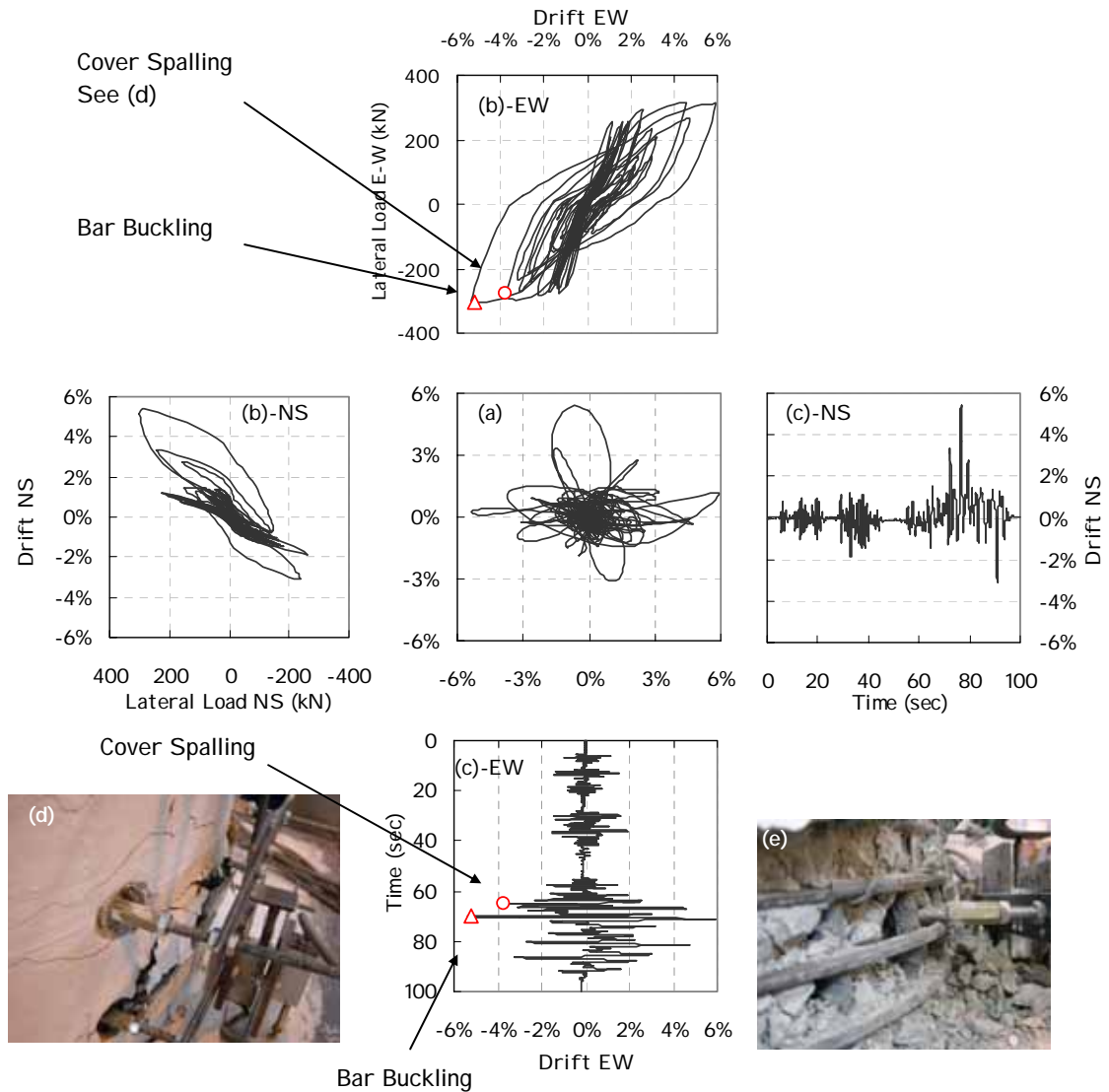


Figure 3-7 Experimental Results of the Seismic Performance of the Caltrans Pier (SP-3) showing (a) Plan view of bi-directional drift orbit; (b) Load Displacement Curve; (c) Time History of the Drift; (d) Photograph showing cover spalling at drift of 3.7%; and (e) at end of test showing bar buckling along with loss of core concrete.

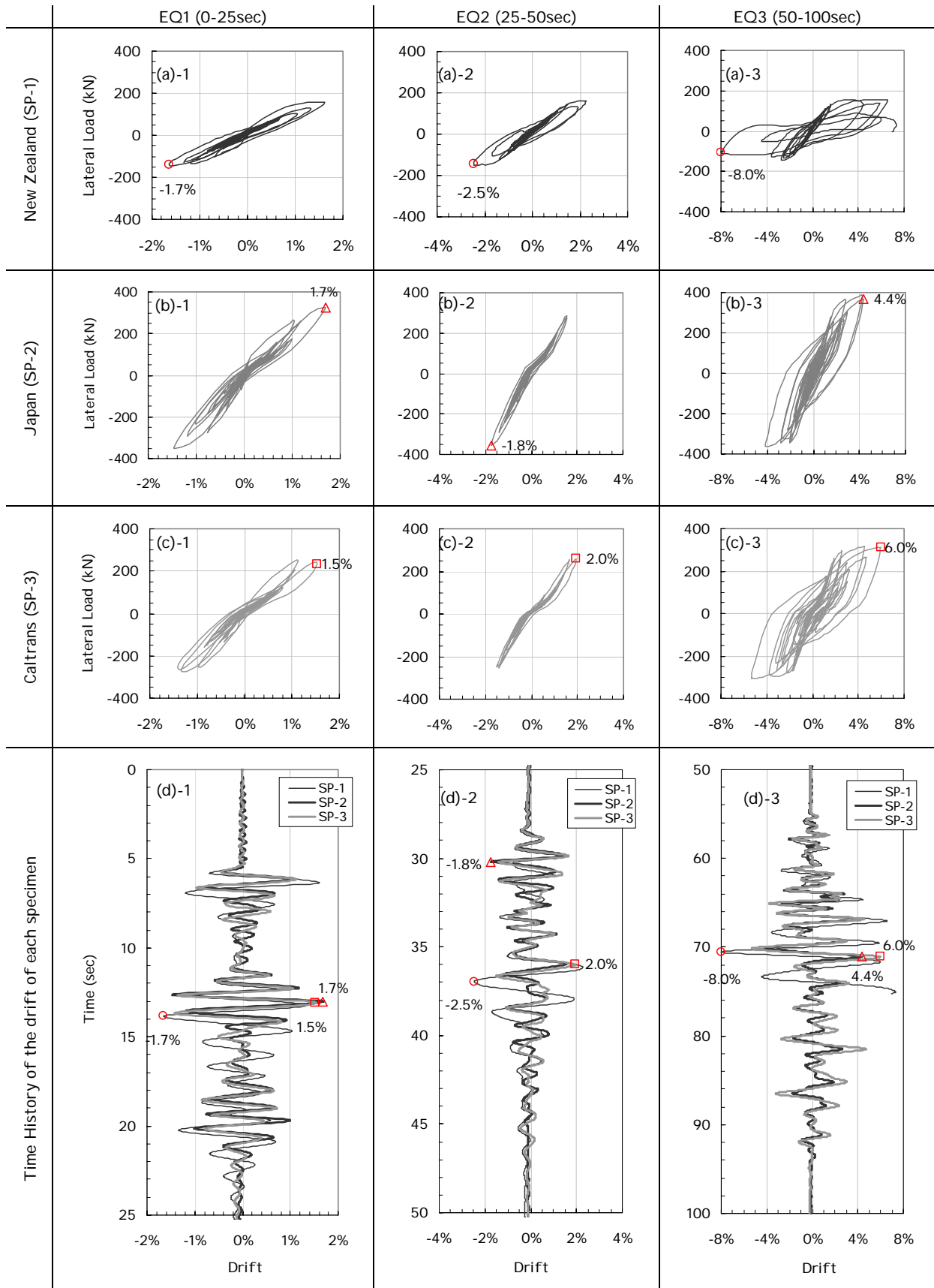
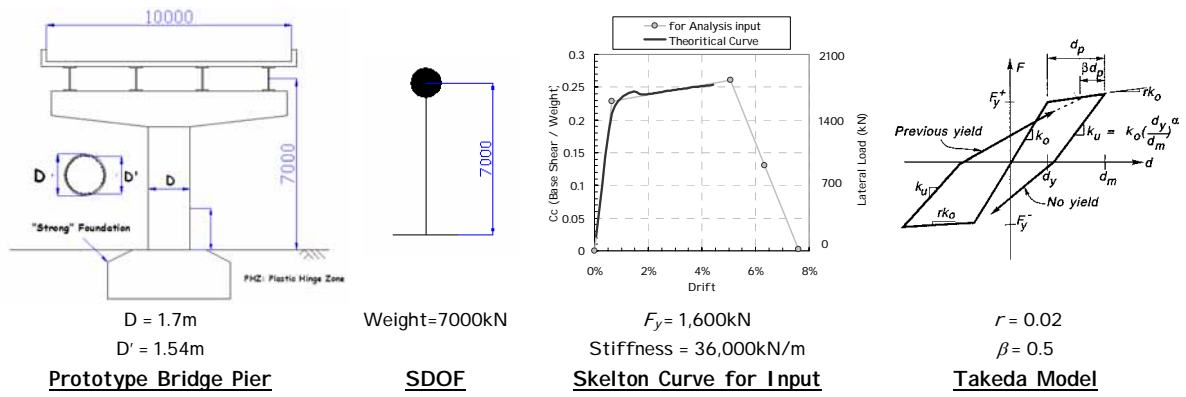
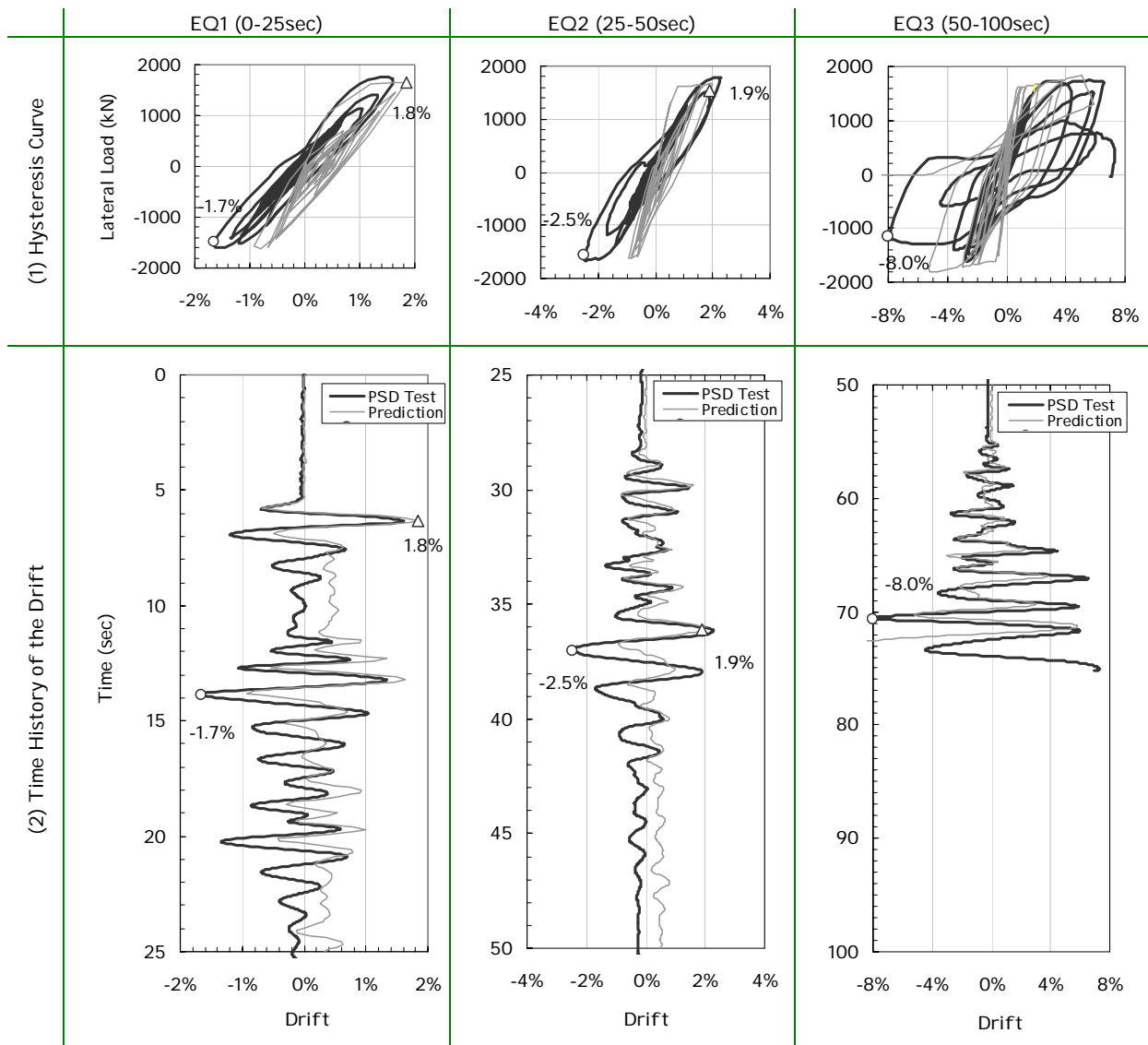


Figure 3-8 Comparison of the Seismic Performance the Specimens



(a) Computational modelling for time history analysis



(b) Comparison between the experimental results and the computational prediction

Figure 3-9 Comparison of the Bi-directional PD tests with the computational prediction for the New Zealand pier (SP-1)

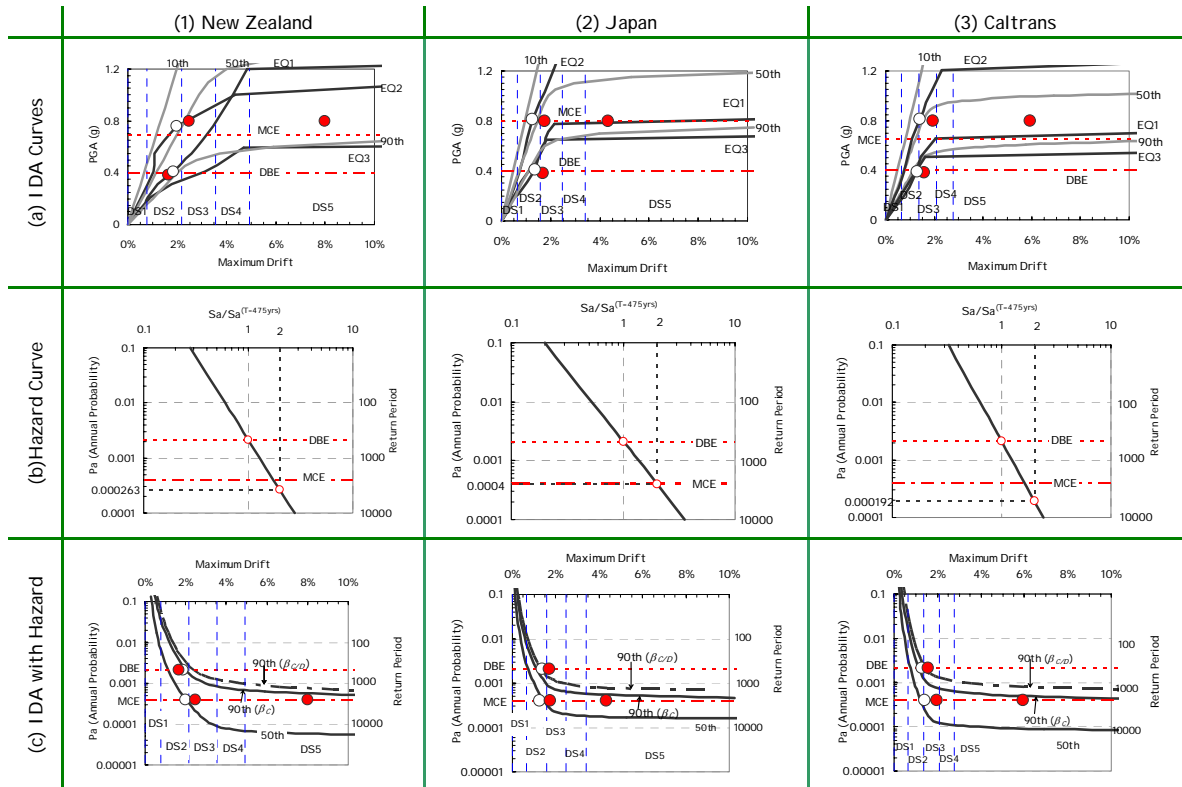


Figure 3-10 Damage State Index and Test Results on the Hazard Curves. The solid bullet points show the observed outcomes, while the open bullets represent the computed prediction.

4 PERFORMANCE OF A DAMAGE PROTECTED HIGHWAY BRIDGE PIER SUBJECTED TO BI-DIRECTIONAL EARTHQUAKE ATTACK

Summary

Recent earthquakes such as Loma Prieta (1989), Northridge (1994) and Kobe (1995) have all shown the need for a new bridge design philosophy that avoids damage in order to ensure post-earthquake serviceability to keep traffic flowing. The use of rocking bridge piers has the potential to achieve this design objective. By adopting the principles of Damage Avoidance Design (DAD) which utilises post-tensioned prestressed concrete piers with an armoured interface alloy, it is possible to achieve the design objective. This section presents an experimental investigation of a pier designed and constructed in accordance with the principles of damage avoidance design and tested under bi-directional loading using the Pseudodynamic test methods. The behaviour of the DAD pier is compared with a companion conventional monolithic pier designed and constructed using the principles of ductility. It is shown that following a design basis earthquake, the DAD pier experiences no damage and there is zero residual drift, whilst the ductile pier sustained considerable damage.

4.1 Introduction

The basic principles of current seismic design have relied on detailing for ductility that permits, under a strong earthquake, energy dissipation within a plastic hinge region, which is normally located at the bottom of the bridge pier. The resulting seismic performance leads to permanent damage mostly concentrated within the plastic hinge region; such behaviour also leads to residual drift. Residual drift may make it difficult to maintain serviceability of the bridge even though life-safety may have been maintained.

Early work on rocking structures dates back to Housner (1963). He showed rocking is an effective means of mitigating seismic damage. Two state-of-the-practice examples can be found in New Zealand: the South Rangitikei Railway Bridge, and an industrial chimney at the Christchurch Airport, (Skinners et al., 1993).

From this background, a Damage Avoidance Design (DAD) philosophy, aimed at maintaining both life safety and serviceability, was proposed by Mander and Cheng (1997) for the design of bridges. A DAD pier can avoid damage by way of the rocking movement on its foundation. High contact stresses between the column and foundation are mitigated through steel armouring of the rocking interfaces. Mander and Cheng (1997) studied seismic performance of DAD pier under the uni-lateral loading as well as shaking table tests. Damage avoidance was confirmed through the experiments. However, the DAD concept has not been tested under a bi-lateral loading condition.

The conduct of bi-lateral loading experiments is a primary objective of the research reported in this section.

The Pseudodynamic (PD) test method was first developed by Takanashi et al. (1975) and has since had considerable use and further algorithm development. The PD testing method consists of a non-linear time-history analysis system coupled with a quasi-static experimental system. The PD test method is well known as an effective approach in assessing

realistic seismic performance under real earthquakes. The bi-lateral PD test method was adopted in this study to realistically investigate the behaviour of a DAD bridge column subjected to bi-directional earthquake motions and to enable comparison with a conventional ductile bridge column designed in accordance with New Zealand specifications.

This chapter describes first the DAD procedure for the prototype highway bridge pier designed in accordance with damage avoidance principles. The prototype pier was then scaled to 30% full size to suit the experimental facilities at the University of Canterbury. The construction and the test configuration are then explained in detail. The bi-directional cyclic loading (CL) and Pseudodynamic (PD) tests were then carried out to investigate the fundamental seismic performance and to examine the realistic behaviour under the bi-directional earthquake loading respectively. A comparison is also made by between the DAD pier and the conventional monolithic New Zealand bridge pier to clarify certain advantages of the DAD approach.

4.2 Experimental Program

4.2.1 Prototype Design

Figure 4-1 presents the prototype DAD bridge pier dimensions. The DAD pier was designed in accordance with damage avoidance principles, and to satisfy the same moment demand (7486kNm), used for the New Zealand monolithic pier described in Chapter 3. The moment capacity, M , of this DAD pier can be determined by multiplication of the axial load, P , (arising from the gravity load of the superstructure and the additional force due to un-bond PC tendons, if necessary) and one-half the Shoe Block width, $B/2$; thus

$$M = P * B/2 \quad (4-1)$$

The additional axial force to satisfy the moment demand was provided by un-bonded tendons and fuses. Detailed design procedures are presented in Appendix B.

The longitudinal and transverse reinforcements were arranged following the New Zealand Concrete Code, NZS 3101 (1995). The DAD pier did not need to consider the post-yield behaviour because earthquake energy is mitigated by the rocking movement and fuse-bar yielding instead of damage to a plastic hinge region. The resulting theoretical push-over curves are shown in Figure 4-1 (b), while the bending moment profiles of demand and capacity are compared in Figure 4-1 (c).

4.2.2 Specimen and Construction

The prototype pier was scaled down to 30% of the prototype to suit the experimental facilities available at the University of Canterbury. The longitudinal and transverse reinforcement ratios, ρ_t and ρ_s , were aimed at keeping the same values as the prototypes. The dimensions and properties of the specimen are summarized in Figure 4-2.

The Base Block and the Pier (column) with the Head Block were constructed separately. Initially, the vertical and horizontal hoop reinforcements (D20 and D25) for the Base Block were assembled. The interface steel plate “A” (700*700*32mm) with a square hole (350*350) in the middle was seated on the top of the reinforcement of the Base Block.

The Pier (column), rocking on the base block under the earthquake conditions, consists of three reinforced concrete (RC) parts, a Shoe Block (500*500*250mm deep), a Pier (ϕ 400*1550mm high) and a Head Block (600*600*550mm deep). First, the longitudinal rebars (16-D10) were placed into the holes drilled on the interface steel plate “B” (500*500*32mm) on the bottom of the Shoe Block and were then welded to the plate to hold the reinforcements in place. The R6 spirals were wrapped around and tied to the longitudinal bars. The Shoe Block had additional horizontal square hoops outside the R6 spirals with a 50mm pitch to mitigate the high end-zone bursting forces and to satisfy minimum reinforcement requirements.

The Head Block reinforcement (8-R6 hoops and 4-D10 longitudinal bars) was assembled and welded to a 10mm thick steel “top plate”. Three Grade 300 “Interface Plates” as shown in Figure 4-2(b), were placed between the Shoe Block and the Base Block to avoid any damage to contact surfaces and to keep the pier centrally located while rocking. Plate “A” at the bottom of the Shoe Block and Plate “C” on the top of the Base Block were always in contact with each other to eliminate any damage at this contact interface. Plate “B” was bolted to Plate “A” to act as a “shear key” to prevent the Shoe Block sliding under lateral loads. For the energy dissipater, R12 (340mm length) threaded bars with the middle 150mm machined down to 7mm diameter, were used, as shown in Figure 4-2 (c).

Compression strength of the concrete cylinders, (100mm diameter and 200mm height) was measured to be $f'_c = 71$ MPa. Plain round 6mm dia. Grade 430 bars and D10, D12 and D16 deformed Grade 500 rebars were respectively used for the transverse and longitudinal reinforcements in the specimens. The tensile strength for each rebar type is given in Figure 4-2 (e). The resulting theoretical push-over curves are shown in Figure 4-2 (f).

4.2.3 Testing procedures

Figure 4-3 (a) shows an elevation view of the DAD specimen in the test apparatus from the north direction. The specimens were set within a 10 MN capacity universal testing machine. Vertical (axial) load to the specimen was applied through two ball joints at the top and bottom of the specimen. A constant axial load of 777 kN was applied; representing the weight of the superstructure (630 kN), and an additional axial load allowance of 147 kN to simulate the tension force of un-bonded post-tensioning tendons. Figure 4-3 (b) presents a plan view of the specimen setup. Two L-shaped loading frames and two weighted baskets for each direction were connected with the Base Block by 30mm diameter high strength threaded bars. Bidirectional lateral loading was applied by two actuators, each having an 800 kN load and 400mm stroke capacity and were attached in the EW and NS directions between the head

block to the load frame with universal joint pinned connection. For the CL and first PD test, the energy dissipaters were screwed vertically into the tapped holes of the steel interface plate on the Base Block and the Shoe Block was clamped down with nuts by a torque wrench to put 50% of the yield stress (150MPa) into the dissipaters.

Next the instrumentation was installed, as shown in Figure 4-4 (a). To monitor the global response, rotary potentiometers were, located 2.1m from the bottom of the Pier. Load cells (1000kN capacity) were installed in each direction (East and South) to measure the lateral load corresponding to the specimen's position. To monitor the rocking response, 8 sprung loaded linear potentiometers were mounted around the perimeter of the Shoe Block. In addition, 6 rotary potentiometers (3 layers in 2 directions) were mounted on isolated instrumentation frames to measure lateral displacements within the lower part of the column, over a height of 2 times the diameter or 0.8m. Strain gauges were affixed to 8 longitudinal reinforcing bars (4 directions on both right and left faces of the longitudinal bars). The strain gauges were used to assess whether yielding of the longitudinal rebars occurred in the column during rocking.

Figure 4-4 (b) shows the PD test concept of the PD testing at the $(n+1)^{\text{th}}$ time step. To conduct the PD test, two main physical systems linked together are required. One is an “analysis and control system”, which analyses the response of the structure based on the equation of motion: $ma_{n+1} + cv_{n+1} + kx_{n+1} = -ma_{g(n+1)}$. This also controls the “experimental system” which plays a role in moving the physical specimen to the position calculated by the “analysis and control system”. In the “analysis and control system”, the position for the next step (x_{n+1}) is calculated and sent to the ‘experimental system’, based on the measured restoring forces ($F_n = k_n x_n$) by the “experimental system” at the current (n)th step and also based on the earthquake ground acceleration at the next step, a_{gn+1} . The “experimental system” then moves the specimen to the next position (x_{n+1}) where the measured restoring

force ($F_{n+1}=k_{n+1} * x_{n+1}$) is sent back to the “analysis and control system”. This cyclic procedure is repeated until the input earthquake data sets are terminated.

The complexities involved with the PD tests were due to the combination of scale factors in the “Analysis and Control System”, including (1) the time step increment, (2) amplitude of input EQ, (3) the mass of the superstructure and (4) the damping factor. However these were solved simply and efficiently. While the values in the “Analysis and Control System” were always kept at full scale, the imposed displacements were scaled to 30% only when being sent out to the “Experimental System”. The measured lateral loads in the “Experimental System” were scaled up by $1/(30\%)^2$ when being sent back into “Analysis and Control System”.

To perform the PD tests, the determined input values were the weight (7000kN), the damping factor and the input earthquake (EQ) motion records in time sequence format. The damping factor for the DAD pier was determined to be 5.75%, as follows:

The total effective damping for the DAD pier can be assessed by the equation below;

$$\xi_{eff} = \xi_0 + \xi_{rocking} \quad (4-2)$$

in which ξ_0 the intrinsic damping; and $\xi_{rocking}$ the effective viscous damping due to the radiation of energy into the foundation half-space as rocking takes place.

The intrinsic damping was assumed to be $\xi_0=2\%$, a standard value often assumed for precast prestressed concrete members. The damping factor representing the rocking motion, described by Mander and Cheng (1997) was found from

$$\xi_{rocking} = \frac{2}{\pi} \times \left(\frac{D_c}{H_c} \right)^2 = \frac{2}{\pi} \times \left(\frac{1.7}{7.0} \right)^2 = 3.75\% \quad (4-3)$$

in which D_c = the width of the bottom of the pier and H_c = the height of the pier. Hence, the input damping factor was $\xi_{eff} = 5.75\%$.

The two input EQs, designated as the 10 percent in 50 years Design Basis EQ (DBE) and the 2 percent in 50 years Maximum Considered Event (MCE), for the PD tests were chosen according from an Incremental Dynamic Analysis (IDA) discussed in the Chapter 2, and as shown in Figure 4-5. The Peak Ground Acceleration (PGA) of the DBE and MCE were taken as 0.4g, and 0.8g respectively. The first 20sec of each earthquake that contains the critical part of each record was used for the PD tests. The two records were connected together with 5sec of zero acceleration data between them. In this way, the residual drift could be measured after each record.

Based on work described in Chapter 3, the time step (Δt) for the numerical integration with the PD algorithm as well as the input earthquakes were chosen as 0.03 sec.

4.3 Test Results

4.3.1 Cyclic Loading Test

The fundamental seismic performance results of the DAD pier tested using a bi-directional loading protocol shown in Figure 4-6, are presented in Figure 4-7 in the forms of (a) the bi-directional drift orbit; (b) the lateral load and drift relationship; and (c) the bi-directional load orbit. The Clover Leaf Loading Path has eight loading loops (leaves), distributed evenly in all quadrants. The results show that the DAD pier behaved mostly elastically. The small degree of hysteretic behaviour in both EW and NS directions is attributed to a combination of friction and partial dissipator yielding. An important feature is that no residual drift was observed. Figure 4-7 (c) shows that the shape of lateral load orbit mostly resembles the shape of the imposed drift orbit.

4.3.2 Pseudo-Dynamic Test

Two PD tests were carried out to establish the seismic performance of a DAD pier (SP-4) first without and then second with the energy dissipaters under bi-directional

earthquake attack. Results of both tests are presented respectively in Figure 4-8 and Figure 4-9 in the following forms: (a) the orbit of response drift; (b) load-displacement hysteresis curves; and (c) the time-history of response drift in accordance with the aforementioned two sequential earthquakes.

The hysteresis curves (b)-EW and (b)-NS in Figure 4-8, of the first test without the energy dissipaters, exhibited good self-centering characteristics of the DAD pier in both directions. As expected, and by design, no residual drift was observed. An interesting reverse looping effect is observed. This shape is attributed to a simultaneous bi-directional load interaction effect. This effect tends to reduce the lateral load capacity in a direction affected by the interaction from the simultaneous orthogonal movement, as shown in Figure 4-8 (b)-EW at approximately -3% drift.

As can be observed in Figure 4-8 (c), the maximum drifts in both EW and NS direction for EQ1 were 2.1% and 1.5% at 6.45sec and 14.2sec respectively. The lateral forces in both EW and NS direction corresponding to the maximum drift were 89.4kN and 68.7kN respectively.

The maximum drifts in both directions for EQ2 were 3.6% and -2.9% at 36.42 and 37.59sec respectively. The lateral loads measured at the maximum drift were 90.1kN and -63.9kN, respectively. Figure 4-8 (d) shows a photograph of entire specimen, while Figure 4-8 (e) presents a photograph of the pier base (shoe block) at -2% in both EW and NS directions approximately at 38sec.

Several small flexural cracks in the middle of the pier were observed during EQ2 but these cracks closed and were invisible by the end of the test. Within the Shoe Block, several minor diagonal cracks were observed at the end of the test.

Figure 4-9 presents the results of the second PD test, which was carried out after the energy dissipaters were installed into the Shoe Block of the specimen. The hysteresis curves,

shown in Figure 4-9 (b) and (c) indicate that the self-centring function of this DAD pier worked successfully with no residual drift at the end of testing. Some simultaneous bi-directional interaction effects were also observed in the EW directional behaviour at approximately -3% drift.

Maximum drifts in the EW direction for both EQ1 and EQ2 were observed at 1.8% and 2.8% at the times of 6.48sec and 36.39sec respectively. The lateral loads corresponding to the maximum drifts were 85.6kN and 93.4kN respectively. Due to the presence of the dissipators, the maximum drift values for each EQ were reduced by 14% and 20% of the corresponding values observed during the first test.

The maximum drift in each direction was identified as -1.5% and -3.0% at the time of 19.05 and 37.6sec respectively. The lateral load values corresponding to the maximum drift were -66.5kN and -72.2kN respectively.

Due to the presence of the dissipators, the maximum lateral load (when the maximum drift was observed) increased from 63.9kN to 72.2kN; 13.0% greater than in the first test where no dissipators were present.

The photograph in Figure 4-9 (d) shows an installed energy dissipater in the Shoe Block, while the photograph in Figure 4-9 (e) shows the uplift effect at -3% drift in both EW and NS directions approximately at 39sec.

4.3.3 Comparison with the New Zealand Code-designed ductile bridge pier

The comparisons of (a) the hysteresis curves, (b) the orbit of the drifts and (c) the time history of the drifts of the two contrasting bridge piers are graphically presented in Figure 4-10. The New Zealand pier was designed with the same lateral load demand (1062kN for the prototype) as the DAD pier, with the design details as described in Chapter 3.

From the hysteresis curve comparison (Figure 4-10 (a)), it can be observed that the lateral load strength varied considerably, although the maximum response drift did not differ significantly. For the first EQ, maximum drift of 1.8% and 1.6% were observed for the DAD and ductile designs, respectively; that is a 10% increase in the case of the rocking details which may be attributed to less strength and damping of the DAD specimen. However, the lateral load for the DAD specimen was 85.6kN, which is 45% smaller than that of the New Zealand pier specimen (155kN). During EQ2, the maximum drift of the DAD pier was 3.0%, which was 20% larger than that of the New Zealand pier (-2.48%). The lateral load (93.4kN) of the DAD pier at the time of maximum drift, was smaller by 33.7% than the New Zealand pier value (-141kN).

Figure 4-9 (b) presents the drift orbits. Somewhat differently, there is a clear NE-SW bias in the movement of both piers.

The time history of the drift in the principal (EW) direction shows again that the residual drift of the DAD pier was negligible, whereas a residual drift of -0.25% was observed for the New Zealand pier. The natural periods of the DAD pier after EQ1 and EQ2, obtained from the drift time history, were 1.29sec and 1.38sec respectively. The natural period of the New Zealand pier after EQ1 and EQ2 increased from 0.99 to 1.32sec. The period lengthening of the New Zealand pier is an indicator of the hysteretic damage that took place.

4.4 Conclusions

Based on the experimental investigation reported herein, the following conclusions are drawn:

1. Using rocking columns with armoured rocking surfaces provides protection against seismically induced damage. Hence a Damage Avoidance Design philosophy can be used instead of the customary ductile design.

2. For a similar design load basis, the damping and overstrength will be less for a DAD column, when compared to its ductile counterpart. Therefore, slightly larger displacements may be expected. This can be partially mitigated by providing supplementary energy dissipating devices.
3. A principal advantage of DAD is that no residual drift occurs, thus post-earthquake serviceability of the highway bridge can be maintained.

4.5 References

Chopra K.A., 2000, *Dynamics of structures (second edition)*, Prentice Hall, New Jersey

Housner, G.W., 1963, *The Behaviour of Inverted Pendulum Structures During Earthquake*, Bulletin of the Seismological Society of America, vol. 53, No. 3, pp. 403-417

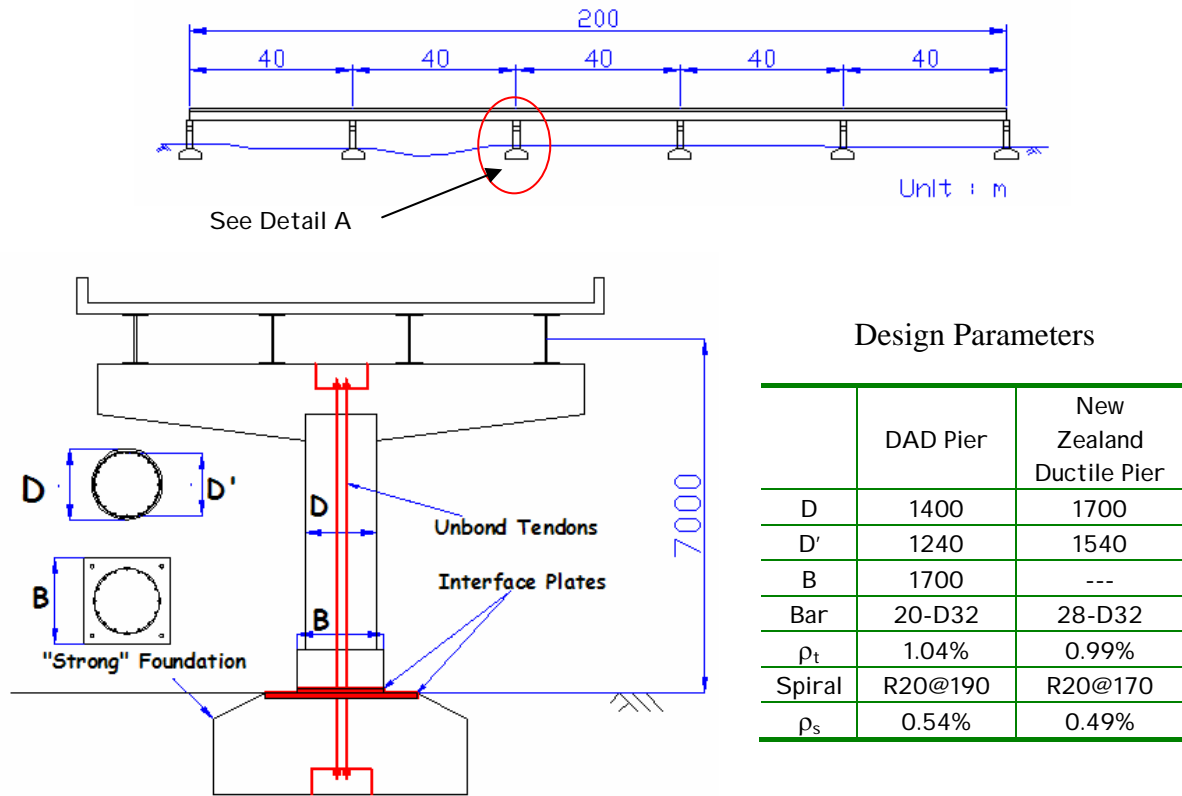
Mander J.B., Cheng C-T., 1997, *Seismic Resistance of Bridge Piers Based on Damage Avoidance Design*, National Centre for Earthquake Engineering Research, Technical Report NCEER-97-0014, December 10

Skinner R.I., Robinson W.H., and McVerry G.H. 1993, *An Introduction to Seismic Isolation*, J. Wiley and Sons, England

Takanashi K., Udagawa M., Seki M., Okada T., and Tanaka H., 1975, Nonlinear earthquake response analysis of structures by a computer-actuator on-line system, *Bulletin of Earthquake Resistant Structure Research Centre & Institute of Industrial Science*, University of Tokyo, Tokyo, Japan

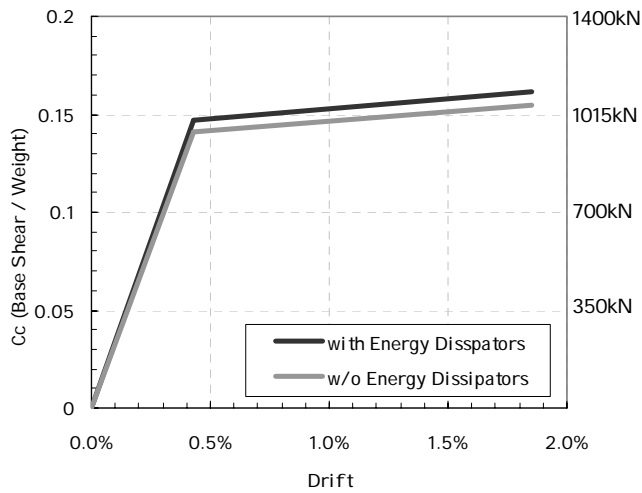
Tanabe, T., 1999, *Comparative Performance of Seismic Design codes for Concrete Structures*, Vol. 1, Elsevier, New York

4.6 Tables and Figures for Chapter 4

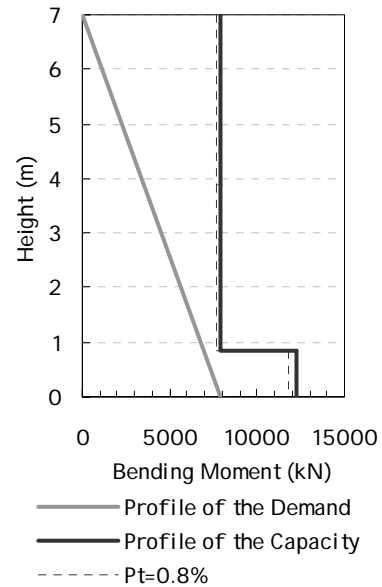


Detail A

(a) Prototype DAD Bridge

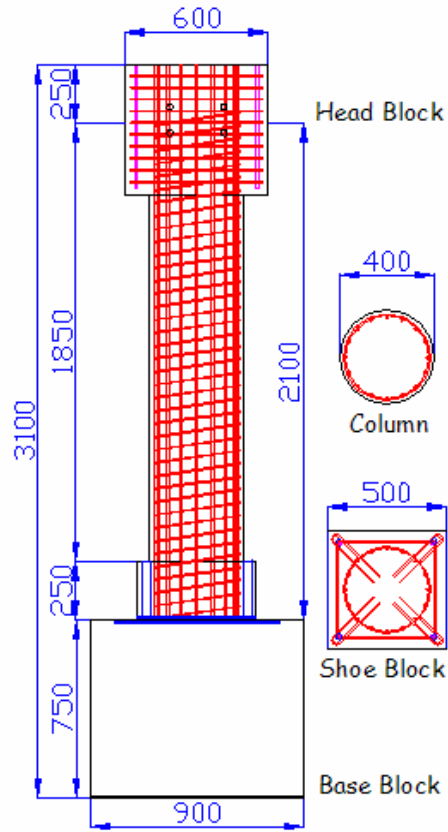


(b) Push-over Curves

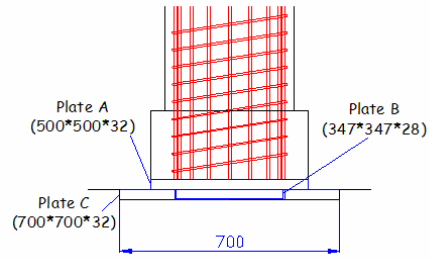


(c) Bending Moment Profile

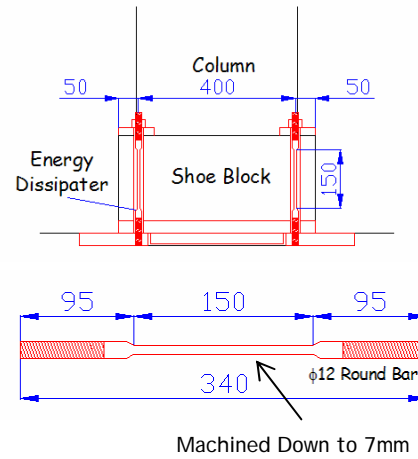
Figure 4-1 Prototype DAD Bridge Pier for the Pseudodynamic Experimentation



(a) Reinforcement Arrangement



(b) Interface Plates Arrangement



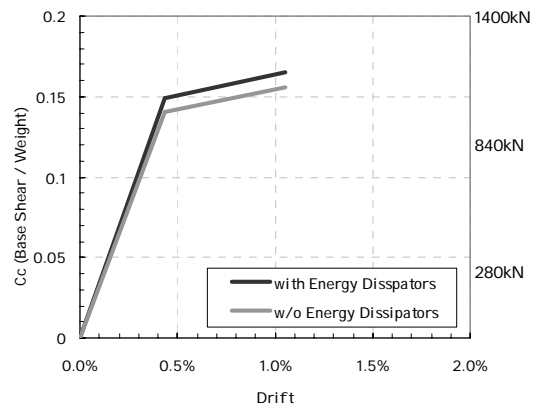
(c) Energy Dissipater Detail

(d) Specimen Dimensions

	Code	Unit	DAD
Diameter	D	mm	400
Gravity Load	P	kN	630
Main Bars			16-D10
	ρ_t	%	1.00
Spirals			R6@55
	ρ_s	%	0.60

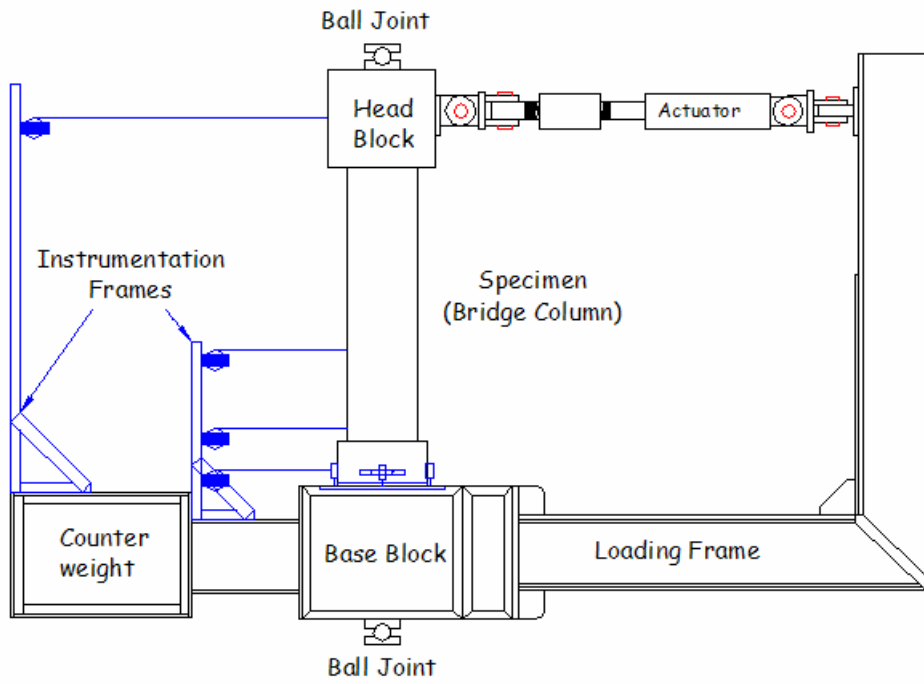
(e) Measured Material Properties

	Code	Unit	DAD
Concrete	f'_c	MPa	70.6
Main Bars	f_{ym}	MPa	539
	f_{um}	MPa	677
	ϵ_{sh}	%	1.8
	ϵ_{su}	%	14.6
Spirals	f_{ym}	MPa	461
	f_{um}	MPa	633
	ϵ_{sh}	%	1.4
	ϵ_{su}	%	19.6

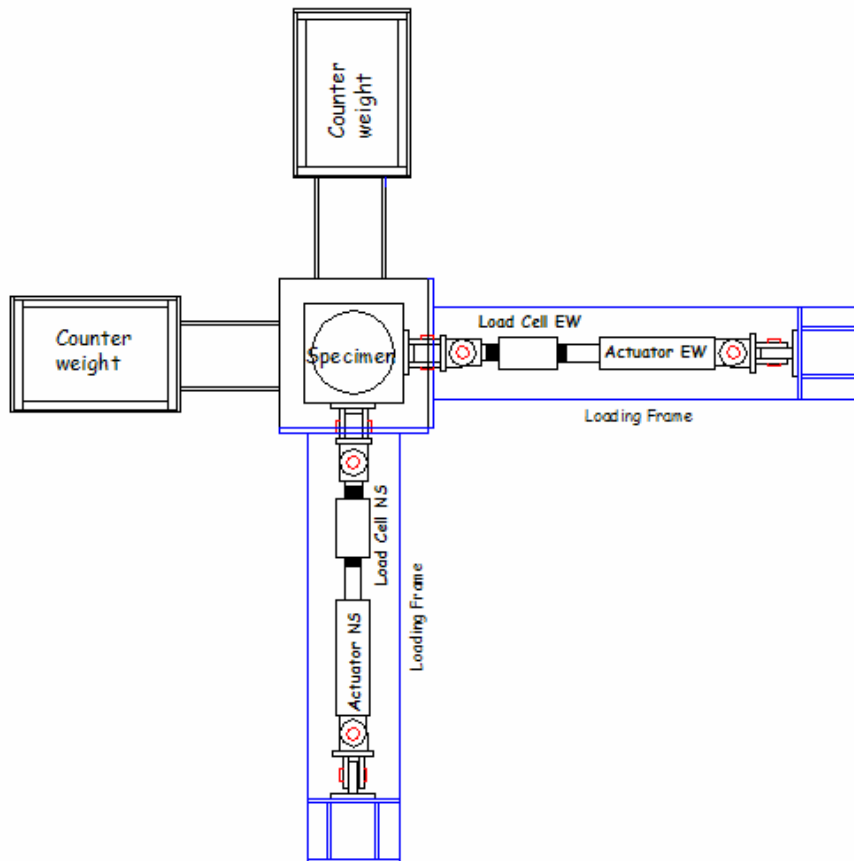


(f) Theoretical Push-over Curve

Figure 4-2 Dimensions and Properties of the DAD specimen



(a) Physical Setup (Elevation View)



(b) Physical Setup (Plan view)

Figure 4-3 Experimental Setup

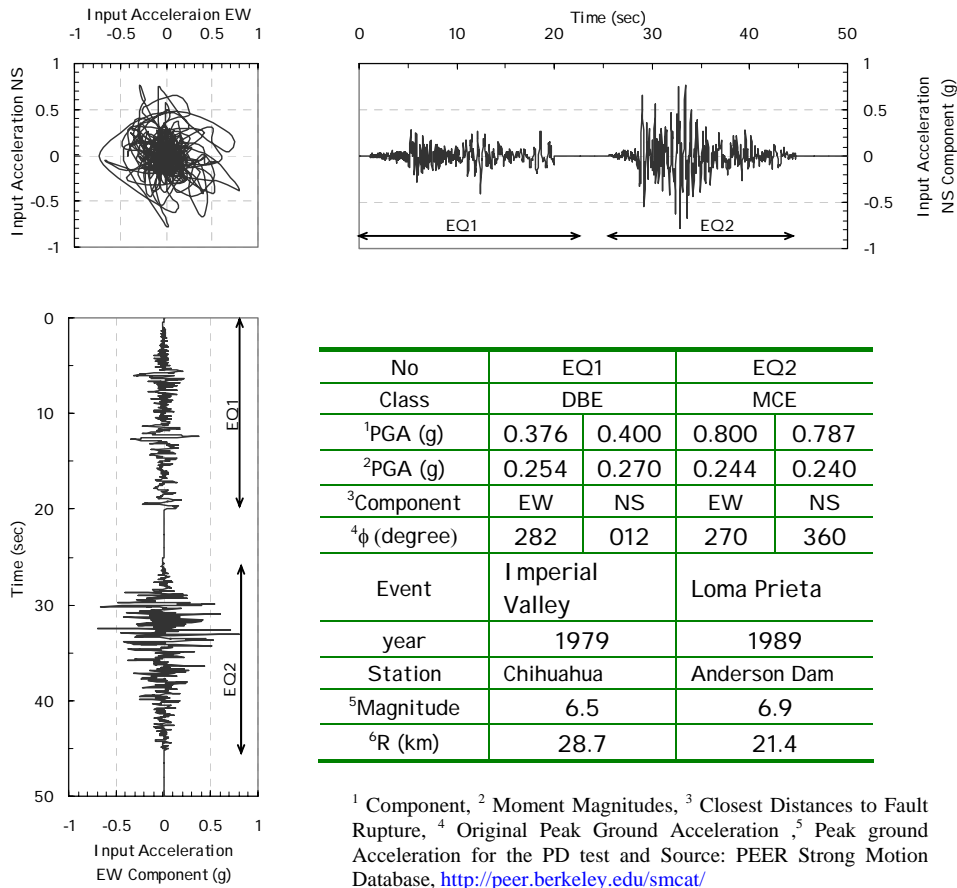


Figure 4-5 Input Acceleration of each component for bi-directional Pseudodynamic test

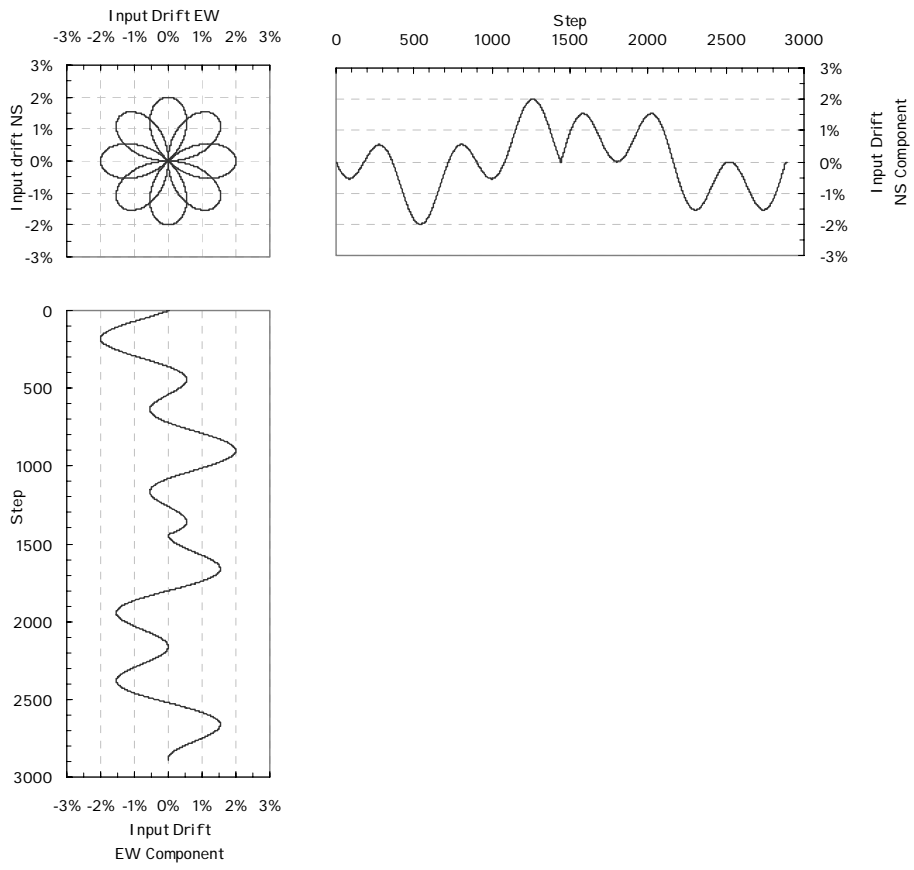


Figure 4-6 Input drift for bi-directional cyclic loading test

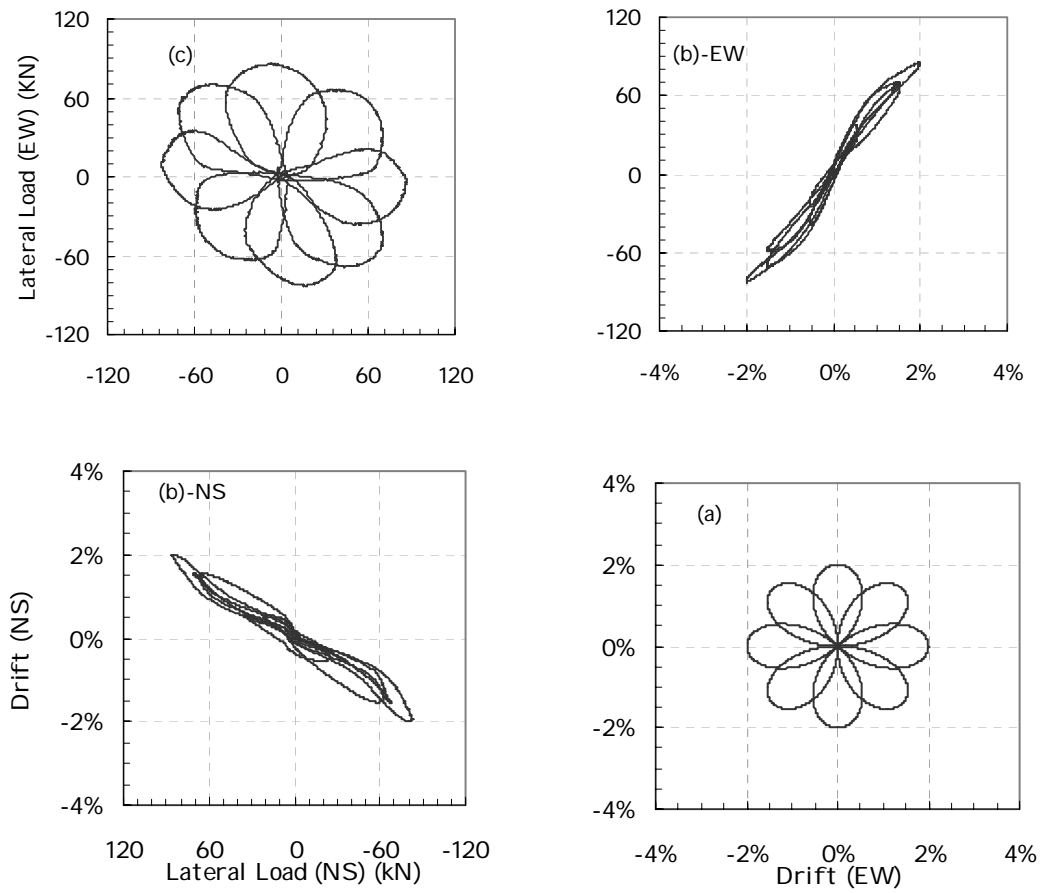


Figure 4-7 Cyclic Loading Test-2 showing (a) Plan view of bi-directional drift orbit; (b) Load Displacement Curve; and (c) Plan view of bi-directional load orbit.

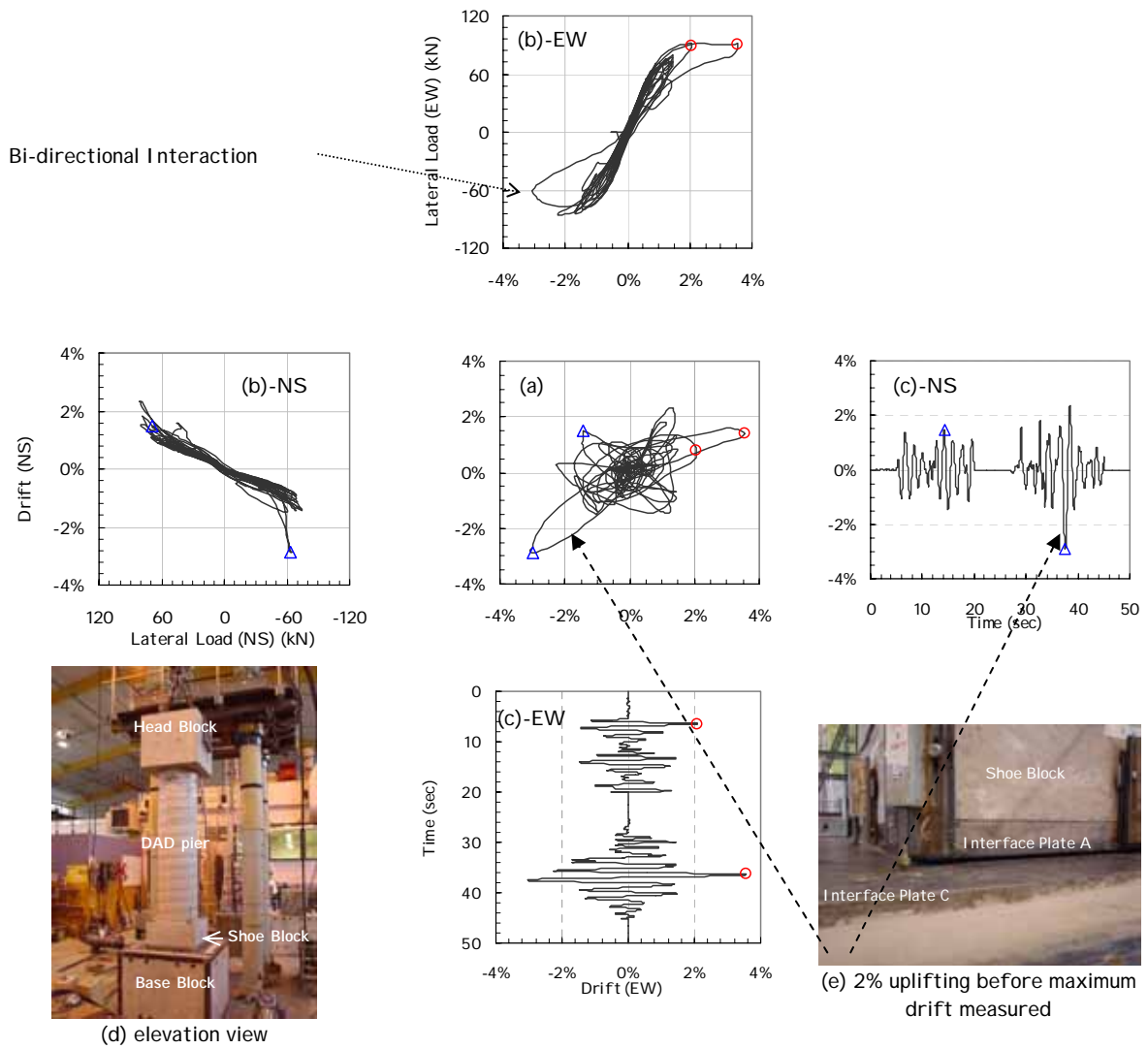


Figure 4-8 Experimental Results of the Seismic Performance of DAD Pier (SP-4) showing (a) Plan view of bi-directional drift orbit; (b) Load Displacement Curve; (c) Time History of the Drift; and Photographs (d) and (e) showing the elevation view and the Shoe Block rocking at 2% drift.

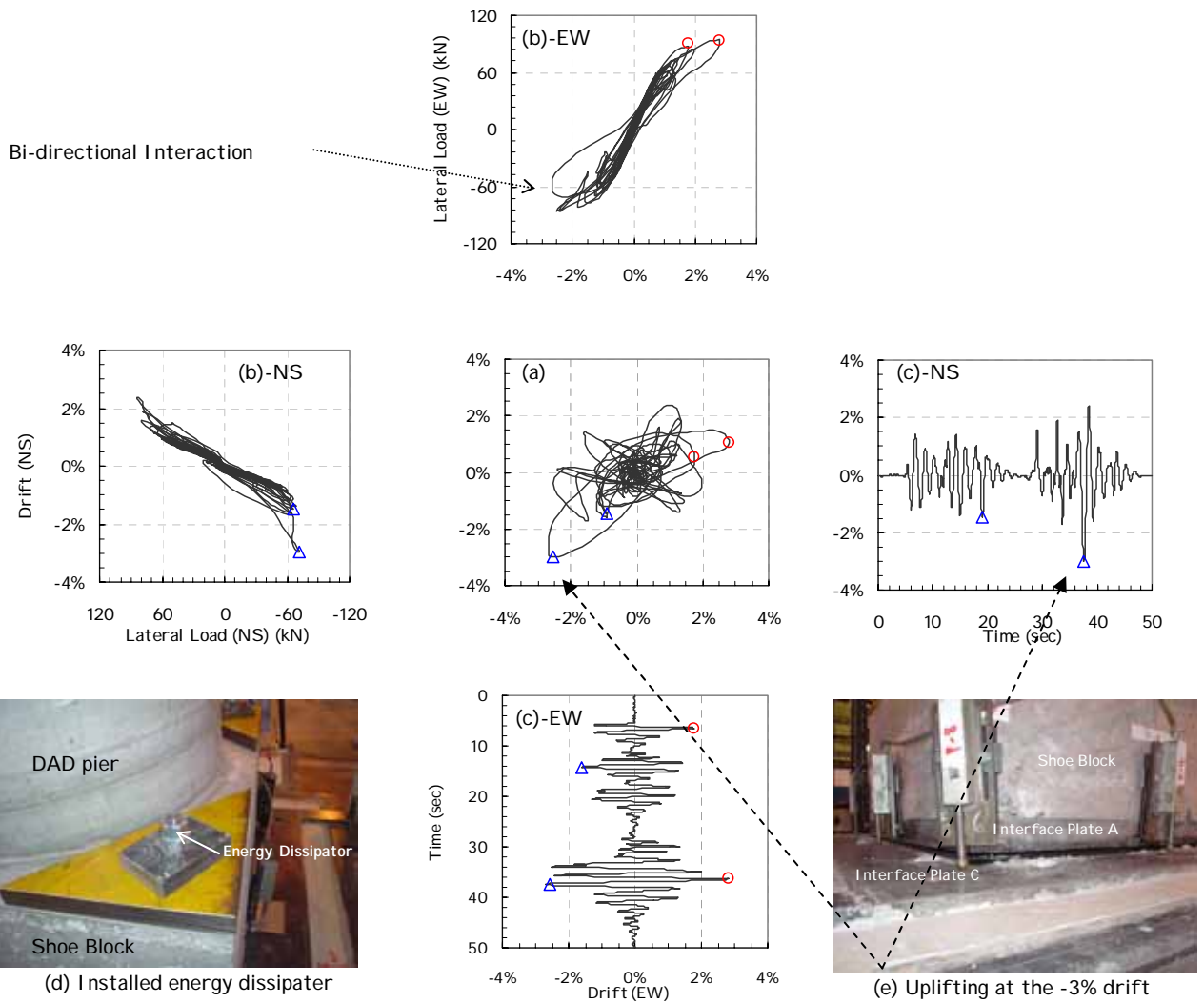


Figure 4-9 Seismic performance with energy dissipaters showing (a) Plan view of bi-directional drift orbit; (b) Load Displacement Curve; (c) Time History of the Drift; and photographs (d) and (e) showing the energy dissipater and the Shoe Block uplifting at 3% respectively.

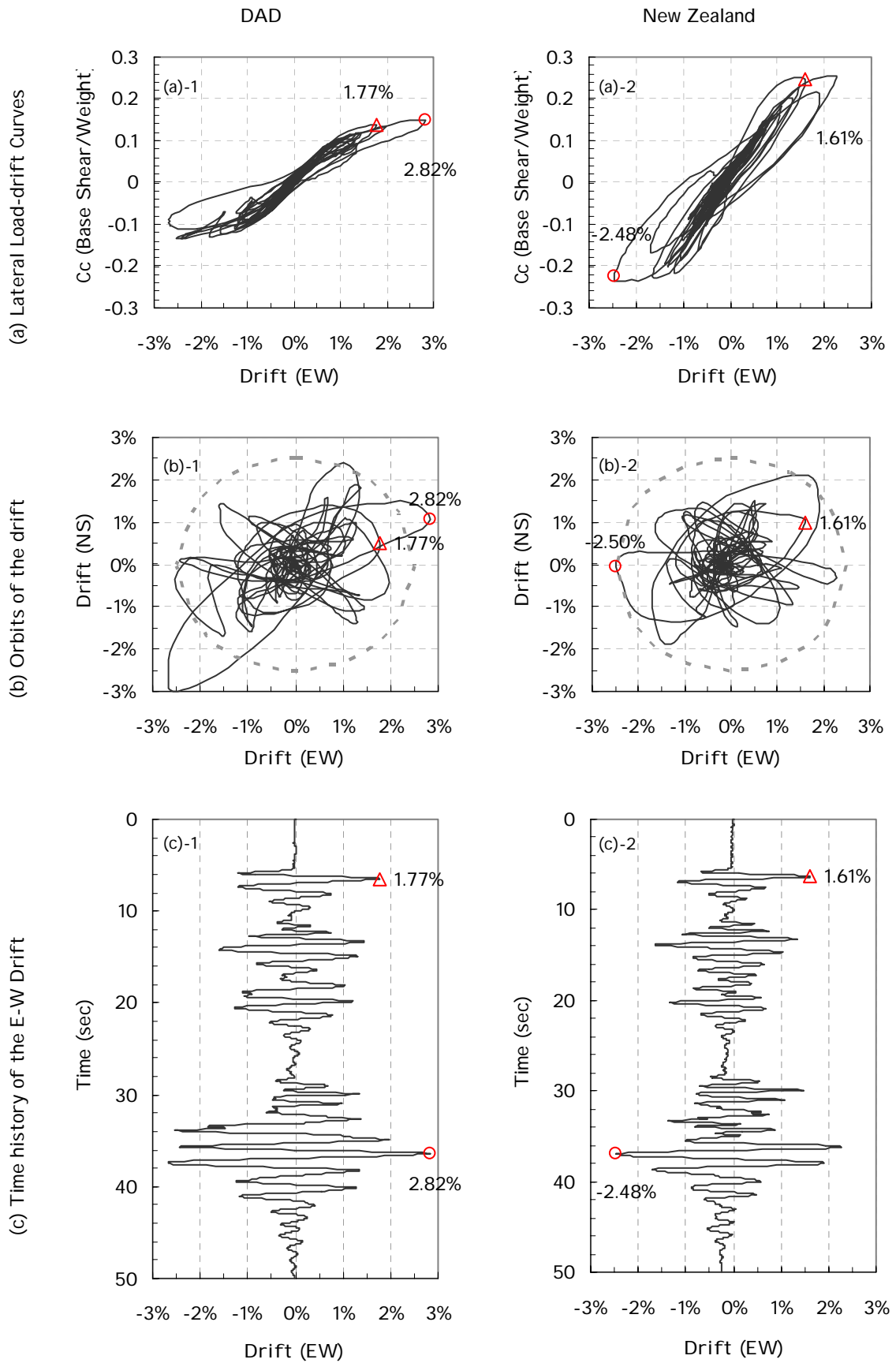


Figure 4-10 Response comparison with the New Zealand Bridge Pier

5 CONCLUSIONS AND RECOMMENDATIONS

5.1 *Research Summary*

Inelastic Dynamic Analysis (IDA) procedures were advanced and then applied to a quantitative risk assessment for bridge structures. This was achieved by combining IDA with site-dependent hazard-recurrence relations and damage outcomes. The IDA procedure was also developed as a way to select a critical earthquake motion record for a one-off destructive experiment.

Three prototype bridge substructures were designed according to the loading and detailing requirements of New Zealand, Japan and Caltrans codes. From these designs 30 percent reduced scale specimens were constructed as part of an experimental investigation. The Pseudodynamic test method was then used to conduct bi-directional experiments on the three specimens using the identified critical earthquake records. The results were presented in a probabilistic risk-based format. The seismic performance differences among the three different countries design codes were examined.

Each of these current seismic design codes rely on ductile behaviour of bridge substructures. Seismic response is expected to be resulting damage may impose post-earthquake serviceability. To overcome this major performance shortcoming, the seismic behaviour under bi-directional lateral loading was investigated for a bridge pier designed and constructed in accordance with Damage Avoidance principal. Due to the presence of steel armoured rocking interface at the base, it was demonstrated that damage could be avoided, but due to the lack of hysteresis it was necessary to add some supplemental damping. Experimental results of the armoured rocking pier under bi-directional loading were compared with a companion ductile design specimen.

5.2 Conclusions

Based on this theoretical development and experimental investigation reported herein, the following principal conclusions are drawn:

1. Seismic Risk Assessment (SRA) methodology was developed by integrating probabilistic recurrence relations with and advanced IDA procedures. Thus based on given level of hazard exposure it is possible to assess the damage outcome for a prescribed degree of confidence.
2. Using the developed SRA methodology, studies on the behaviour of design to New Zealand, Japan and Caltrans specifications were carried out both analytically and experimentally. Results show that for each of the three countries owner can clarify a high degree of confidence in the performance under DBE where only slight damage is expected along with a rapid return to service. However, under MCE events there is a reasonable (30%) chance that irreparable damage or collapse may occur.
3. Damage Avoidance Design of bridge piers offers several advantages. As demonstrated in the experiments the DAD pier performed well under both DBE and MCE, neither damage nor residual drift was identified. The DAD pier had only 65 percent of the strength of the companion New Zealand designed bridge pier, but showed that although the drifts were some 15 percent greater there was no damage that would lead to loss of amenity of the structure. Thus, in terms of the superior post-earthquake serviceability along with the economical benefits gained from pre-casting and rapid construction, DAD of bridge piers has considerable promise.

5.3 Recommendations for Future Research

Based on the study presented herein, the following topics are recommended for future research.

1. The SRA methodology developed herein was applied to single degree freedom bridge systems. It would be of interest to extend the approach to the more complex structures such as multi-storey buildings or bridge with variable spans and piers heights and other multi degree of freedom structures with stiffness, strength and mass eccentricities.
2. The columns were designed for a DBE with $PGA=0.4g$. This was a single level design process, and it became evident that the high damage outcomes for the MCE are not desirable. Therefore, it would be interesting to repeat this study where a earthquake design is used whereby no collapse could be ensured for MCE.
3. It would be interesting to repeat the experiments where the vertical component of earthquake ground motion was used in conjunction with near field earthquake effect.
4. It became evident from the present experiment the DAD column that there was a lack of diagonal reinforcing within the shoe block of the column specimen. It would be interesting to repeat this experiment with this deficiency corrected.

Appendix A – Spread Sheet for Spiral Designs

Spiral Reinforcing Arrangement Design

NZS										
Summary of the shear strength										
Demand of the Proto type										
		N*=0.8Wt			N*=1.3Wt					
V _u =		1856	kN		2131	kN				
Capacity of the proto type										
		0.8Wt			1.3Wt					
V _c =		659	kN		1893	kN				
V _s =		2798	kN		2798	kN				
V _n =		3457	kN		4691	kN				
Capacity of the circular type										
		0.8Wt			1.3Wt					
V _c		342	kN		1399	kN				
V _s		2347	kN		2347	kN				
V _n		2689	kN		3746	kN				
Calculation sheets										
1. Sheer strength										
		0.8Wt			1.3Wt					
*	V _c =	342	kN		1399	kN				
	v _c =	0.17			0.68					
	v _b =	0.65								
*	p _w =	0.006								
	f'' _c =	25								
	N* =	5909	kN		9602	kN				
	A _g =	2269801								
	V _s =	2347	kN		2347	kN				
	A _v =	628	mm ²							
	f _{yt} =	480	Mpa							
*	d=	1323	mm							
	s=	170	mm							
	V _n for	N*=0.8Wt=	2689	kN	>	1856	kN	OK !	1.45	
	V _n for	N*=1.3Wt=	3746	kN	>	2131	kN	OK !	1.76	
2-1 Minimum requirement of transvers reinforcements										
A _{sh} shall not be less than that given by the greater of Eq 8-23 or Eq. 8-26										
	A _{sh} =	-1025.387	mm ²		-678	mm ²				
		N*=0.8Wt			N*=1.3Wt					
	p _t m=	0.233								
	m=f _y /(0.85f' _c)	23.5								
	S _h h''=	263500	mm ²							
	A _g /A _c	1.2								
	f' _c /f _y	0.052								
	N*/(f'*f' _c *A _g)	0.10			0.17					
	f=	1.00								
Because A _{sh} by equation 8-26 is negative, the equation 8-23 is applied										
	A _{te} =	SA _b f _y /f _{yt} / 96*s/d _b	=	312	mm ²					
	A _b =	5630	mm ²							
ratio of the tensile rebars										
	Area of	D20	=	314	mm ²	>	312	mm ²	OK !!	1.01 <- critical !!
2-2 Vertical spacing not to exceed the smaller of h/4 or 6db										
	spacing=	170								
	limitation=	192	mm	>	170	mm	OK !!	1.13		
2-3 Horizontal spacing not exceed the larger of h/4 or 200mm										
	spacing=	170								
	limitation=	425	mm	>	170	mm	OK !!	2.50		

Summary of the shear strength

Demand of the Proto type

Vu= 4237 kN

Capacity of the proto type

Vc= 1408 kN

Vs= 3363 kN

Vyd= 4771 kN

Capacity of the circular type

Vc 1102 kN

Vs 3145 kN

Vn 4246 kN

Calculation sheets

1. shear strength

Vc= 1432 /gb= 1102 kN
 bd= 0.849
 bp= 0.959 0.45
 bn= 1.030
 Md 19986 kNm
 Nd 7556 kN
 M0 601.3 kNm
 f_{vcd}= 0.58
 b_w d= 2921286
 Vs= 3616 /gb= 3145 kN
 A_w 628
 f_{wyd} 480
 s_s 115
 z 1379
 V_{yd}= 4246 kN > 4237 kN OK ! 1.00 <--critical !!

2-1 Vertical spacing (s_v)

s_v should be smaller than 12d_b
 12d_b= 612 mm
 s_v= 115 mm < 612 mm OK !! 5.32
 s_v shall not be exceeding a 1/2 of the D
 1/2D= 1000 mm
 s_v= 115 mm < 1000 mm OK !! 8.70
 s shall be smaller than that is smaller 1/5 of d_{sp} or 80mm (especially for the spiral)
 1/5 of d_{sp}= 370 mm
 smaller value is 80 mm
 s= 115 mm > 80 mm NG 0.7

2-2 Lateral spacing (s_l) (sepecially for the rectangular shape)

s_l shall not exceeding 48d_b of trans rabar
 48d_b= 960 mm
 s_l= 1850 mm > 960 mm check only the rectangular cases

Summary of the shear strength

Demand of the Proto type (Nominal Shear strength) $V_u < F V_n$ $V_u = 3385$

$V_n = 3982$ kN $f = 0.85$

Capacity of the proto type (from the book)

	general	(end)	hinge
V_c	2888	1644	1644
V_s	3869	5860	6461
V_n	6757	7504	8105

Capacity of the circular type

	general	(end)	hinge
V_c	3327	1899	1899
V_s	2757	4030	6163
V_n	6084	5929	8062

Calculation sheets

1-1 shear strength (carried by concrete)

general region

$V_c = 3327$ kN 747815 lbf
 $P_e = 7386$ kN 2E+06 lbf
 $A_g = 3141593$ mm² 5027 inch²
 $F'_c = 32.5$ Mpa 4714 lbf/inch²
 $A_e = 2921286$ mm² 4674 inch²

end region

$V_c = 1899$ kN 426911 lbf
 $P_e = 7386$ kN 2E+06 lbf
 $A_g = 3141593$ mm² 5027 inch²
 $F'_c = 32.5$ Mpa 4714 lbf/inch²
 $A_e = 2921286$ mm² 4674 inch²

1-2 shear strength (carried by rebars)

General region

$A_v = V_s * s / f_y h / d = 612$ mm²
 $V_s = f_0 * V_n - V_c = 2687$ kN
 $f_y h = 1.1 f_y = 528$ Mpa
 $s = 190$ mm
 $d = 1579$ mm
 $A_h = 628$ mm² > 612 mm² OK !! 1.03
 $V_s = A_h * f_y h * d / s = 2757$ kN

End region

$A_v = V_s * s / f_y h / d = 613$ mm²
 $V_s = f_0 * V_n - V_c = 3932$ kN
 $f_y h = 1.1 f_y = 528$ Mpa
 $s = 130$ mm
 $d = 1579$ mm
 $A_h = 628$ mm² > 613 mm² OK !! 1.02
 $V_s = A_h * f_y h * d / s = 4030$ kN

Hinge region

$A_v = V_s * s / f_y h / d = 401$ mm²
 $V_s = f_0 * V_n - V_c = 3932$ kN
 $f_y h = 1.1 f_y = 528$ Mpa
 $s = 85$ mm
 $d = 1579$ mm
 $A_h = 628$ mm² > 401 mm² OK !! 1.57
 $V_s = A_h * f_y h * d / s = 6163$ kN

2-1 Verification of minimum reinforcement									
Av>(50bw*s)/fyh (lb, in)									
*	b _w	1850	mm		72.8	inch			
	f _{yh}	528	MPa		76580	lbf/inch ²			
General rigion									
	s	190	mm		7.48	inch			
*	Av=50b _w *s/f _{yh}	229	mm ²		0.356	inch ²			
	A _h	628	mm ²	>	229	mm ²	OK !!	2.74	
End region									
	s	130	mm		5.12	inch			
	Av=50b _w *s/f _{yh}	229	mm ²		0.36	inch ²			
	A _h	628	mm ²	>	229	mm ²	OK !!	2.74	
Hinge rigion									
	s _t	85	mm						
	h _c	1850	mm						
	f' _{ce} =1.3f' _c	31.2	MPa						
	f _{ye} =1.1f _y	528	MPa						
	P	7386	kN						
	A _g	3E+06	mm ²						
	r _i =r _t	1.34%							
	A _{sh}	628	mm ²						
	A _h	628	mm ²	>	628.1	mm ²	OK !!	1.00	<----- critical !!
2-2 Assessment of maximum reinforcement									
V _s <8*f' _c ^{0.5} *b _w *d									
*	b _w d=	3E+06	mm ²		4528	inch ²			
	f _{yh} =	528	MPa		76580	lbf/inch ²			
	f' _c =	24	MPa		3481	lbf/inch ³			
	Limitaion	9507	kN		2E+06	lbf			
General region									
*	V _s =A _h *f _{yh} *d/s	2757	kN	<	9507	kN	OK!!	3.45	
End Rigion									
	V _s =A _h *f _{yh} *d/s	4030	kN	<	9507	kN	OK!!	2.36	
Hinge rigion									
	V _s =A _h *f _{yh} *d/s	6163	kN	<	9507	kN	OK!!	1.54	
2-3 Verification of minimum spacing of trans. reinforcement									
	s1=0.2b _w or 0.2h	400	mm						
	s2=6db	246	mm						
	s3=20cm(8inch)	203	mm						
General									
	min(s1,s2,s3)	203	mm	>	190	mm	OK!!	1.07	
End									
	min(s1,s2,s3)	203	mm	>	130	mm	OK!!	1.56	
Hinge rigion									
	min(s1,s2,s3)	203	mm	>	85	mm	OK!!	2.39	

The initial conditions for spiral calculations

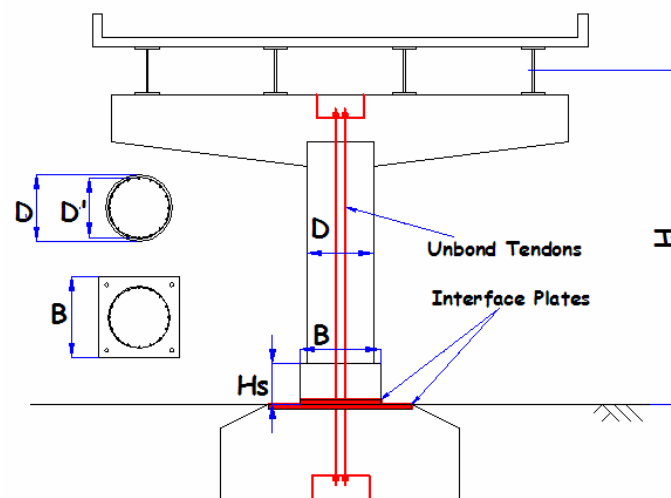
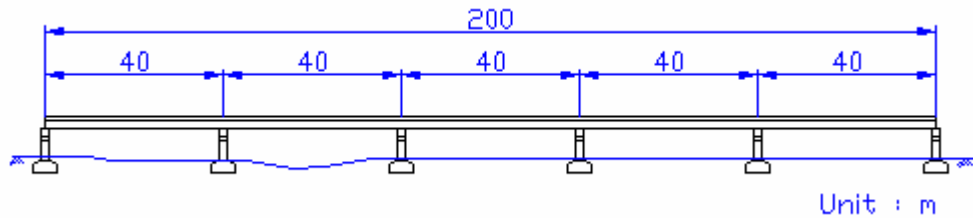
1. Prototype (square section by Tanabe et al (1999 and 2000))								
				NZS	JSCE	Caltrans		
Dimensions	D		mm	1500	1800	1800		
	B		mm	1500	1800	1800		
	H		mm	7000	7000	7000		
Reinforcement	Longi.	f_y	Mpa	345	345	345		
		r_t	A_s/A_g	40 D32 1.43%	40 D51 2.52%	64 D35 1.90%		
		F_t	MN	11.1	28.2	21.2		
	Transv.			8 D13	4 D19	general region 4 D13 4 D13	end region 4 D16 4 D16	hinge region 2 D19 6 D16
		A_w	mm ²	1062	1134	1062	1608	1773
		Space	mm	180	150	150	150	150
	r_s	$A_w/b/s$	0.47%	0.47%	0.44%	0.67%	0.74%	

2. Prototype, changed to circular section								
				NZS	JSCE	Caltrans		
Dimension	D		mm	1700	2000	2000		
	H		mm	7000	7000	7000		
	Pure cover		mm	75	75	75		
Reinforcements	Longitudinal	f_y	MPa	500	500	500		
		r_t	mm ²	28 D32 0.99% 1.44%	28 D51 1.82% 2.64%	32 D41 1.34% 1.95%		
		F_t	MN	11.3 101%	28.6 101%	21.1 99%		
		Space	S/ d_b	141.9 4.4	156.6 3.1	140.6 3.4		
	Transverse	f_y	MPa	480 2 D20	480 2 D20	480 2 D20	480 2 D20	480 2 D20
		A_w	mm ²	628	628	628	628	
space		mm	170	115	190	130	85	
	r_s	V_w/V	0.49%	0.61%	0.37%	0.53%	0.78%	

3. Specimen				Scale factor =		0.3	
				PGA=400 gal			
				NZS	JSCE	Caltrans	
Dimen	D		mm	500	600	600	
	H		mm	2100	2100	2100	
	pure cover		mm	22.5	22.5	22.5	
Reinforcements	Longitudinal	f_y	Mpa	500	500	500	
		r_t	mm ²	24 D10 0.96%	24 D16 1.71%	32 D12 1.28%	
		F_t	demand	1.00	2.54	1.91	
		F_t	capacity	0.94 94%	2.41 95%	1.81 95%	
	Space	mm	48.3 4.8	54.6 3.41	41.3 3.4		
	Transverse	f_y	Mpa	480 2 R6.0	480 2 R6.0	480 2 R6.0	480 2 R6.0
space		mm	51 50	34.5 35	57 60	39 40	25.5 25
r_s		V_w/V	0.51%	0.60%	0.35%	0.52%	0.83%

Appendix B – DAD Procedure Details

1. Initial conditions



Diameter of the column	D	1,400	mm	
Height	H	7,000	mm	
Width of Shoe Block	B	1,700	mm	
Axial load by gravity	P_a	7,292	kN	by superstructure and column
Concrete strength	f'_c	50	MPa	
Tendon strength	f_{py}	900	MPa	
Reinforcing strength	f_y	500	MPa	
Moment Demand	M^*	7,436	kN m	Determined to be the same as the New Zealand Column in Chapter 3
Shear Demand	V^*	1,062	kN	

2. Design the Main System (Unbond PC tendons and Energy

Dissipators (fuse bars))

2-1 Assess the Moment Capacity, M (capacity)

Calculate the additional axial force (P_{pc} and P_f) by PC tendons and Fuse bars

Use four $\phi 24$ Thread bars with 900 MPa yield strength

$$P_{pc} = 4 * \pi * 24^2 / 4 * 900 = \underline{1,629kN}$$

Use four $\Phi 22$ threaded rod machined downed from D28 reinforcement

$$P_f = 4 * \pi * 20^2 / 4 * 300 = \underline{377kN}$$

Hence, M (capacity) = $(P_a + P_p + P_f) * (B/2)$

$$= (7,292 + 1,629 + 377) * (1,700/2)$$

$$= \underline{7,903kN m} > 7,436kN m \quad \text{--} \quad \text{OK!!}$$

2-2 Assess the Load-Displacement Performance

Calculate the force at Uplift, F_{up}

Use 50 % of Pre-stress in threaded bars,

$$P_{up} = P_a + 0.5 P_p = 7,292 + 0.5 * 1,629kN$$

$$= 8,106kN$$

$$F_{up} = P_{up} * e / H = 7,826 * (1.7 / 2) / 7.0$$

$$= \underline{984kN}$$

Calculate the displacement at Uplift, Δ_{up}

$$I_{col} = \pi / 64 * d^4 = \pi / 64 * 1.4^4 = 0.189 \text{ m}^4$$

$$f'_c = 50 \text{ MPa}, E_c = 4700 * f'_c^{0.5} = 33,234 \text{ MPa}$$

$$\text{Assume } EI_{eff} = 0.6 EI_g = 0.6 * 33,234 * 0.189 = 3,760$$

$$\Delta_{up} = \frac{F_{up} \times L^3}{3EI_{eff}} = \frac{0.984 \times 7.0^3}{3 \times 3,760} = \underline{0.0299 \text{ m (0.43\% drift)}}$$

Calculate the yield of Column, F_y , due to the fuse bars yield, P_{yf}

$$P_{yf} = P_a + 0.5P_p + P_f = 8,483 \text{ kN}$$

$$F_y = P_{yf} * e / H = 8,483 * 1.7/2 / 7.0$$

$$= \underline{1,030 \text{ kN}}$$

Calculate the maximum Displacement, D_{max} , and Force, F_{max}

$$F_{max} = M_{max}/H = (P_a+P_p+P_f)*(B/2)/H$$

$$= (7,292+1,629+377)*(1.7/2)/7.0$$

$$= \underline{1,129 \text{ kN}}$$

Calculate Δ_{pmax} due to the Elongation of the tendons at yield

$$\Delta_{pmax} = FL/EA = 0.5*P_p*H/EA$$

$$= (0.5*1,629*7.0) / (200,000*\pi/4*24^2*4)$$

$$= 0.0158 \text{ m (1.9\%)}$$

$$\Delta_{max} = \Delta_{pmax} * H / (B/2) = 0.0158*7.0/(1.7/2) = \underline{0.130 \text{ m}}$$

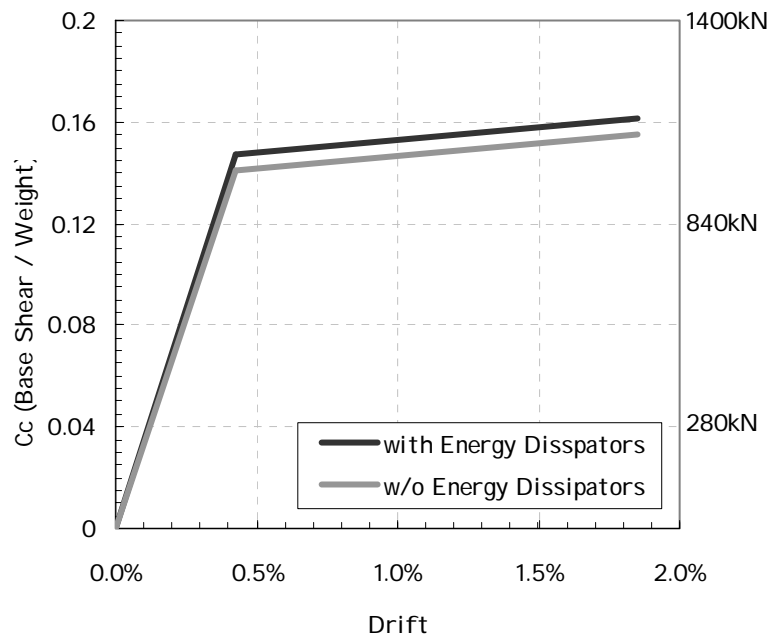


Figure 1 Push-over curves of DAD column

2. Reinforcing arrangements

2-1 longitudinal reinforcing

Calculate the range of minimum and nominal reinforcing

Check the p.s.c column for allowable stresses.

$$\text{Use } f_{t\max} = 1.0 f_c^{0.5} = 7.07 \text{ MPa}$$

$$M_{cr} = (f_{t\max} + P_{\text{total}}/A) * S_x = (7.07 + 9298 / (\pi 1.4^2 / 4)) * \pi 1.4^3 / 32$$
$$= 3,532 \text{ kN m, } (F_{cr} = 505 \text{ kN})$$

$$M_{\max} = 7,903 \text{ kN m, } (F_{\max} = 1129 \text{ kN})$$

Therefore, the nominal and minimum reinforcing range is arranged as follows;

Nominal reinforcing range is from bottom (0m) to 3.9m high

Minimum reinforcing range is from 3.9m high to the top (7m)

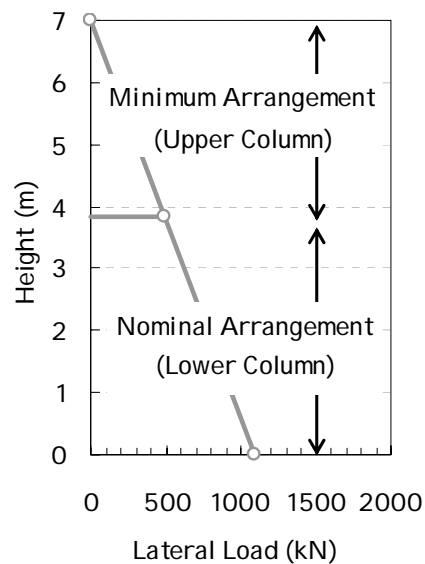


Figure 2 The range of minimum and nominal reinforcing

Calculate the reinforcing bar for each range

The reinforcing are designed according to the *New Zealand Reinforced Concrete Design Handbook* (2001), then modified, considering construction conveniences as follows;

(1) Lower column

$$M_i = 7,903 \text{ kN m}, N_i = 9,007 \text{ kN}, M_i/D^3 = 2.88 \text{ MPa} \text{ and } N_i/D^2 = 4.6 \text{ MPa}$$

According to the design chart $p_t = 1.00\%$ is required.

Therefore, use 20 of D32 rebars and $p_t = 1.04\% > 1.00\%$

The moment capacity is more than 7665kN m (1095kN)

(2) Upper column

Minimum requirement of $p_t = 0.8\%$, therefore use 16 of D32, which equivalent of $0.84\% > 0.8\%$.

The moment capacity of the upper column is 7,272 kN m (1039kN).

(3) Pedestal Base

The minimum reinforcing ratio, p_t is 0.8%, but assume to arrange 20 of D32 as same as the lower column, hence, $p_t = 0.72\%$.

$$g=0.729, N_i/D^2 = 4.6 \text{ MPa} \text{ and } M_i/D^3 = 2.88 \text{ MPa}, \text{ therefore,}$$

$$M_i = 11,791 \text{ kN m (1684kN)}$$

Then, the final reinforcing arrangements are modified by the judgments below

- ❖ The upper column reinforcing follows the lower column arrangement due to the construction consideration.
- ❖ Pedestal base (shoe block) also follows the arrangement of lower column considering construction consideration, because the capacity exceeds the demand.

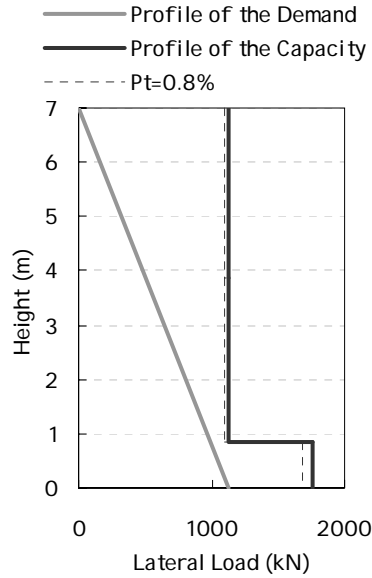


Figure 3 The lateral load profile

2.2 Spiral arrangements

See the spread sheet on the next page

3. Design of the length of the energy dissipators (L_f) and the Shoe Block Height

Assume the maximum drift of the DAD column $\theta_u=0.03$, then $\Delta_u=51$ mm.

Ultimate strain on fuse bars can be explained by $\epsilon_{su}=\Delta/L_f = \theta_u \cdot B/L_f$.

Accordingly, $L_f=\theta_u \cdot B/\epsilon_{su}$ or $L_f/B=\theta_u/\epsilon_{su}$

Assume the $\epsilon_{su} = 0.12$,

Consequently, $L_f/B=\theta_u/\epsilon_{su}= 0.03/0.12 = 0.25$

Hence, the L_f can be assumed to be 500mm




$L_f/B = 500/1700 = 0.29 > 0.25$ ----- OK!!




Subsequently, the height of pedestal base is decided as the half, 0.5, of the B

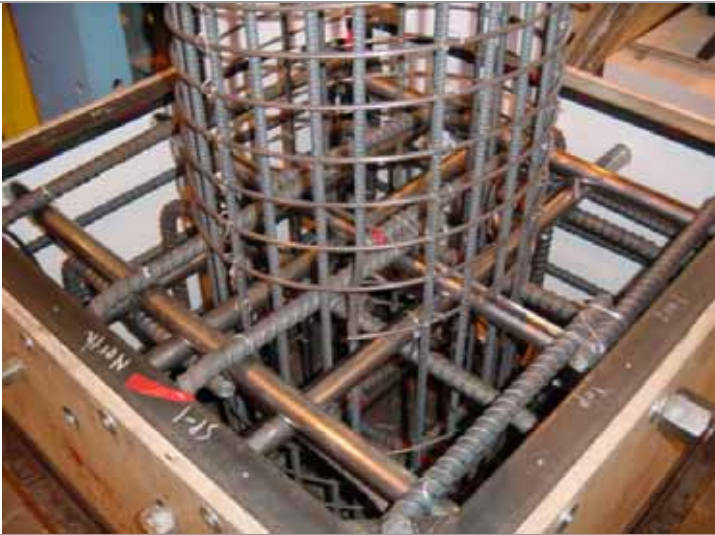
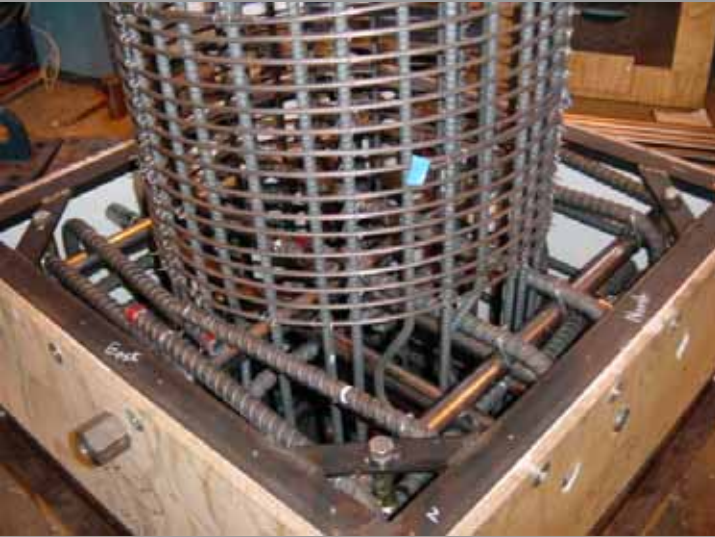

$y= 1700 \cdot 0.5 = \underline{850mm} > 500mm$ ----- OK!!

Spiral reinforcing arrangements							
Summary of the shear strength							
Demand of the Proto type							
		$N^*=0.8W_t$		$N^*=1.3W_t$			
$V_u=$		1856 kN		2131 kN			
Capacity of the circular type							
		$0.8W_t$		$1.3W_t$			
V_c		659 kN		1419 kN			
V_s		1694 kN		1694 kN			
V_n		2353 kN		3113 kN			
Calculation sheets							
1. Sheer strength							
		$0.8W_t$		$1.3W_t$			
*	$V_c=$	659.5 kN		1419 kN			
	$v_c=$	0.494		1.064			
	$v_b=$	0.857					
*	p_w	0.007					
	f''_c	40					
	N^*	7438 kN		12087 kN			
	A_g	1539380					
	$V_s=$	1694 kN		1694 kN			
	A_v	628 mm ²					
	f_{yt}	480 Mpa					
*	d	1067 mm					
	s	190 mm					
	V_n for	$N^*=0.8W_t=$	2353 kN	>	1856 kN	OK!	1.27
	V_n for	$N^*=1.3W_t=$	3113 kN	>	2131 kN	OK!	1.46
2-1 Minimum requirement of transverse reinforcement							
A_{sh} shall not be less than that given by the greater of Eq 8-23 or Eq. 8-26							
	$A_{sh}=$		-467 mm ²		131.7 mm ²		
			$N^*=0.8W_t$		$N^*=1.3W_t$		
	$p_t m=$		0.246				
	$m=f_y/(0.85f'_c)$		23.5				
	$s_h h''=$		237500 mm ²				
	A_g/A_c		1.25				
	f'_c/f_y		0.08				
	$N^*/(f'_c A_g)$		0.12		0.20		
	$f=$		1.00				
Because A_{sh} by equation 8-26 is negative, the equation 8-23 is applied							
	$A_{te}=$	$S A_b f_y/f_{yt} / 96*s/d_b$	=		249 mm ²		
	$A_b=$	4021 mm ²					
ratio of the tensile rebars							
	Area of	D20 =	314 mm ²	>	249 mm ²	OK !!	1.26
2-2 Vertical spacing not to exceed the smaller of h/4 or 6db							
	spacing=	190					
	limitation=		192 mm	>	190 mm	OK !!	1.01
2-3 Horizontal spacing not exceed the larger of h/4 or 200mm							
	spacing=	190					
	limitation=		350 mm	>	190 mm	OK !!	1.84




Appendix C – Photo Albums




Construction		
1	 A photograph showing a collection of steel reinforcing bars in a workshop. Some bars are bundled together on a hand truck, while others are laid out on the floor. The bars are arranged in various shapes, including spirals and straight lengths.	Reinforcing for the Base block and spirals
2	 A photograph showing several long, straight steel reinforcing bars laid out on a concrete floor. The bars are arranged in a parallel fashion, showing their length and thickness.	Longitudinal bars
3	 A photograph showing a large, rectangular concrete base block in a workshop. The block is surrounded by various tools, equipment, and materials. The workshop environment is visible in the background, including workbenches and structural elements.	The Base Block for DAD Pier (SP-4)




Construction		
4		Reinforcing arrangement for (SP-1)
5		Reinforcing arrangement of SP-1, 2 and 3
6		Reinforcing arrangement of SP-1, 2 and 3

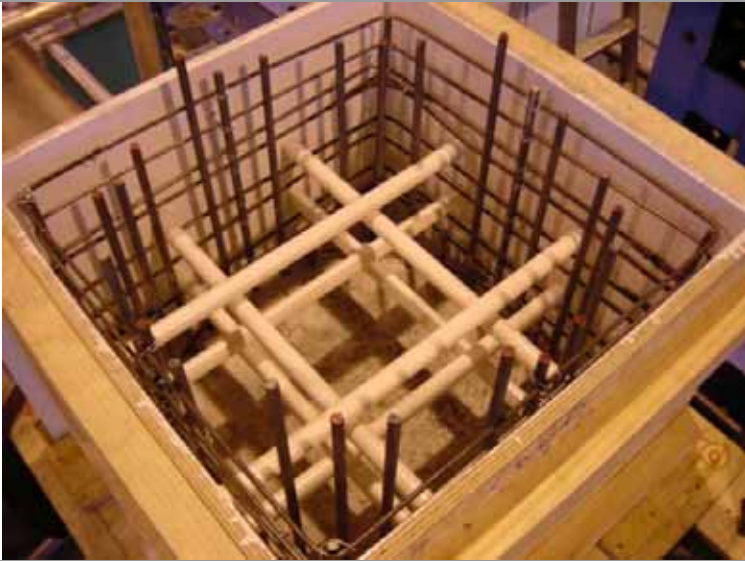


Construction		
7	 A photograph showing the construction of a cylindrical concrete structure. The structure is formed within a wooden formwork. The reinforcement consists of a dense grid of vertical and horizontal steel bars. The vertical bars are spaced closely together, and the horizontal bars are also closely spaced, creating a mesh-like structure. The formwork is made of light-colored wood and is bolted together. A red-handled tool is visible near the bottom left corner of the formwork.	Reinforcing bars (SP-1)
8	 A photograph showing the construction of a cylindrical concrete structure, similar to the previous one. The structure is formed within a wooden formwork. The reinforcement consists of a dense grid of vertical and horizontal steel bars. The vertical bars are spaced closely together, and the horizontal bars are also closely spaced, creating a mesh-like structure. The formwork is made of light-colored wood and is bolted together. A blue-handled tool is visible near the bottom left corner of the formwork.	Reinforcing bars (SP-2)
9	 A photograph showing the construction of a cylindrical concrete structure, similar to the previous ones. The structure is formed within a wooden formwork. The reinforcement consists of a dense grid of vertical and horizontal steel bars. The vertical bars are spaced closely together, and the horizontal bars are also closely spaced, creating a mesh-like structure. The formwork is made of light-colored wood and is bolted together. A red-handled tool is visible near the bottom left corner of the formwork.	Reinforcing bars (SP-3)




Construction		
10		Concrete pouring for the Base Block
11		Concrete pouring for the Base Block
12		Concrete pouring for the Base Block




Construction		
13	 A cylindrical metal reinforcing cage for pier SP-2, mounted on a wooden base. A white label is attached to the cage.	The pier reinforcing (SP-2)
14	 A cylindrical metal reinforcing cage for pier SP-3, mounted on a wooden base. A white label is attached to the cage.	The pier reinforcing (SP-2)
15	 A cylindrical metal reinforcing cage for pier SP-3, mounted on a wooden base. A white label is attached to the cage.	The pier reinforcing (SP-3)




Construction		
16	 <p>A photograph showing the reinforcing arrangement for the Shoe Block of SP-4. A pink sign is placed on top of the rebar cage. The sign reads: "SP-4", "Damage Avoidance Design", "Ø 400", "16-D10", and "R6@55". The rebar cage is a cylindrical structure with vertical longitudinal bars and horizontal spiral bars, sitting on a wooden base.</p>	Reinforcing arrangement for the Shoe Block of SP-4
17	 <p>A photograph showing the process of pouring concrete for the Shoe Block. The rebar cage is now partially filled with concrete, and the concrete is being poured from a height into the center of the cage. The wooden formwork is visible around the base.</p>	Pouring concrete for the Shoe Block
18	 <p>A photograph showing the longitudinal reinforcement for the SP-4. The rebar cage is now fully filled with concrete, and the longitudinal bars are clearly visible. The wooden formwork is visible around the base.</p>	Longitudinal Reinforcement for the SP-4


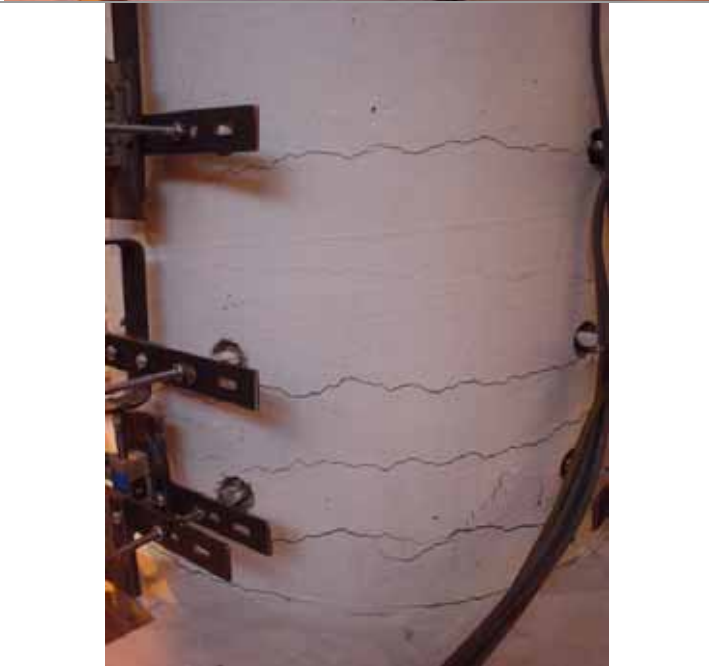
Construction		
19		The formworks for the Piers
20		The formworks for the DAD pier
21		The threaded bars for the curvature measurement inside cardboard tube




Construction		
22		bar arrangement for the Head Block
23		The top plate for the Head block
24		The formworks for the Head Blocks



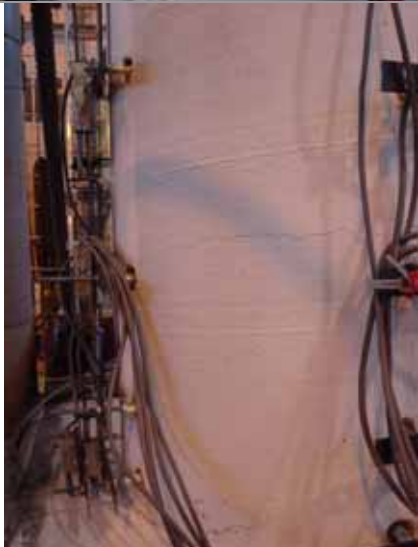
Construction		
25		The completion of the construction of SP-1, 2 and 3
26		The completion of the construction of SP-4, 2, 3 and 1 (front to backward)
27		After white painting of SP-1, 3 and 2 (from front raw)

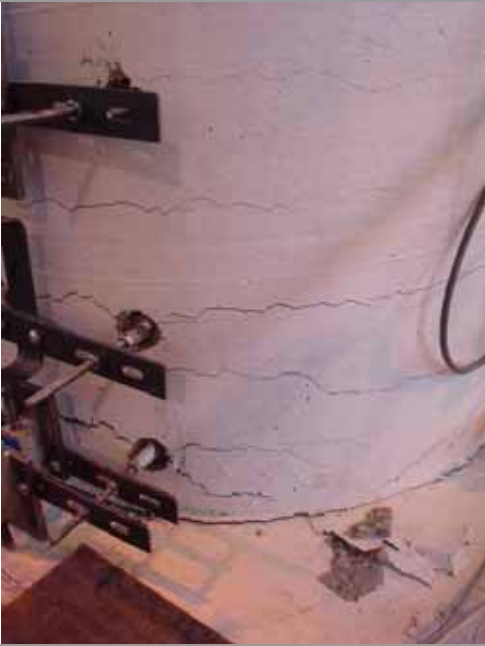


Setup		
28		The ball joint at the bottom
29		The ball joint at the top
30		Control PC and Data acquisition PC


Setup		
31		<p>The rams arrangement from the South West</p>
32		<p>The hydraulic controller</p>
33		<p>Whole setup view</p>




	SP-1	
34		Instrumentation
35		during EQ1 DBE
36		during EQ2 MCE




SP-1		
37		Spalling
38		Buckling
39		Initial fracture




	SP-2	
40		Instrumentation
41		during EQ1 DBE
42		during EQ2 MCE1

		SP-2	
43			Cracks under EQ3 MCE2
44			Spalling
45			at the test end

		SP-3	
46			Instrumentation
47			during EQ1 DBE
48			during EQ2 MCE1

	SP-3	
49		spalling
50		Buckling
51		at the test end

52	<p style="text-align: center;">SP-4</p> 	Instrumentation
53		Energy Dissipator
54		Top of view

SP-4		
55		Rocking approximately at 1% drift
56		about 2% drift
57		after the test (elevation view)